



**HAL**  
open science

# Experimental and numerical investigation of the progressive collapse resistance of reinforced concrete beam-column sub-assemblages

Guoqiang Zhao

► **To cite this version:**

Guoqiang Zhao. Experimental and numerical investigation of the progressive collapse resistance of reinforced concrete beam-column sub-assemblages. Other [cond-mat.other]. Université Grenoble Alpes, 2019. English. NNT: 2019GREAI043 . tel-02304705

**HAL Id: tel-02304705**

**<https://theses.hal.science/tel-02304705>**

Submitted on 3 Oct 2019

**HAL** is a multi-disciplinary open access archive for the deposit and dissemination of scientific research documents, whether they are published or not. The documents may come from teaching and research institutions in France or abroad, or from public or private research centers.

L'archive ouverte pluridisciplinaire **HAL**, est destinée au dépôt et à la diffusion de documents scientifiques de niveau recherche, publiés ou non, émanant des établissements d'enseignement et de recherche français ou étrangers, des laboratoires publics ou privés.

## THÈSE

Pour obtenir le grade de

### **DOCTEUR DE LA COMMUNAUTE UNIVERSITE GRENOBLE ALPES**

Spécialité : 2MGE : Matériaux, Mécanique, Genie civil

Arrêté ministériel : 25 mai 2016

Présentée par

**Guoqiang ZHAO**

Thèse dirigée par **Pascal FORQUIN** et  
co-dirigée par **Yann MALECOT**

préparée au sein du **Laboratoire Sols, Solides, Structures et  
Risques**

dans l'**École Doctorale I-MEP2- Ingénierie - Matériaux,  
Mécanique, Environnement, Énergétique, Procédés,  
Production**

## **Etude expérimentale et numérique de la résistance à l'effondrement progressif de sous-assemblages poteaux-poutres en béton armé**

Thèse soutenue publiquement le **3 juillet 2019**,  
devant le jury composé de :

**Monsieur Emmanuel FERRIER**

Professeur, Université Claude Bernard - Lyon 1, Président

**Madame Evelyne TOUSSAINT**

Professeur, Université Clermont Auvergne, Rapporteur

**Monsieur Stéphane GRANGE**

Professeur, INSA de Lyon, Rapporteur

**Madame Wen CHEN**

Maître de Conférences, Université de Lorraine, Examineur

**Monsieur Pascal FORQUIN**

Professeur, Université Grenoble Alpes, Directeur de thèse

**Monsieur Yann MALECOT**

Professeur, Université Grenoble Alpes, Co-directeur de thèse



## **THESIS**

To obtain the grade of

### **DOCTOR OF THE COMMUNAUTE UNIVERSITE GRENOBLE ALPES**

Specialty: 2MGE: Matériaux, Mécanique, Genie civil

Ministerial decree: 25 mai 2016

Presented by

**Guoqiang ZHAO**

Thesis directed by **Pascal FORQUIN** and  
co-directed by **Yann MALECOT**

Prepared in the **Laboratory Sols, Solides, Structures et  
Risques**  
in the **École Doctorale I-MEP2- Ingénierie - Matériaux,  
Mécanique, Environnement, Energétique, Procédés,  
Production**

## **Experimental and numerical investigation of the progressive collapse resistance of reinforced concrete beam-column sub- assemblages**

Thesis publicly defended on **July 3, 2019**

In front of the defense jury composed of:

**Mr. Emmanuel FERRIER**

Professor, Université Claude Bernard - Lyon 1, President

**Mrs. Evelyne TOUSSAINT**

Professor, Université Clermont Auvergne, Reviewer

**Mr. Stéphane GRANGE**

Professor, INSA de Lyon, Reviewer

**Mrs. Wen CHEN**

Associate professor, Université de Lorraine, Examiner

**Mr. Pascal FORQUIN**

Professor, Université Grenoble Alpes, Thesis director

**Mr. Yann MALECOT**

Professor, Université Grenoble Alpes, Thesis co-director





## Acknowledgements

This Ph.D. dissertation has been one of the most significant challenges that I have faced in my study. Last year, my family and I went through a hard time. Due to family affairs, progress was barely made in my work during a long time. Under pressure, the study was too stressful to be continued and I would like even to give it up. However, my professors gave me invaluable advices and supports in my study. Their diligence, motivation and rigorous attitudes in research make me understand that I should accomplish my dissertation. As an old Chinese saying, “start well an end well”, so that I conquered the difficulties and completed the dissertation. Thus, I would like to express my gratitude to all people who gave me help and support during my Ph.D. study in 3SR laboratory.

First and foremost I would like to acknowledge my advisors, Professor Pascal Forquin and Professor Yann Malecot, for their patience, guidance and encouragement during my study and experiment design. They introduced me into the field of “dynamic experiment” and taught me how to be a good researcher. Without their support and guidance, this dissertation would have been impossible to complete. I will always be grateful for this and thank you for everything you have done for me.

Next, I want to give my sincere gratitude to all the members of the jury. Thank you for taking time out of your busy schedule to attend my defense. Special thanks go to Mrs. Toussaint and Mr. Grange for their invaluable feedback and constructive criticisms in their reports. Thanks is also due to Mrs. Chen for her intelligent questions and detailed comments. Finally, I am also thankful to Mr. Emmanuel for accepting to be the president of the jury and for his insightful suggestions. A fruitful scientific discussion on the day of the defense helped me understand my research area better.

I would like to sincerely thank to Dr. Briffaut Matthieu for helping in software and hardware. I also appreciate the help provided by Dr. Lukic Bratislav, Dr. Chao Yuan, Dr. Zhao Hua Li and all the colleagues in our team. We often discussed problems respecting numerical simulation

and it was unforgettable experience of cooperation.

Further appreciation extends to the master students Luis Calos Arevalo, Dmitriy Baturkin and Hui Hu who helped to make specimens of the test. Besides, I would like to thank the technicians of the 3SR laboratory, Mehideb Karim, Toni Jean-benot, and Decosne Jean-luc for their support in the experiment.

This work was supported by Country China Scholarship Council (CSC) . Thanks to CSC for offering me an opportunity of study in France.

Finally, I would like to thank my parents, my wife, my son and my daughter for their uncompromising support. Their smile makes me feel warm and give me the impetus to move forward. I appreciate them very much. I love you.

## **Abstract**

Important buildings may be subjected to accidental loads, such as explosions or impacts, during their service life. It is, therefore, necessary not only to evaluate their safety under traditional loads and seismic action. The structural performances related to progressive collapse scenarios need to be investigated.

The study of progressive collapse involves a dynamic problem, but unfortunately dynamic experiments on the behavior of the civil engineering structures under dynamic conditions are rare. In this research, beam-column sub-assembly specimens were tested under dynamic load. The loading program consists in placing a large mass, as a dead load, on the top of the middle column of a beam-column sub-assembly. The support under the middle column is suddenly removed for simulating the sudden loss of a column and the damage that will result in the structure. The loading system and supporting devices were specially designed for this test. The upper dead load can be changed by increasing or decreasing the applied mass to different specimens. The supports for the side column have a controlled rigidity in the horizontal direction and are designed to restrain rotation of the side-column. Thus, the boundary conditions are supposed to be similar to real situations. During the test, a laser was installed under the middle pillar to collect the falling velocity and a high-speed camera was used to visualize the whole process of failure. The images obtained from the camera were processed by Digital Image Correlation (DIC) technology to get the corresponding displacements and strain fields. By these means, all the information of the structure under dynamic loading was captured and recorded, such as the period of vibration, frequency, velocity and displacement. Based on these experimental data, the effect of section and span of the specimen on dynamic response was discussed and the damage of the specimens under different loads was analyzed by the damage factor. Time history of resistance force curves and resistance force versus vertical displacement curves were produced. The performance of the beam-column assemblies under dynamic loads is different from the previous published quasi-static experiments in terms of structural mechanisms, crack patterns, damage mode. And it demonstrate that the beam-column assembly test with the designed support device can be used to analyze the dynamic behavior

of the local structure.

In addition, numerical simulations were developed for simulating the failing process of the structure. A technique named “connector” was proposed into beam-column finite element model by adding a series of springs to investigate the interaction between steel rebars and concrete. A concrete damage model, named DFH-KST model, was used to characterize the development of concrete crack and damage. The versatility of the adopted methodology allows assessing the influence of the material nonlinear behavior and the geometry of the tested structure. Calibration and validation studies show that the proposed model can successfully represent the resistance of structure and behavior.

## Résumé

Au cours de leur durée de vie, les bâtiments importants sont susceptibles d'être soumis à des charges accidentelles, telles que des explosions ou des impacts. Evaluer leur stabilité vis-à-vis de charges traditionnelles statiques et sismiques ne suffit pas. Leurs performances structurelles liées à des scénarios d'effondrement progressif doivent également être examinées.

L'étude de l'effondrement progressif est un problème dynamique. Malheureusement, les expériences sur le comportement des structures de génie civil dans des conditions dynamiques sont rares car difficiles à réaliser. Dans cette étude, des sous-assemblages poteaux-poutres en béton armé ont été testés sous chargement dynamique. Le chargement a consisté à placer une masse importante jouant le rôle de « charge morte » sur la colonne centrale d'un sous-assemblage simulant la liaison de 3 poteaux avec 2 poutres. Une pièce fusible jouant le rôle de support sous la colonne centrale est brutalement déverrouillée pour simuler la perte de portance soudaine de cette colonne. Le comportement dynamique et les dommages locaux causés à la structure ont été mesurés et étudiés. Le bâti de chargement et les dispositifs de support ont été conçus spécialement pour cet essai. La charge morte supérieure peut être modifiée et appliquées à différents spécimens. Les supports des colonnes latérales ont une rigidité horizontale contrôlée et sont conçus pour limiter la rotation de ces mêmes colonnes. Ainsi, les conditions aux limites des essais réalisés sont supposées être représentatives de situations réalistes. Au cours des essais, un laser a été installé sous la colonne centrale pour mesurer la vitesse de chute. Une caméra numérique rapide a été utilisée pour visualiser l'ensemble du processus de ruine du sous-assemblage. Les images obtenues de la caméra ont été traitées par une technique de DIC (Digital Image Correlation) afin d'obtenir le champ de déplacement et les déformations correspondantes. Grâce à ces mesures dynamiques, des données importantes ont été produites et enregistrées, notamment la période de vibration, la fréquence, la vitesse et le déplacement des différents échantillons testés. Sur la base de ces données expérimentales, l'effet de la section et de la portée des poutres sur la réponse dynamique et sur le mode d'endommagement des sous-assemblages a été discuté. Cette étude montre que les résultats expérimentaux obtenus, en termes de mécanismes structurels, de schéma de fissuration, de mode d'endommagement,

peuvent être utilisés pour analyser le comportement de sous-assemblages de structures réelles.

De plus, une modélisation numérique des essais a été établie pour simuler le processus de ruine de la structure. Une technique appelée «connecteur» a été proposée dans le modèle aux éléments finis du sous-assemblage poteaux-poutres. Cette technique consiste à ajouter une série de ressorts pour étudier le rôle de l'interaction entre les armatures en acier et le béton. Un modèle d'endommagement anisotrope, appelé modèle DFH-KST, a été utilisé pour caractériser l'évolution de la fissuration et l'endommagement du béton.

La polyvalence de la méthodologie adoptée permet d'évaluer l'influence du comportement non-linéaire du matériau et celle de la géométrie de la structure testée. Les études numériques de calibration et de validation montrent que le modèle proposé peut reproduire le comportement et la résistance de la structure avec succès.

**Table of contents**

- CHAPTER 1 INTRODUCTION .....1**
- 1.1 BACKGROUND .....1
- 1.2 SCOPE AND OBJECTIVES .....4
- 1.3 ORGANIZATION THE DISSERTATION .....6
- CHAPTER 2 LITERATURE REVIEW .....8**
- 2.1 REGULATIONS AND PROVISIONS FOR RESISTANCE PROGRESSIVE COLLAPSE IN CODES AND STANDARDS .....8
- 2.1.1 European standard .....8
- 2.1.2 American standards and guidelines .....9
- 2.2 EXPERIMENTAL RESEARCH PROGRESS .....18
- 2.2.1 Experiment study performed with RC frames .....18
- 2.2.2 Beam-column sub-assemblages experiment .....21
- 2.3 NUMERICAL SIMULATION ANALYSIS .....33
- 2.4 STUDY OF INTERACTION PROPERTIES BETWEEN REBARS AND CONCRETE .....39
- CHAPTER 3 EXPERIMENTAL AND ANALYTICAL EVALUATION OF RESPONSE OF A RC BEAM-COLUMN SUB-ASSEMBLAGES UNDER A REMOVAL SUPPORT .....43**
- 3.1 INTRODUCTION .....43
- 3.2 SPECIMEN DESIGN .....44
- 3.2.1 Dimensions of specimens .....45
- 3.2.2 Material .....48
- 3.2.3 Fabrication of specimen .....50
- 3.2.4 Estimation of the bearing capacity by traditional design method and identification of the range of failure loads .....52
- 3.3 EXPERIMENTAL SET UP .....55
- 3.3.1 The loading system .....55

3.3.2 Design of the support for the side columns .....	57
3.3.3 Unloading device under the middle column .....	61
3.3.4 Instrumentation .....	61
3.4 EXPERIMENTAL PROCEDURE .....	63
3.5 TEST RESULTS .....	64
3.5.1 Specimen 1-1 L=2m 110mm×180mm.....	64
3.5.2 Specimen 2-1 L=3m 110mm×180mm.....	69
3.5.3 Specimen 2-2 L=3m 110mm×180mm.....	76
3.5.4 Specimen 3-1 L=3m 110mm×270mm.....	78
3.6 THE DYNAMIC ANALYSIS OF THE BEAM-COLUMN ASSEMBLAGES.....	82
3.6.1 Calculation of vibration properties $\zeta$ , $\omega D$ , $TD$ .....	82
3.5.2 Evaluation of the damage state of the sub-assemblages under dynamic loads	87
<b>CHAPTER 4 APPLICATION OF CONNECTOR IN SIMULATING BOND-SLIP</b>	
<b>BEHAVIOR .....</b>	<b>89</b>
4.1 INTRODUCTION .....	89
4.2 THE CONCRETE CONSTITUTIVE MODEL .....	89
4.3 CONNECTOR TECHNOLOGY .....	91
4.3.1 Connector elements .....	91
4.3.2 Connector behavior .....	91
4.4 IDENTIFICATION AND VALIDATION OF PARAMETERS FROM PULL-OUT TESTS .....	93
4.4.1 Identification of parameters .....	93
4.4.2 Numerical model of pull-out test .....	94
4.4.3 Identification the connector parameters (D12mm) .....	95
4.4.4 The effect of different restrain modes on the beam.....	96
<b>CHAPTER 5 NUMERICAL INVESTIGATION OF REINFORCED CONCRETE</b>	
<b>STRUCTURE IN PROGRESSIVE COLLAPSE.....</b>	<b>102</b>
5.1 DESIGN SUPPORT FOR THE SIDE STUB COLUMNS.....	102

5.1.1 Assessment of the design of the support for the side columns .....	102
5.1.2 Analysis of the stress and strain of the supports .....	103
5.2 NUMERICAL SIMULATION THE BEAM-COLUMN ASSEMBLAGES UNDER THE REMOVAL OF THE MIDDLE SUPPORT.....	108
5.2.1 Evaluation the resistance of beam-column assemblages subjected to the middle support removal in the quasi-static state loading .....	109
5.2.2 Numerical simulation study of the dynamic behavior of beam-column assemblages subjected to middle support removal .....	118
<b>CHAPTER 6 CONCLUSIONS AND RECOMMENDATIONS .....</b>	<b>125</b>
6.1 CONCLUSIONS.....	125
6.2 RECOMMENDATIONS FOR FUTURE RESEARCH .....	128
6.2.1 Experimental research .....	128
6.2.2 Numerical simulation .....	129
REFERENCE .....	131

## List of figures

Figure 1. 1 Ronan point apartment collapse, 1968.....	2
Figure 1. 2 Murrah Federal Office building, 1995 .....	2
Figure 1. 3 World trade center, 2001 .....	3
Figure 1. 4 Bankers trust, New York .....	4
Figure 2. 1 Measurement of $\theta$ after formation of plastic hinges .....	14
Figure 2. 2 (a) Collapse limit state of model frame; (b) middle column load versus unloading displacement of failed middle column; (c) effect of downward displacement of middle column on horizontal displacement of columns at first floor.( Yi et al 2008) .....	19
Figure 2. 3(a) South-east view of evaluated building; (b) Locations of strain gauges on first floor columns; (c) Strain gauge histories installed on first floor Column A1. (Sasani and Sagiroglu, 2008) .....	20
Figure 2. 4 The circled columns on North Side of the Building were Removed During the Experiment (Sezen and Song, 2009).....	20
Figure 2. 5 (a) Model of frame; (b) static collapse test setup; (c) frame horizontal displacement (He, 2009) .....	21
Figure 2. 6 Force-displacement relationships (Sasani and Kropelnicki, 2008) .....	22
Figure 2. 7 (a) Test setup; (b) effect of flexural reinforcement ratio; (b) effect of ratio of beam span to depth. (Su et al. 2008) .....	23
Figure 2. 8 (a) The specimen and the boundary conditions;(b) The detailing of the beam-column specimen; (c) The relationship between the applied force and the middle joint displacement; (d) The relationship between the horizontal reaction force and the middle joint displacement. (Yu and Tan, 2010) .....	24
Figure 2. 9 (a) Test set-up for the beam-column; (b) Load-displacement relationships; (c) Reinforcement detailing of the specimen ;(d) Damage mode of the specimen (H.Choi, J.Kim 2011) 5S: 5 storey, seismic-load resisting; 5G: 5 storey, gravity-load resisting ....	26
Figure 2. 10 (a) Illustration of moment redistribution and deformed shape; (b) the test set-up. (Yap and Li, 2011) .....	27
Figure 2. 11 (a) Overview of a specimen prior testing; (b) Reaction force versus vertical displacement responses (Qian and Li, 2012) .....	27
Figure 2. 12 (a) experimental set-up; (b) Vertical load versus displacement of the middle column (Lanhui Guo et. al, 2013).....	28
Figure 2. 13 Pictures of RC structures after the experiments. Macro-cracks are visible near the middle joint. (a) Rebar $\varnothing 8$ h=180mm; (b) Rebar $\varnothing 12$ h=180mm (P. Forquin and W. Chen, 2014) .....	29
Figure 2. 14 (a) overview of test setup; (b) configuration of middle column; (c) testing procedure at 30ms; (d) at the end of the test. (Jun Yu et al., 2013) .....	30
Figure 2. 15 Failure mode of beam-column assemblages .....	33
Figure 2. 16 P-I curves for different damage degrees D (Shi et al., 2010).....	37
Figure 2. 17 (a) Single story reinforced concrete frame model for blast analysis; (b) Damage contour of the detailed model; (c) Damage contour of the simplified model (Kim et al., 2013) .....	37

Figure 2. 18 Collapse evolution for structures with increasing $\alpha$ (Masoero et al. 2010) .....	38
Figure 2. 19 Pull out test: Failure types for concrete specimen with and without confinement (W.Yeih et al. 1997) .....	40
Figure 2. 20 (a) Bond failure at the steel concrete interface; (b) Steel bar failure (J. Humbert et al. 2009) .....	40
Figure 2. 21 (a) Mode failure of specimen without rings (0D); (b) Mode failure of specimen with rings (4D40) (Tastani and Pantazopoulou, 2002) .....	41
Figure 2. 22 (a) Slip curve of DTP-BT of steel bars with different arrangements of loose metal rings along the anchorage; (b) comparative values of bond strength obtained by two test setups (Tastani and Pantazopoulou, 2002) .....	41
Figure 2. 23 (a) Radial stress; (b) Longitudinal stress (Mahran, 2008) .....	42
Figure 3. 1 The prototype building and local sub-assembly used for the test .....	45
Figure 3. 2 Boundaries of removed elements based on GSA .....	45
Figure 3. 3 Specimen S1 180x110 L=2000mm .....	47
Figure 3. 4 Specimen S2 180x110 L=3000mm .....	47
Figure 3. 5 Specimen S3 270x110 L=3000mm .....	48
Figure 3. 6 Stress-strain curve of steel rebar.....	50
Figure 3. 7 Making of specimens (a) Reinforcement cage and mould; (b) concrete constituents; (c) Casting the specimen; (d) Spraying the specimen .....	51
Figure 3. 8 Flowchart of the concrete mixing .....	52
Figure 3. 9 Rectangular stress distribution (Eurocode 1-1).....	53
Figure 3. 10 Bending moment diagram .....	54
Figure 3. 11 Layout of test set-up.....	56
Figure 3. 12 (a) front elevation of the loading system; (b) lateral view of the loading system	57
Figure 3. 13 The support for side columns .....	58
Figure 3. 14 Deformation of structure after the removal of the middle support.....	59
Figure 3. 15 Simplified diagram of the deformed shape of the support connector plate .....	59
Figure 3. 16 designed support for side columns .....	60
Figure 3. 17 Unloading device .....	61
Figure 3. 18 Measurement device .....	63
Figure 3. 19 Layout of set-up before the test .....	64
Figure 3. 20 Calculation sketch of the resistance force.....	65
Figure 3. 21 Velocity of the middle column of the specimen 1-1 under the dynamic load 2662kg. The maximum velocity is 0.43m/s. ....	67
Figure 3. 22 Time history of vertical displacement of the middle column and the strain field under the load 2662kg.....	67
Figure 3. 23 The vertical displacement of the middle column versus time and the damage under the load 2662kg.....	67
Figure 3. 24 (a) Resistance force versus vertical displacement of middle column; (b) The stain field near the middle joint by the DIC (S1-1 Load=2662kg).....	68
Figure 3. 25 Calculation diagram of the displacement of the support.....	69
Figure 3. 26 Concrete crack pattern on the specimen (S1-1 Load=2662kg) .....	69
Figure 3. 27 Set up of the specimen S 2-1 .....	70

Figure 3. 28 Velocity versus time under several successive loadings of 675kg .....	71
Figure 3. 29 Vertical displacement of the middle column versus time for the first loading at 675kg and strain fields in the horizontal direction .....	72
Figure 3. 30 Vertical displacement of the middle column versus time under the load of 675kg for the second time and the strain in the horizontal direction .....	72
Figure 3. 31 Velocity versus time under the load of 994kg .....	72
Figure 3. 32 Vertical displacement of the middle column versus time under the load of 994kg for the first time and the strain field in the horizontal direction.....	73
Figure 3. 33 Crack development after the first loading at 994kg.....	73
Figure 3. 34 Vertical displacement of the middle column versus time under the third loading at 994 kg and the strain of the side column in the horizontal direction.....	73
Figure 3. 35 Crack development under the third loading at 994 kg.....	74
Figure 3. 36 Velocity versus time under a loading of 2063kg and after undergoing previous loading of 675kg and 994kg.....	75
Figure 3. 37 Vertical displacement of the middle column versus time under the load of 2063kg .....	75
Figure 3. 38 Failure mode of the structure under the load of 2063kg .....	75
Figure 3. 39 Velocity versus time under a loading of 2063kg (the specimen 2-1 was previously loaded with multiple smaller loading; the specimen 2-2 was loaded with a unique load of 2063kg.) .....	77
Figure 3. 40 Vertical displacement of the middle column versus time under a load of 2063kg .....	77
Figure 3. 41 (a) Time history of vertical resistance force; (b) Resistance force versus vertical displacement of middle column (S2-1 Load=2063kg, S2-2 Load=2063kg) .....	78
Figure 3. 42 Velocity versus time under successive loads of 994kg .....	80
Figure 3. 43 Vertical displacement of the middle column versus time and strain field under the load of 994kg (first loading time).....	80
Figure 3. 44 Vertical displacement of the middle column versus time and the strain under the load of 994kg (second loading time) .....	80
Figure 3. 45 Velocity versus time under the load 2737kg (third loading time) .....	81
Figure 3. 46 Vertical displacement of the middle column versus time and strain field under the load 2737kg (third loading time) .....	81
Figure 3. 47 Damage of structure under the load of 2737kg at the end of the test .....	81
Figure 3. 48 (a) Time history of vertical resistance force; (b) Resistance force versus vertical displacement of middle column (S3-1 Load=2737kg) .....	82
Figure 3. 49 Dynamic analysis diagram .....	83
Figure 4. 1 Connector damage evolution.....	91
Figure 4. 2 Evolution of force versus displacement for the pull out tests .....	94
Figure 4. 3 Boundary and loading conditions for the FE model.....	95
Figure 4. 4 Schematic representation of connector in FE model .....	95
Figure 4. 5 (a) Pull out force versus displacement of steel bar; (b) The response of the single connector (D12mm) .....	96
Figure 4. 6 The numerical model of the beam-column assemblage.....	97

Figure 4. 7 Numerical model of reinforcement cage for the three studied cases .....	98
Figure 4. 8 Effect of different constraint modes of rebars on bearing capacity (D12mm) of beams .....	99
Figure 4. 9 Cracking development .....	100
Figure 5. 1 Calculation sketch diagram .....	102
Figure 5. 2 Force diagram of beam-column assemblage in elastic state (a) horizontal force; (b) vertical force; (c) bending moment.....	103
Figure 5. 3 Details of the support (thickness=5mm, 4 slices).....	104
Figure 5. 4 Details of the support (thickness=5mm, 6 slices).....	104
Figure 5. 5 Details of the support (thickness=4mm, 6 slices).....	105
Figure 5. 6 (a) Mises stress in the support; (b) Lateral displacement of the support (thickness=5mm, 4 slices).....	106
Figure 5. 7 (a) Mises stress in the support; (b) Lateral displacement of the support (thickness=5mm, 6 slices).....	107
Figure 5. 8 (a) Mises stress in the support; (b) Lateral displacement of the support (thickness=4mm, 6 slices).....	108
Figure 5. 9 Numerical model used in ABAQUS representing the quarter of a beam .....	110
Figure 5. 10 Additional connectors in the plastic zone.....	110
Figure 5. 11 Middle column load versus vertical displacement of failed middle column.....	112
Figure 5. 12 Effect of downward displacement of middle column on horizontal displacement .....	113
Figure 5. 13 PEEQ of tension reinforcement at middle and end sections .....	116
Figure 5. 14 Damage development in the specimen .....	118
Figure 5. 15 Numerical model used in ABAQUS and gravitational field .....	118
Figure 5. 16 Resistance force versus vertical displacement of middle column .....	120
Figure 5. 17 Comparison of experimental and numerical results for the vertical displacement history of the middle joint .....	121
Figure 5. 18 Damage development in the specimen .....	124

## List of tables

Table 2. 1 Strength-increase factor for various construction materials .....	14
Table 2. 2 Size of specimens in different experiments .....	33
Table 3. 1 Span-depth ratio of the specimen .....	48
Table 3. 2 specimen properties .....	48
Table 3. 3 Composition and properties of R30A7 concrete [22] [77] .....	49
Table 3. 4 Material properties of steel reinforcement [22] .....	50
Table 3. 5 Consumption of materials for each type of specimen .....	51
Table 3. 6 Basic configuration of specimens and bearing capacity .....	55
Table 3. 7 The summary of experimental results .....	82
Table 3. 8 The stiffness of the beam .....	83
Table 3. 9 The frequency and period of damped vibration .....	87
Table 3. 10 Damage factor of the structure under different level loads .....	88
Table 4. 1 Parameters of connector law (with hardening) for D12mm .....	94
Table 5. 1 Force at critical point of reaction force-displacement curves .....	115

# Chapter 1 Introduction

## 1.1 Background

Generally, a building is designed by taking into account the applied static dead load, live load, and depending on the location of the building, seismic and climate related loads. While some important existing buildings could be subjected to abnormal loadings such as earthquake, explosion or other man-made or natural hazards. These accidental events may induce local structural damage. This local failure leads to a load redistribution in the structure and may cause a chain reaction of key structure load-carrying members' failures disproportionate to the initial damage, leading to more widespread failure of the surrounding members and partial or complete structure collapse. This type of collapse is named "progressive collapse". The General Services Administration of the United States (2003) defines this phenomenon as "a situation where local failure of a primary structural component leads to the collapse of adjoining members which, in turn, leads to additional collapse.[1]" Other definition is from ASCE/SEI 7 (2010) "the spread of an initial local failure from element to element, eventually resulting in the collapse of an entire structure or disproportionately large part of it. [2]" The key characteristic of both is that the total damage is disproportionate to the original cause.

One of the earliest well-known example of progressive collapse was the collapse of Ronan Point apartment. On the morning of 6 May 1968, Ronan point apartment tower in east London, partially collapsed due to a gas explosion, which pulled down the precast concrete panels near the corner of the building. The loss of support at the 18th floor led to the floors above to collapse. Four people died in this accident. The impact of the upper floors on the lower ones led to a sequential failure all the way down to the ground level [3]. As a result, the entire corner of the building collapsed, as can be observed in Figure 1. 1. This partial collapse was attributed to the inability of the structure to redirect loads after the loss of a load-carrying member. It is a particularly representative example since the magnitude of the collapse was completely out of proportion with respect to the triggering event [3]. Since the collapse of the Ronan Point, the progressive collapse resistance of building structures has attracted the attention of engineers and researchers. People began to recognize the importance of progressive collapse resistance.

After that event, there have been more global progressive collapse accidents due to various reasons.



Figure 1. 1 Ronan point apartment collapse, 1968

On 19 April 1995, the Murrah Federal Office building in Oklahoma City collapsed consequently to a bomb attack [4], which only destroyed three columns initially. The failure was transferred from location columns to adjacent girders causing the progressive collapse of the upper stories. Finally, the whole building was destroyed (Figure 1. 2.) and 168 people were killed as well as more than 800 people were injured in this terrorist attack.



Figure 1. 2 Murrah Federal Office building, 1995

The World Trade Center in New York City was attacked by terrorists on 11 September 2001. A Boeing 767 airplane crashed into the building at a very high speed (see Figure 1.3). The crash caused a fire hazard so that the internal steel components softened and lost their ability to support load above. It resulted in a progression of failures extending from the impact zone to the ground. According to the report prepared by the National Institute of Standards and Technology (NIST, 2008a) the fireproofing on the Twin Towers' steel infrastructures was blown off by the initial impact of the planes and concluded that, if this had not occurred, the towers would likely have remained standing [5]. It was a horrible disaster. More than a thousand people lost their lives in that event. In fact, as early as 1993, the World Trade Center was already attacked by a car bomb, which exploded in the underground garage [6]. The explosion resulted in severe damage in the garage, however, the building didn't collapse.



Figure 1.3 World Trade Center, 2001

Debris from the collapse of WTC 2 removed an exterior column over a partial height of the Bankers Trust building (see Figure 1.4). The redundancy of the structure above provided the necessary bridge to transfer loads from the lost column.



Figure 1. 4 Bankers trust, New York

With the recent collapse of the Federal Building, World Trade Center, and subsequently a series of accident during this decade, it is noted that large-scale public buildings are much easier to suffer from destruction. When this kind of building collapse, it often causes costly damages and massive casualties and can have very bad social consequences. In the international structural engineering academic circles, “progressive collapse” and “disproportionate collapse” have become common vocabulary. Reinforced concrete structures are widely used in civil engineering throughout the world as well as for large infrastructures or buildings. Abnormal loads may induce local structural damage that occurs firstly at the beam-column joint leading to more widespread failure of the surrounding members and to partial or complete structure collapse. Therefore, apart from ensuring the security and reliability of the structure in strength, stability and rigidity when it bears its service design load designed from regular design methods, a reinforced concrete structure also should be able to resist to abnormal load caused by a local damage or by a sudden change in the support system.

## **1.2 Scope and objectives**

In observing above cases of collapse, although progressive collapse involves the global structure with partial or full collapse, the crucial issue is the behavior of the local structure subjected to accidental load. Beam-column system is a very common structural building system that can be chosen as a typical structure. In experimental work, the beam-column is then a

subassembly often used as a laboratory testing object. Based on the two federal guidelines GSA 2003 and DoD 2005 that provided the strategy and proposed threat independent-analysis procedures to evaluate the potential of progressive collapse of a structure following the notional removal of major loading bearing elements, one of the most probable scenarios is the loss of exterior ground column. In that case, the effect of abnormal load on the adjacent elements can be considered apart from testing object. In terms of experimental studies in the literature, there are few dynamic tests conducted to investigate the response of structures by removing the middle vertical supporting element. Using a well designed fusing support for the middle column, this test can reproduce a typical dynamic local failure process.

A partial damage of the structure due to accidental load could trigger progressive collapse, which involves a series of nonlinear problems such as brittle damage of concrete, interaction between concrete and steel bar as well as large deformation of members beyond the traditional scope of design. In numerical simulation studies, these efforts focus on material (brittle damage) and geometric (interaction between concrete and steel bars) nonlinearities in the process of component failure. For this purpose, a concrete anisotropic damage model, named DFH model, was used in this numerical calculation. In addition, a type of spring wire connector was applied for the detailed modeling of reinforced concrete structures with the commercial finite element code ABAQUS.

The overall objective of this research is to characterize the resisting mechanisms and to better understand the dynamic response of the reinforced concrete structure after the loss of a vertical supporting component. In conjunction with the general objective, dynamic tests of beam-column sub-assemblages with different sections and span lengths were conducted to investigate the effect of reinforcement ratio and the effect of span-depth ratio (span of beam divided by the depth of the beam) on the behavior of beam-column assemblages. The characterization of the resisting mechanisms has been done using the results of the experiments and thanks to analytical studies. In addition, the research was devoted to the development of an experimental equipment including the loading and unloading system as well as the support system for the testing specimens [7]–[9].

Another objective is to propose and to validate a numerical simulation approach which is able to deal with the nonlinear problem that constitute the simulation of progressive collapse of reinforced concrete building.

### **1.3 Organization the dissertation**

This dissertation is organized as follows:

Chapter 1 presents the background of progressive collapse and gives a series of examples of progressive collapse. The scope and the objectives of this research work are also presented. The last part presents the organization of dissertation.

Chapter 2 summarizes regulations, provision and analysis techniques in current codes and standards concerning progressive collapse resistance and introduces research progresses of recent years.

A dynamic test of beam-column assemblies is designed and presented in Chapter 3, including design of specimens, test set-up and obtained results. Four beam-column specimens with different sizes were tested under middle support removal scenario. It is highlighted that a new type of steel support was adopted in this test instead of common pin or fixed supports constraint so that it can supply a boundary conditions close to the member in the real frame would do. This section also discusses the results for successive increasing loading process.

Chapter 4 mainly presents connector skill. Connector model is built to describe the nonlinear relationship between two nodes. On the basis of this model, the interaction of concrete and reinforcement bars can be studied. This connector model was used to simulate the pull-out test successfully. The effect of parameters on the model is also studied.

Numerical simulation work is reported in Chapter 5. In this section, the dynamic tests are simulated. The connector element is used in the beam-column numerical model in order to analyze the influence of reinforcement bar in the overload resistance.

A discussion of the overall findings is given in chapter 6, together with some conclusions and

recommendations. Finally, some further prospecting works are presented.

## Chapter 2 Literature review

In the literature, it is found that the bond strength of reinforcing steel bar and concrete has a great influence on the bearing capacity of components [5][10]. Considering this, the review literature was divided into four parts, codes and standards, experimental works, numerical simulation works and studying of bond slip behavior between reinforcing steel bar and concrete.

### 2.1 Regulations and provisions for resistance progressive collapse in codes and standards

#### 2.1.1 European standard

The Eurocodes are detailed and comprehensive standards covering various aspects of structural design. They are divided into packages by groups Eurocodes for each of building materials, reinforced concrete, steel, composite concrete and steel, timber and so on. Eurocode- basis of structural design states that *“A structure shall be designed and executed in such a way that it will not be damaged by events such as explosion, impact, and the consequences of human errors, to an extent disproportionate to the original cause”*[11]. It indicates potential damage shall be avoided or limited by appropriate choice of one or more of the following:

- *avoiding, eliminating or reducing the hazards to which the structure can be subjected;*
- *selecting a structural form which has low sensitivity to the hazards considered;*
- *selecting a structural form and design that can survive adequately the accidental removal of an individual member or a limited part of the structure, or the occurrence of acceptable localized damage;*
- *avoiding as far as possible structural systems that can collapse without warning;*
- *tying the structural members together.*

Part 1-7 of Eurocode 1 provides principles and rules for safety of the buildings and other civil engineering works against identifiable and unidentifiable accidental actions. It emphasizes that structures shall be designed to resist to a progressive collapse resulting from an internal explosion.

Eurocode 2 mainly concerns concrete structure design and civil engineering works in plain, reinforced and prestressed concrete. The chapters that refer to robustness of concrete structure

can be found in the part 1-1. In the section 5 of part 1-1, it presents nonlinear analysis method and plastic analysis in design structure by selecting or changing the calculation parameters of material in order to improve the ductility of the structure.

These sections mainly indicate the basic requirements to meet in the design or the selection of structural form. However, they do not seem to give specific approach or practical information about how meet these requirements in the structural design and no quantitative method can be found in these chapters.

### **2.1.2 American standards and guidelines**

#### **ASCE 7-02**

The American Society of Civil Engineers *Minimum Design Loads for Buildings and Other Structures* (ASCE, 2002) has a section about “general structural integrity” that mentions “Buildings and other structures shall be designed to sustain local damage with the structural system as a whole remaining stable and not being damaged to an extent disproportionate to the original local damage. This shall be achieved through an arrangement of the structural elements that provides stability to the entire structural system by transferring loads from any locally damaged region to adjacent regions capable of resisting those loads without collapse. This shall be accomplished by providing sufficient continuity, redundancy, or energy-dissipating capacity (ductility), or a combination thereof, in the members of the structure [3].” In the early days, standard from ASCE mainly focus on redundancy and alternate load paths for avoiding disproportionate collapse. The degree of redundancy is not specified, and the requirements are entirely threat-independent. However, the ASCE 7-10 Standard provides recommendations for enhancing the ductility, continuity and redundancy of the structure.

Direct method is that certain elements considered as key elements are designed to be able to resist the load combination of Equation 2.1, or are checked after removal of an important structural element to provide the required resistance to withstand the gravity load combination of Equation 2.2 and to provide the required lateral stability resistance for the notional lateral force of Equation 2.3 [2] [12].

*Alternate load path method:*

$$(0.9 \text{ or } 1.2)D + 0.5L + 0.2(L_r \text{ or } S \text{ or } R) \quad (2.1)$$

*Key elements designs:*

$$(0.9 \text{ or } 1.2)D + A_k + 0.5L + 0.2S \quad (2.2)$$

*Lateral stability:*

$$N_i = 0.002 \sum P_i \quad (2.3)$$

*Where: D, L, L<sub>r</sub>, S and R are the dead, live, roof live, snow and rain loads respectively;*

*A<sub>k</sub> is the load effect arising from an abnormal event;*

*∑ P<sub>i</sub> is the gravity force acting at level i.*

### **ACI 318-11**

Similarly, the American Concrete Institute *Building Code Requirements for Structural Concrete* (ACI, 2002) includes requirements for structural integrity in the chapter 7 about details of reinforcement [13]. The recommendation says in the detailing of reinforcement and connections, members of a structure shall be effectively tied together to improve integrity of the overall structure.

We can also find some prescriptive requirements for continuity of reinforcing steel bars and interconnection members such as following:

- At least one-sixth of the tension reinforcement required for negative moment at the support, but not less than two bars;
- At least one-quarter of the tension reinforcement required for positive moment at midspan, but not less than two bars.

The commentary states that it is the intent of this section of the code to improve the redundancy and ductility in structures. Thus, in the event of damage to a major supporting element or due to an abnormal loading event, the resulting damage may be confined to a relatively small area and the structure will have a better chance to maintain its overall stability.

### **GSA PBS Facilities Standards 2000**

The 2000 edition of the GSA's *Facilities Standards for the Public Buildings Service* (GSA, 2000) included a "Progressive Collapse" heading in the "Structural Considerations" section: "The

structure must be able to sustain local damage without destabilizing the whole structure. The failure of a beam, slab, or column shall not result in failure of the structural system below, above, or in adjacent bays. In the case of column failure, damage in the beams and girders above the column shall be limited to large deflections. Collapse of floors or roofs must not be permitted.”

This is an absolute and unequivocal requirement for one-member (beam, slab, or column) redundancy, unrelated to the degree of vulnerability of the member or the level of threat to the structure[3].

### **Progressive Collapse Analysis and Design Guidelines for New Federal Office Buildings and Major Modernization Projects (GSA, 2003)**

In order to assist in the reduction of the potential for progressive collapse of Federal Office Building and in order to assist in the assessment of the potential for progressive collapse of existing Federal Office Buildings, the U.S. General Services Administration (GSA) published the “Progressive Collapse Analysis and Design Guidelines for New Federal Office Buildings and Major Modernization Projects”. The GSA document provides an insight to current thinking related to mitigating of progressive collapse. This approach is the concept of multiple load paths and structural redundancy which will produce a robust structure. The GSA criteria for new and existing structures, contains guidelines for the analyses of “typical” and “atypical” structural systems [1]. A typical structure is defined as having relatively simple layout with no unusual structural configurations. Unlike the codes of the past, these guidelines provides an independent methodology and a series criteria for improving design and reducing the risk of progressive collapse.

The guidelines give a procedure to estimate progressive collapse potential of the new as well as existing structures. Generally, it can be summarized in four steps [1]

- (a) Identify if the building is important and/or big enough to be targeted;*
- (b) Identify if the design of the frame is prone to progressive collapse;*
- (c) Conduct the analysis to verify the building sensitivity to progressive collapse;*
- (d) Apply structural modifications and restart from step (b).*

To determine the potential of progressive collapse for a typical structure, designers can perform structural analyses in which the instantaneous loss of one of the following first floor columns at a time is assumed:

- 1. An exterior column near the middle of the long side of the building.*
- 2. An exterior column near the middle of the short side of the building.*
- 3. A column located at the corner of the building.*
- 4. A column interior to the perimeter column lines for facilities that have underground parking and/or uncontrolled public ground floor areas.*

Designers may use linear elastic static analyses or non-linear dynamic analysis to check structural members in the alternate path structure, i.e. the structure after removal of a single column.

For static analysis purposes the following gravity load is applied to each structural member of the alternate path structure:

$$\text{Load} = 2(\text{DL} + 0.25\text{LL}) \quad (2.4)$$

For dynamic analysis procedure, the structure is required to be analyzed under vertical load combination as follows:

$$\text{Load} = \text{DL} + 0.25\text{LL} \quad (2.5)$$

Where, DL = Dead load; LL = Floor Live load (higher of the design live load or the code live load). The coefficient 2 in the load combination to be used in the static analysis procedure is used to take into account the dynamic effects.

In the section 4 of the guidelines, the Demand Capacity Ratio (DCR) is presented. An examination of the linear elastic analysis results shall be performed to identify the magnitudes and distribution of potential demands on both the primary and secondary structural elements for quantifying potential collapse areas. The magnitude and distribution of these demands can be indicated by DCR. It is calculated from the following equation:

$$DCR = Q_{UD}/Q_{CE} \quad (2.6)$$

Where  $Q_{UD}$  =Acting force (demand) determined in component or connection/joint (moment, axial force, shear, and possible combined forces);  $Q_{CE}$  =Expected ultimate, un-factored capacity of the component and/or connection/joint (moment, axial force, shear and possible combined forces).

In order to prevent collapse of the alternate path structure, the DCR values for each structural element must be less than or equal to the following:

$$DCR \leq 2.0 \text{ for typical structural configuration;}$$

$$DCR \leq 1.5 \text{ for atypical structural configuration.}$$

Structural elements that have DCR values exceeding the above limits will not have additional capacity for effectively redistributing loads, are considered failed, and can, therefore, result in collapse of the entire structure. The above DCR methodology is based on NEHRP (National Earthquake Hazards Reduction Program) guidelines for the seismic Rehabilitation of Buildings issued by FEMA in 1997.

In addition, these guidelines also refer to the material strengths in static linear elastic analysis approach. The guidelines point out that the design material strengths may be increased by a strength-increase factor to determine the expected material strength (for determining capacities, etc.) as the following table 2.1. To determine the ultimate capacity of the structural component, a material strength increase of 25% is allowed for concrete and reinforcing steel. These should be used only in cases where the designer or analyst is confident in the actual state of the facility's materials.

Table 2. 1 Strength-increase factor for various construction materials

Construction material	strength increase factor
Reinforced concrete	
Concrete compressive strength	1.25
Reinforcing steel (tensile and yield strength)	1.25
Concrete unit masonry	
Compressive strength	1.00
Flexural tensile strength	1.00
Shear strength	1.00
Wood and light metal framing	
All components	1.00

Compared to linear analysis procedure, nonlinear analysis procedure is generally a more sophisticated analysis approach to characterize the performance of a structure. The guidelines based upon the plastic hinge rotation and displacement ductility ratios set up a group of acceptance criteria for nonlinear analysis according to various component combinations. It can be used to predict the potential collapse of a structural element. For example, the maximum allowable rotation  $\theta$  for reinforced concrete beam is 6 degrees [14] [15]. If a beam rotates beyond than 6 degrees, it has the possibility of collapsing. Rotation for members can be determined using Figure 2. 1 provided below.

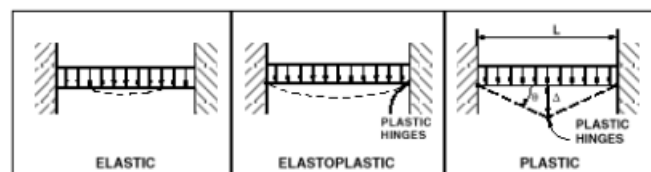


Figure 2. 1 Measurement of  $\theta$  after formation of plastic hinges

The GSA guidelines represent the state-of-the-practice in blast engineering of buildings but, similar to current building codes for seismic design, make use of indirect methods of analysis and prescriptive procedures of unknown reliability [16]. In fact, most calculations are based on previous experience. In the actual analysis, because of the time cost factors, people still conduct mostly static linear analysis. The reliability of the results urgently need a lot of dynamic experimental data for reference.

## **Design of Buildings to Resist Progressive Collapse (UFC 4-023-03) (The Department of Defense (DOD), 2005)**

In 1999 and 2001, the department of Defense (DOD) developed interim guidelines to reduce the risk of progressive collapse. These threat independent guidelines were developed to provide resistance to collapse propagating outside of a local collapse region.

In 2004, DOD began an effort to develop a Unified Facilities Criteria (UFC) on the Design of Buildings to Resist Progressive Collapse to provide designers of its facilities with specific, enforceable design criteria for mitigation of progressive collapse due to blast, severe impact or other natural or manmade events. In an effort to update and expand the DOD Interim guidelines, the DOD searched and then adapted the best available approaches from different organizations and countries.

In UFC 4-023-03, structural analyses must consider the “removal” of external columns near the middle of the each side and at the corner of the building. Columns must also be removed at locations where the plan geometry of the structure changes significantly or at locations where there is an abrupt change in loads, member geometry, or bay sizes. The GSA guidelines require only removal of ground floor elements while UFC 4-023-03 requires that analyses to be performed for each floor, one at a time. The motivation for the DOD requirement is that facilities could be attacked with direct or indirect fire weapons, which could damage a structure at upper floors.

DOD has additional prescriptive requirements that increase resistance to progressive collapse.

For all Levels of Protection (use UFC 4-020-01 to define a level of protection) [17]:

- *All multistory vertical load carrying elements must be capable of supporting the vertical load after the loss of lateral support at any floor level (i.e., a laterally unsupported length equal to two stories must be used in the design or analysis). The loads from the “removed” story should not be applied to the wall or column.*
- *All floors and roofs must be able to withstand a prescribed net upward load applied to each bay. The uplift loads are not applied concurrently to all bays. For Medium and High Levels of Protection:*

- *All perimeter columns must have sufficient shear capacity to develop the full plastic flexural moment.*

The UFC defines four Occupancy Category (OC) according to the level of occupancy and building function and then sets different levels of design requirements for each category of protection level. Three approaches are presented to design existing and new structures to resist progressive collapse, including tie force, alternate path method and enhanced local resistance.

1. Tie Forces, which prescribe a tensile force strength of the floor or roof system, to allow the transfer of load from the damaged portion of the structure to the undamaged portion; there are three horizontal ties that must be provided: longitudinal, transverse, and peripheral. Vertical ties are required in columns and load bearing walls.

Required tie strength for the longitudinal or transverse ties:

$$F_i = 3w_F L_1 \quad (2.7)$$

Required peripheral tie strength for the frame structures and two-way load-bearing wall buildings:

$$F_i = 6w_F L_1 L_p + 3W_c \quad (2.8)$$

$w_F$  is the floor load;  $W_c$  is 1.2 time the dead load of cladding over the length of  $L_1$ , where 1.2 is the dead load factor;  $L_1$  is the largest of the distances between the centers of the columns, frames, or walls supporting any two adjacent floor spaces in the direction under consideration;  $L_p$  is 1m.

2. Alternate Path method, in which the building must bridge across a removed element. Following the general philosophy of the standard Load and Resistance Factor Design (LRFD) approach, the design strength is taken as the product of the strength reduction factor  $\phi$  and the nominal strength  $R_n$  calculated in accordance with the requirements and assumptions of applicable material specific codes. The design strength must be larger than or equal to the required strength:

$$\phi R_n \geq R_u \quad (2.9)$$

where  $\phi R_n$  is the design strength;  $\phi$  is the strength reduction factor;  $R_n$  corresponds to the nominal strength ;  $R_u$  is the required strength.

3. Enhanced Local Resistance, in which the shear and flexural strength of the perimeter columns and walls are increased to provide additional protection by reducing the probability of extent of initial damage.

Taking into account local strengthening in the design easily leads to a large section or size of the component, greatly increases costs and reduces used space. Therefore, these guidelines are more suitable for large-scale public buildings.

In summary, many of the provisions exposed in previous paragraph agreed on common features-ductility, continuity and energy absorption-that structures should possess to help preventing progressive collapse. These guides supply two design methods to consider progressive collapse of structure, indirect design and direct design. The former emphasizes passively providing minimum levels of strength, continuity, and ductility to insure structural integrity. The latter contains the specific load resistance and the alternate path approaches. Few of them offered any quantitative analytical methods for evaluating the potential for progressive collapse.

In addition, researchers found that both the GSA and DoD methods may not give reliable predictions of structural progressive collapse and usually underestimate the stress and strain response at the joint of adjacent columns [16][18]. Besides, the prediction and estimation of the progressive collapse capacity of structure have still absence of efficient method. In order to understand completely the behavior of a structure under progressive collapse, two methods are usually combined: experiment and numerical simulation. It is then necessary to do more bibliography about experimental aspect and numerical simulation analysis that way offer a detail design method for resisting to progressive collapse.

## **2.2 Experimental research progress**

### **2.2.1 Experiment study performed with RC frames**

General services administration describes progressive collapse as follow: “a situation where local failure of a primary structural component leads to the collapse of adjoining members which, in turn, lead to additional collapse.” Many of these collapses are due to explosion, terrorist attack, or other incidental events. Generally, traditional design approach only considered the performance of construction material from elastic to plastic phase, while the progressive collapse of a building more concerns the structure or members in the whole process from plastic to destruction [19].

From the progressive collapse of the Ronan Point apartment tower in 1968, the research on progressive collapse went through three stages. The key point of research transferred from structure system to process simulation and collapse mechanism step by step. Last decade, many people were enthusiastic about studying progressive collapse through the experimental approach, including both components experimentation and frames experimentation. This subject can be approach from two different perspectives: one for which an ideal collapse of the structure is aimed to be achieved and corresponds to the controlled demolition of a building and another which treats the mitigation of the potential of progressive collapse of structures.

Yi et al. [20] did a static experiment to investigate progressive failure of a RC frame structure. This frame experiment influenced the research developed in LEM3 and 3SR laboratory [21], [22]. A test model as following (see Figure 2. 2 (a)) was tested. It was a four-bay and three story one-third scale model representing a segment of a larger planar frame structure. A constant vertical load of 109 kN was applied on the top of the middle column by a servo-hydraulic actuator. Initially, the load applied by the servo-hydraulic actuator was transmitted to the lower jack through the middle column. Then the step-by-step unloading process was initiated by moving down the mechanical lower jack. In the paper, the authors have thought that failure resulting from progressive collapse of the RC concrete frame structure was ultimately controlled by the rupture of the reinforcing steel bars in the floor beams (step D). This is different from the normal limit state for beam bending, which is controlled either by crushing

of concrete in compression or shear failure. As shown in Figure 2. 2 (b), the process of collapse can be divided into five stages: elastic stage, elastoplastic stage, plastic stage, catenary stage and rebar failure. One can note that the resistance gradually increased after plastic stage. On the curve of load-displacement any softening behavior due to the concrete crushing or tension cracks does appear. It indicates that longitudinal bars have an important effect on the bearing capacity during catenary stage. Figure 2. 2 (c) shows the horizontal displacement of the first-floor frame column. It illustrates that the motion of adjacent joints to the middle column also plays an influence in the bearing capacity.

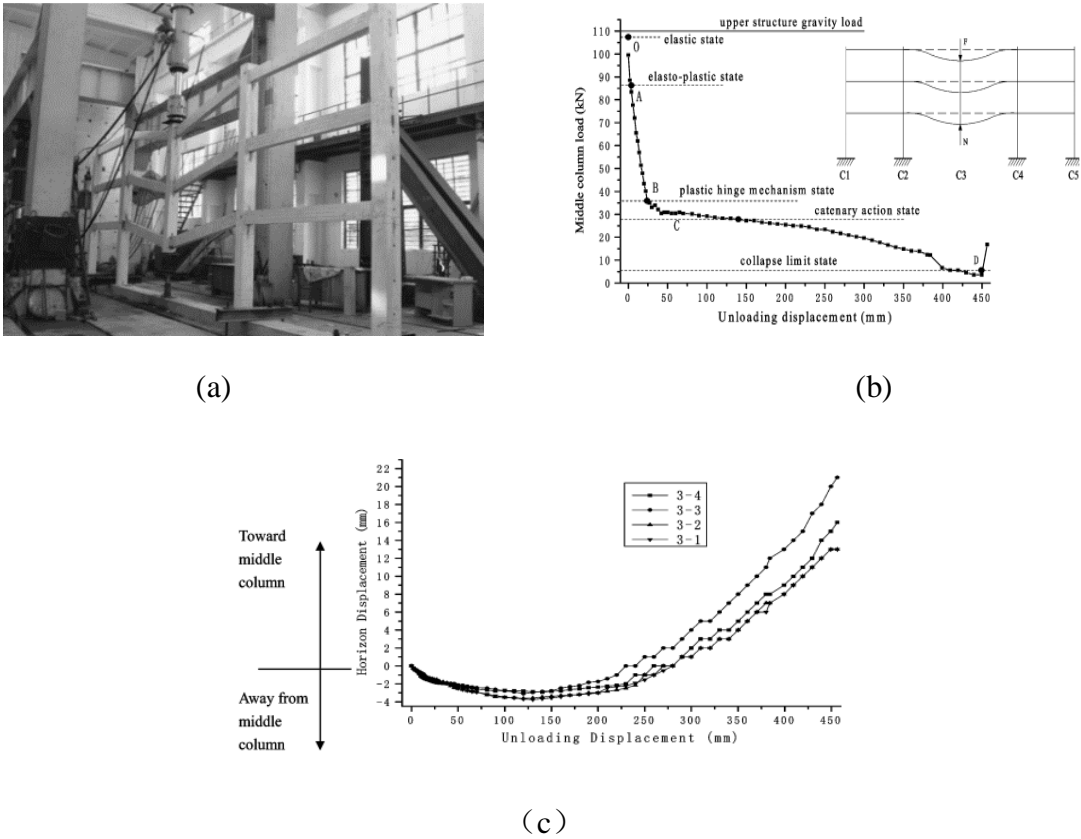


Figure 2. 2 (a) Collapse limit state of model frame; (b) middle column load versus unloading displacement of failed middle column; (c) effect of downward displacement of middle column on horizontal displacement of columns at first floor.( Yi et al 2008 )

The same year, Sasani and Sagioglu [18] reported experimental and analytical data from the testing of a building located in San Diego, California. They studied the progressive collapse potential of Hotel San Diego. The Hotel San Diego building was instrumented with similar strain gauges to measure the strain while two of the exterior columns were removed (see Figure 2. 3). A valuable insight on how a structure would respond when faced with abnormal

conditions. In this paper, authors also discussed the applicability of GSA (2003) but did not calculate some indexes such as DCR to evaluate each member. The following year, Sezen and Song [23] investigated the progressive collapse performance of an actual steel frame building. The Ohio State Union building was tested by physically removing four of first story columns from one of the long perimeter frames prior to building's scheduled demolition (see Figure 2. 4). They followed the GSA (2003) guidelines and calculated the DCR values when four exterior columns were removed from the structure. Their research compared the predicted and calculated building static responses using the GSA (2003) as a guideline. The results shows that the GAS elastic static analysis method is more conservative.

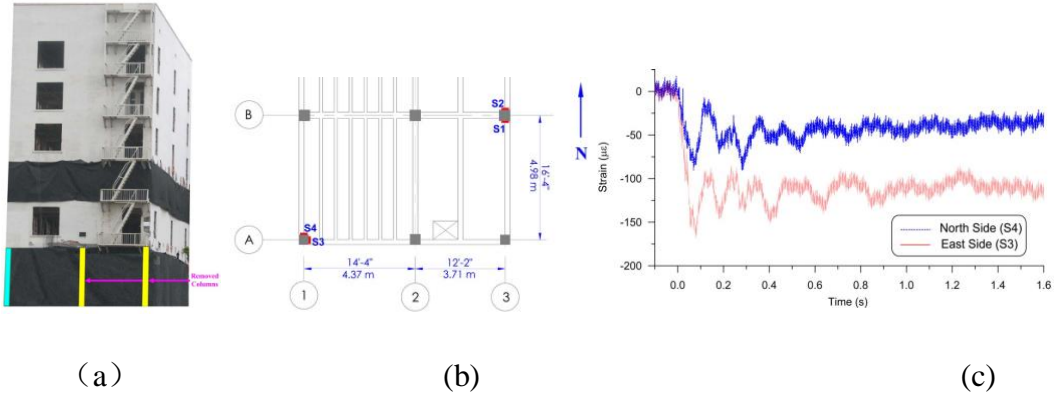


Figure 2. 3(a) South-east view of evaluated building; (b) Locations of strain gauges on first floor columns; (c) Strain gauge histories installed on first floor Column A1. (Sasani and Sagioglu, 2008)



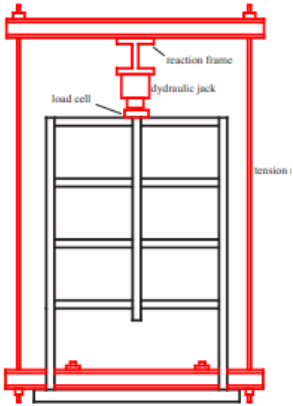
Figure 2. 4 The circled columns on North Side of the Building were Removed During the Experiment (Sezen and Song, 2009)

He et al [24] performed an 1:3 scaled concrete reinforcement (RC) frame model to investigate the response of building under the middle column sudden removal, followed by a static collapse test under controlled displacement. The experimental model is shown on Figure 2. 5 (a) and the

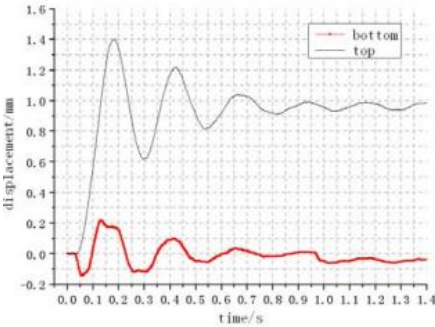
static collapse test setup on Figure 2. 5 (b). After explosion the bottom column is removed, the vertical or horizontal displacements are only up to several millimeters as show on Figure 2. 5 (c). The whole frame remains in an elastic state. Then, the displacement load was applied at a speed of 10mm/s to the residual frame. This research shows that the catenary action in the frame can transmit a part of gravity load, however, because of the limited lateral stiffness of side columns in the frame, the capacity of the frame could not be markedly raised by catenary action. What a pity is this research did not apply any dynamic load to the residual frame in order to observer the dynamic behavior of the frame. A large number of data should be also dug further.



(a)



(b)



(c)

Figure 2. 5 (a) Model of frame; (b) static collapse test setup; (c) frame horizontal displacement (He, 2009)

**2.2.2 Beam-column sub-assemblages experiment**

Besides frame test, considering the economy and feasibility, a great number of component tests were conducted by many researchers to investigate the performance of RC structures in progressive collapse.

Sasani and Kropelnicki [25] performed an experiment with a 3/8 scaled perimeter beam component model to evaluate the behavior of the beam following the loss of the supporting column. The beam-column model was constructed with fixed boundary conditions. The displacement was applied at the middle column at a rate of 5.08cm/s. The relationships between the vertical force and the displacement of the beam center point obtained is shown in the Figure 2. 6. The bottom bars were broken at the first peak in the curve. Following the bars failure, catenary action provided by the top reinforcement leads in an increasing resistance of the beam.

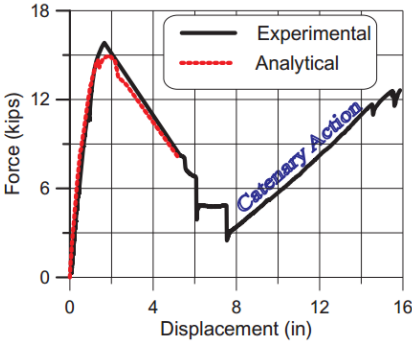
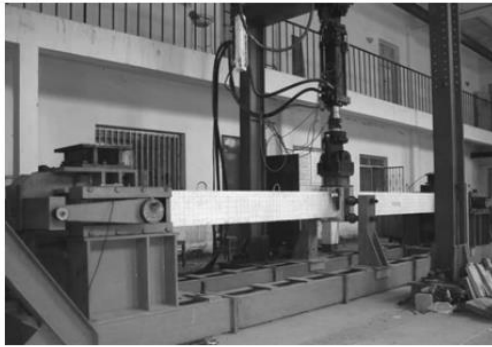
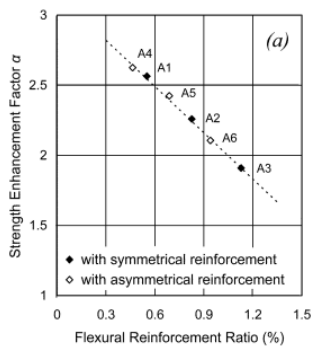


Figure 2. 6 Force-displacement relationships (Sasani and Kropelnicki, 2008)

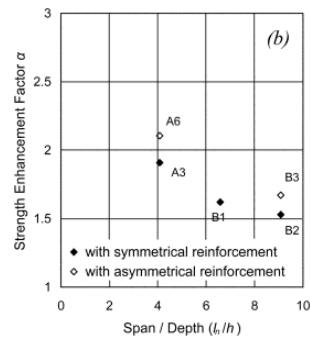
In the same year, Su et al. [26] tested twelve specimens in order to study the effect of axially-restrained boundary conditions on progressive collapse resistance. These specimens were designed with different sections and spans. Each specimen represented a two-bay beam resulting from the removal of a supporting column. The results show that the compressive arch action due to longitudinal restraint can significantly enhance the flexural strength of a beam subjected to vertical loads. In the Figure 2. 7 (b), the strength enhancement factor was observed to decrease in an approximately linear pattern from 2.63 to 1.91 as the reinforcement ratio increased from 0.46 to 1.13%. Figure 2. 7 (c) indicates that the strength enhancement factor  $\alpha$  that measures the beneficial compressive arch effect on beam gravity load capacity decreases as the  $l_n/h$  increases.



(a)



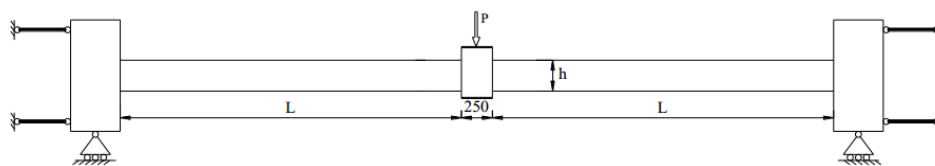
(b)



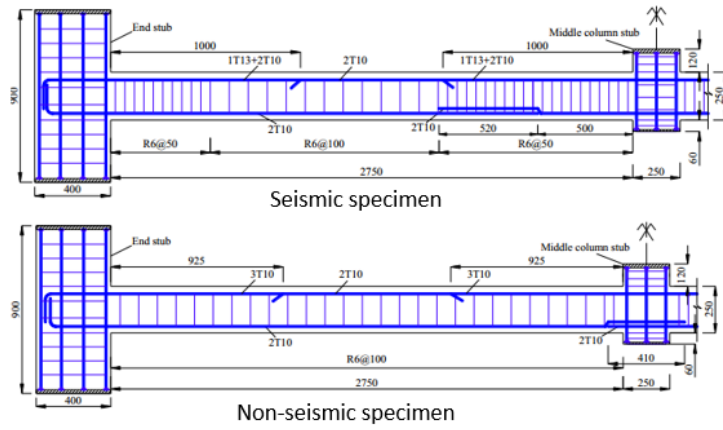
(c)

Figure 2. 7 (a) Test setup; (b) effect of flexural reinforcement ratio; (b) effect of ratio of beam span to depth. (Su et al. 2008)

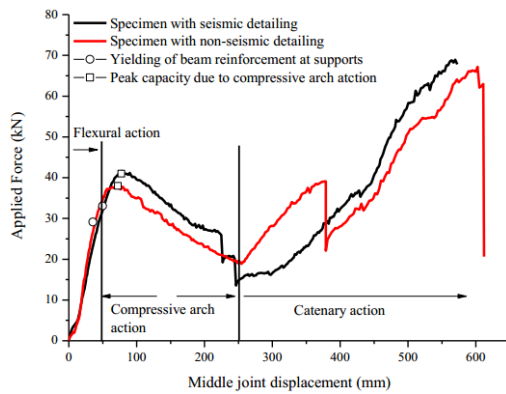
In 2010, Yu and Tan [27] studied the resistance property of RC beam-column sub-assemblages by experimental approaches with either seismic or non-seismic design. One-half scaled specimens were designed and tested under a middle column removal scenario. Each end of specimens was restrained by two rods and pin on rollers as show on Figure 2. 8 (a). Test data on Figure 2. 8 (b) indicate that there is no obvious difference in structural performance due to different design rules. The paper also point out that the conventional plastic hinge mechanism can be used to compute the capacity of flexural action and Park's model can be modified for calculating the capacity of compressive arch action with an acceptable accuracy.



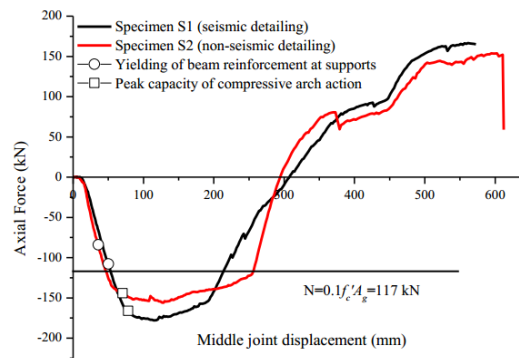
(a)



(b)



(c)

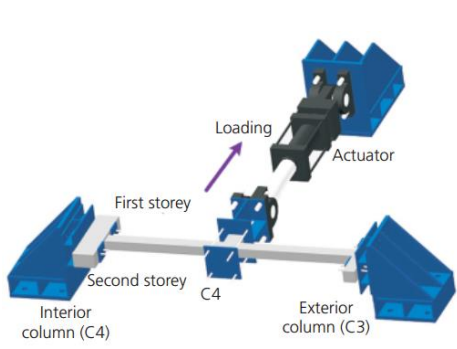


(d)

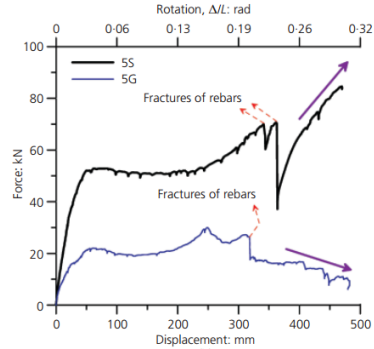
Figure 2. 8 (a) The specimen and the boundary conditions;(b) The detailing of the beam-column specimen; (c) The relationship between the applied force and the middle joint displacement; (d) The relationship between the horizontal reaction force and the middle joint displacement. (Yu and Tan, 2010)

H. Choi and J. Kim [28] carried out experiments to investigate the progressive collapse-resisting capacity of RC beam-column sub-assemblages built with and without seismic design. The right and left hand columns were fixed to the jigs and the actuator was connected to the middle column. Contrary to above mentioned tests, a monotonically increasing load was applied at the middle column of the specimens in the horizontal direction rather than in vertical direction as show on Figure 2. 9 (a). Force–displacement relationships are plotted in the Figure 2. 9 (b). It was observed that the non-seismically designed specimen failed by crushing of concrete at the exterior column–girder joint of the left-hand girder before catenary action was activated. While, the force–displacement relationship of the specimen designed for seismic load continues to increase after fracture of the girder lower rebars near the middle column due to the catenary

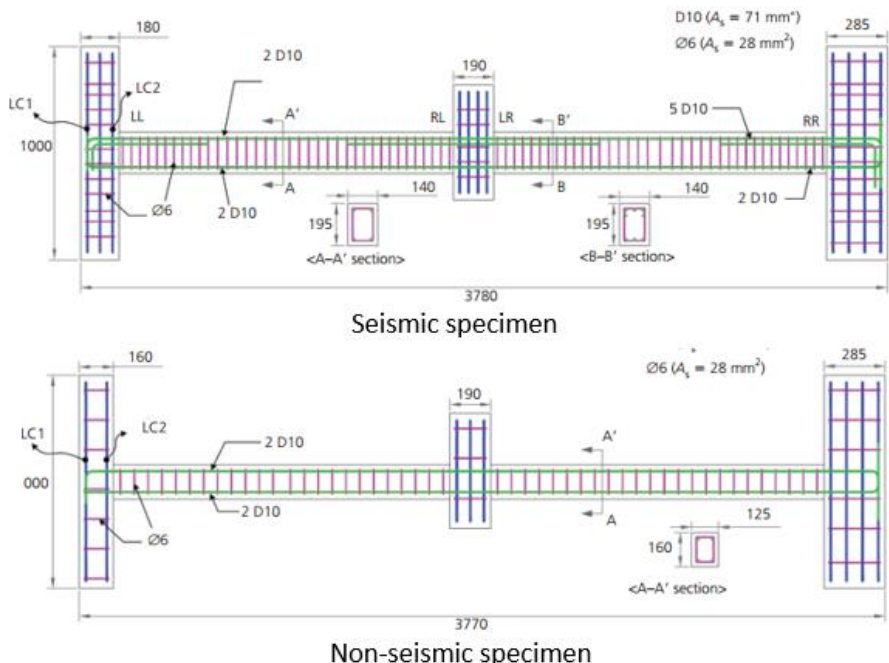
force of upper rebars. The authors thought that significant catenary action of girders could be induced in reinforced concrete moment-resisting buildings seismic design codes against progressive collapse initiated by sudden loss of a column. As previously above mentioned, on the contrary, with the same reinforcement bar, the results from Jun Yu and Kang-Hai Tan's test [29] show there was no obvious difference in structural performance due to seismic design. Hence, other parameters may have an influence in activating catenary action and this needs to be studied further.



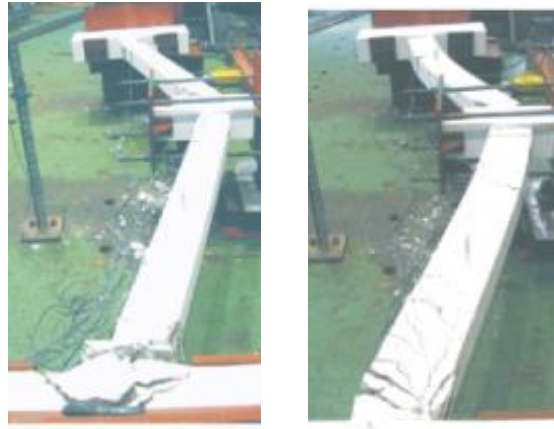
(a)



(b)



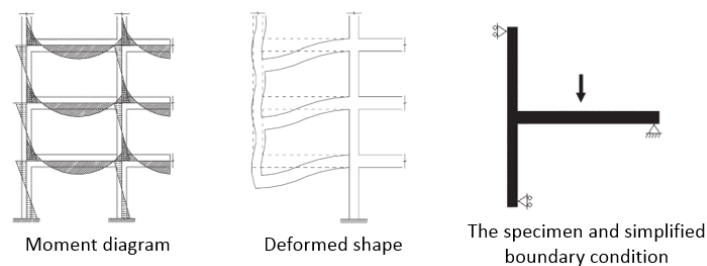
(c)



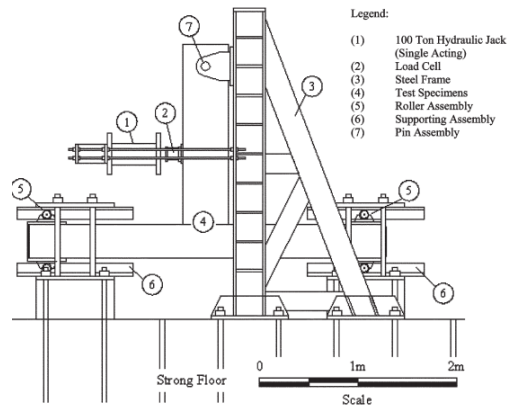
(d)

Figure 2. 9 (a) Test set-up for the beam-column; (b) Load-displacement relationships; (c) Reinforcement detailing of the specimen ;(d) Damage mode of the specimen (H.Choi, J.Kim 2011) 5S: 5 storey, seismic-load resisting; 5G: 5 storey, gravity-load resisting

In 2011, Yap and Li [30] conducted experiments to investigate the performance of reinforced concrete exterior beam-column sub-assemblages in progressive collapse. In order to ensure loading and boundary conditions closed to actual scenario, the specimens were designed by the bending moment diagram and deformed shape of the assumed structural frame as shown in the Figure 2. 10 (a). The test results indicate the increase in the percentage of transverse reinforcement in the joint region improved the shear strength of the joint through the development of the truss mechanism. A bond failure was observed in the beam bars in specimens without improved design. If the adjacent components cannot carry the increase in load, it may result in a collapse.



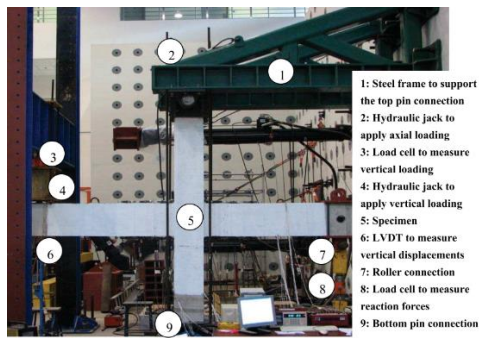
(a)



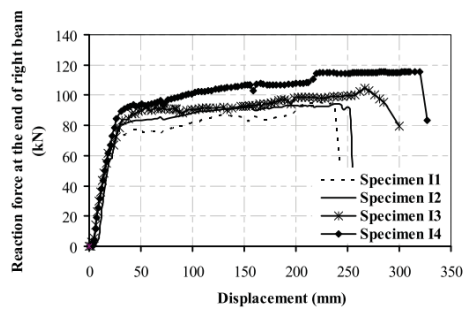
(b)

Figure 2. 10 (a) Illustration of moment redistribution and deformed shape; (b) the test set-up. (Yap and Li, 2011)

After one year, Qian and Li [31] carried out similar test to study the performance of interior beam-column sub-assemblages. Four full-scale interior beam-column sub-assemblages with varying degrees of non-seismic detailing were designed. A monotonic load was applied statically to the side of left beam to simulate the effects of redistributed gravity loads on the sub-assemblages after the loss of a support. The specimen and test set-up is shown on the Figure 2. 11. Compared to previous frame testing, this kind of beam-column structure can provide better results and more realistic response. However, fixing each side of the specimen is more difficult and complex, particularly the fixing of the top of the column.



(a)



(b)

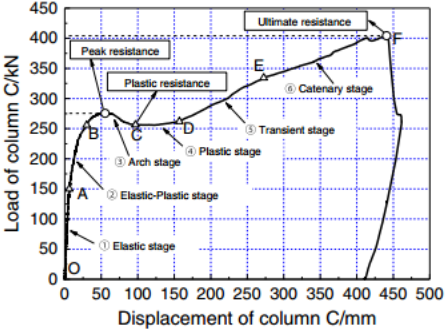
Figure 2. 11 (a) Overview of a specimen prior testing; (b) Reaction force versus vertical displacement responses (Qian and Li, 2012)

Lanhui Guo et. al [32] studied the progressive collapse resistance of steel-concrete composite frames. A 1-storey composite frame with 4-bay was designed and fabricated in one-third scale.

Steel beam were fully welded to the flanges of Steel column to make rigid connections as shown in the Figure 2. 12 (a). Compared with steel joints and reinforcement concrete joints, rigid composite joints consisting in steel beams and reinforced concrete slabs exhibit a higher load-carrying capacity and a better deformation ability [33]–[35]. Actually, this test demonstrated the effect of reinforced concrete slab on the progressive collapse resistance. The results further illustrate that the tie force or the joint connection may have a significant influence in the response of the frame and progressive collapse resistance after concrete splitting and damage.



(a)



(b)

Figure 2. 12 (a) experimental set-up; (b) Vertical load versus displacement of the middle column (Lanhui Guo et. al, 2013)

Forquin and Chen [21] carried out a set of quasi-static tests to evaluate the risk of progressive collapse of beam-column reinforced concrete structures under a column removal scenario. The study considered the effect of the reinforcement ratio on the fracturing and bearing capacity of the structures. The crack propagation of the concrete is analyzed through a Digital Image Correlation technique (see the Figure 2. 13). The results show the progressive collapse behavior of the beam-column structure is driven by the resistance of longitudinal reinforcement steel bars used in the beam. In addition, this paper also proposed a simplified analytical method to predict the structural resistance of such structures. The analytical solution is in good agreement with the experimental data.

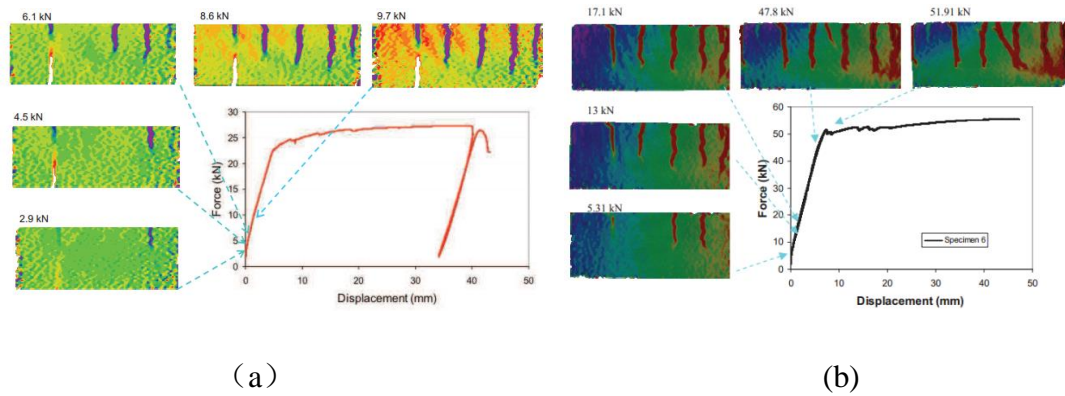


Figure 2. 13 Pictures of RC structures after the experiments. Macro-cracks are visible near the middle joint. (a) Rebar  $\text{Ø}8$   $h=180\text{mm}$ ; (b) Rebar  $\text{Ø}12$   $h=180\text{mm}$  (P. Forquin and W. Chen, 2014)

All the tests previously mentioned are static tests, whatever the load is controlled by displacement or force. Very few dynamic tests can be found in the literatures. Although these studies prove that static experiments are a valid technique to reproduce progressive collapse due to supporting element failure, in the same time, these research indicate that dynamic experiments are necessary and more realistic.

Chang Liu et. al. [36] conducted both dynamic and static tests to investigate the behavior of web cleat connection subjected to sudden column removal scenario. Test results showed that the maximum displacement of the web cleat connection under dynamic load is significantly increased compared with the one under static loading condition. The dynamic loading capacity of the web cleat connection is much lower (about 2.8 times) than the capacity under static load. Concerning reinforced concrete structure, Yu et.al.[37] carried out a more realistic dynamic test by a combination of dead weight loading and a contact detonation. The specimen was a typical beam-column assemblages consisting in two single-bay beams, two end-column stubs and one middle column. Each end-column stub of the sub-assembly was seated onto a steel roller and anchored onto a heavy concrete ring with four horizontal bolts. The specimen and test equipment is shown in the Figure 2. 14 (a). The dead load contributed by two concrete blocks and a steel transfer frame was applied to the top of middle column as shown in Figure 2. 14 (b). An explosive charge was placed between the bottom of the middle column and bricks. After the charge was burst (Figure 2. 14 (c)), the bricks and the bottom end of the middle column were explosively removed. So the upper dead load was redistributed suddenly to the beam-column

subassembly. Eventually, the test was stopped when the two concrete blocks and the middle column touched the ground as shown in Figure 2. 14 (d). The dynamic results are represented systematically at different stages and compared with previous published quasi-static experiments in terms of structural mechanisms, crack patterns and local failure modes. Moreover, the dynamic increase factor (DIF) of reinforcing bars and the dynamic load amplification factor (DLAF) are investigated and discussed. Following the above comparisons and the findings of the dynamic tests, previous quasi-static test results can be linked to actual progressive collapse behavior more convincingly. Finally, the dynamic tests also highlight the effect of contact detonation on structures, which are often not considered in quasi-static tests and design guidelines. The test results indicated that contact detonation causes uplift and out-of-plane actions to the sub-assembly before their downward movement under gravity load, in which the strain rate of reinforcement is in between  $10^{-2}/s$  and  $10^{-1}/s$ . Moreover, the structural mechanisms are similar in both quasi-static and dynamic tests.

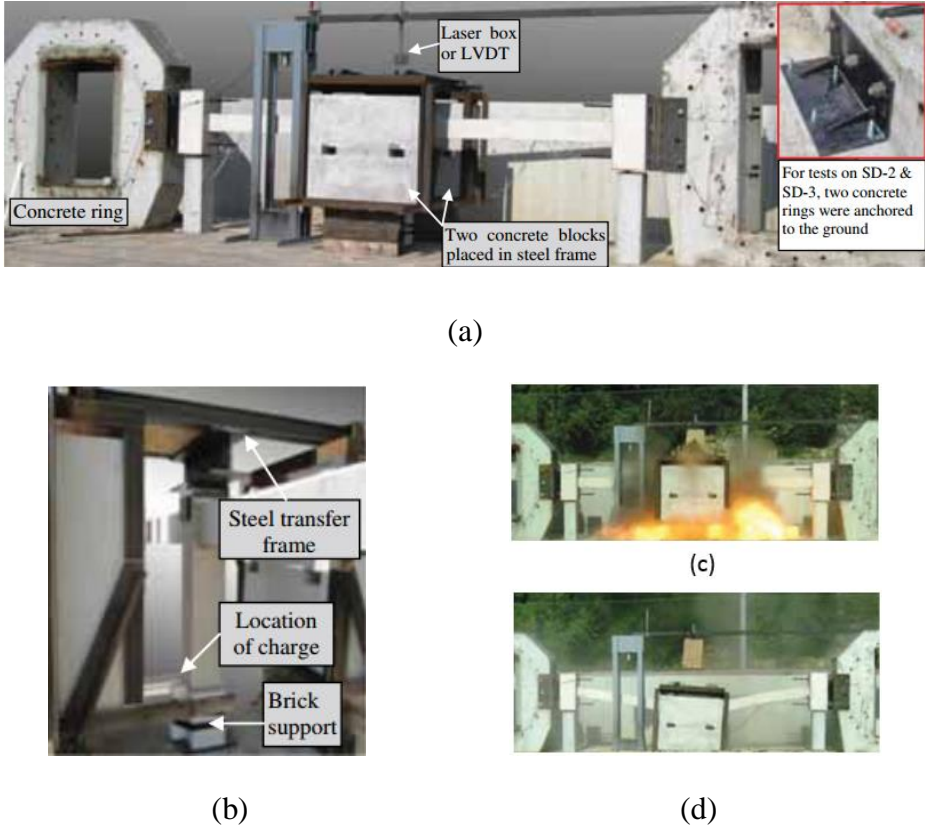


Figure 2. 14 (a) overview of test setup; (b) configuration of middle column; (c) testing procedure at 30ms; (d) at the end of the test. (Jun Yu et al., 2013)

After this literature review, a brief summary can be done:

About the scaling of specimen: few researchers used full-scale specimen in their experiments due to limited space and capacity conditions. Generally, the scale of specimen is about 1/3 to 1/2. For the section of beams, the width of the beam is about 100mm to 150mm and the height is about 160 to 250mm. In these experiments, we cannot know precisely the gap between full-scale experiments and reduce scale experiments. However, based on the experiments previously shown, we can deduce that the mechanical behavior of full-scale components may be distinct from reduce scale components [38]. In addition, it is obvious that there is a close relationship between the height of beam, the ratio between the span and the height of beam ( $l/h$ ) and the vertical displacement of the middle column. When the vertical displacement equals the height of beam, the damage is related to compressive arch action. When the vertical displacement exceeds the beam height, the catenary action may start acting if fixing supports are considered. When the displacement reaches about twice the height of beam, the beam-column joint totally fail [39]–[41].

About concrete strength: It is known that concrete strength is playing an important role on the bond resistance at concrete steel bars interfaces. Choi [28] presented a specifically designed specimen with low-strength concrete such that it failed by joint failure before catenary action was activated. So there is a straightforward effect on activating catenary action.

About reinforcement: In the cited experiments, there was several deduction about the effect of reinforcements [42]:

- (a) Increasing the longitudinal steel bars cross section area at the top of the beam enhances tensile resistance of the structure.
- (b) Adding stirrups and decreasing the space between stirrups enhances shear failure resistance of the structure.
- (c) The effect on the resistance of the specimens of the seismic design in accordance to the code such as ACI.

The presented experimental data show that the maximum vertical displacement of the middle column does not decrease with an increasing ratio of longitudinal reinforcement but it is controlled by the height of the beam. Both methods of adding stirrups and doing a seismic

design can only enhance the shear resistance of the component but are not very effective in improving catenary action. Besides, we can observe that anchoring the joint have an important effect on the failure mode according to experiment of Choi and Kim [28]. In their test, the damage area appears on the beam rather than in the beam-column joint as long as catenary action occurred (see Figure 2. 9 (c)).

About boundary conditions: According to the open literature, most of experimental works deal with boundary condition simply by fixing both sides of columns [28][29][31][32][43]. On the contrary, Forquin and Chen [21] tested 1-column 2 bay beam and 3-column 2 bay beam RC sub-assembly with sliding pin connections and fixed pin connections to study the failure process of the beam under lost a middle support. In the experiment of Yi et al. [20], done on an entire RC frame, there is a horizontal displacement at the top of adjacent columns when the middle joint has a vertical displacement after removing the middle column. As it can be seen from others test, if we just set a fixed boundary condition, we may not obtain realistic results such as bearing capacity and maximum displacement of the middle joint. Indeed, bearing capacity if there is enough concrete strength may also be increased during catenary action if exterior columns are fixed, as they support much larger tension force. On the contrary, if without fixing the exterior columns, the top of adjacent columns will move the middle column so that the vertical displacement of the middle joint will be larger than other experimental results and give a smaller bearing capacity. The problem on how to set representative boundary conditions is one of the keys to make a successful experiment.

About damage mode: the presented experiments show the process and the location of damage and collapse from the start of loading to the total failure. It can be divided into elastic, elastoplastic, plastic, catenary action or, flexural action, compressive arch action, catenary action, as shown in Figure 2. 15. Based on these experiments, the total failure in most of the structures is due to the fracture of the top and bottom steel rebars under catenary action [44].

By comparing experiments of Yi et al. [20], we observe that there is no sharp decrease and rise of force in the force-displacement diagram. Others experiments have an obvious leap in the

force-displacement diagram due to the failure of steel rebars [27] [43]. They have different views about the start of catenary action. Some thought it is catenary action after plastic stage; some thought it is catenary action after fracture of bottom steel bars and rise of the bearing capacity. Under dynamic condition, also no definite conclusion has been reached about catenary action.

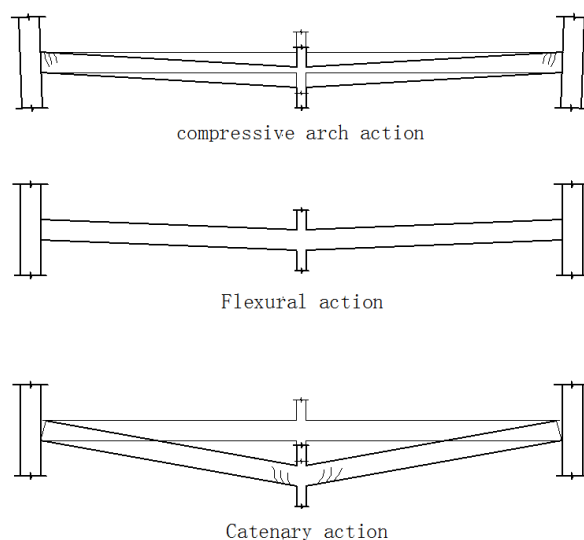


Figure 2. 15 Failure mode of beam-column assemblages

Table 2. 2 Size of specimens in different experiments

author	Year	Column specimen	beam(bxh) specimen	span(mm)
Ohno T, Nishioka T	1984	400x400		
wei-jian yi et al	2008	200x200	100x200	
H.Choi, J.Kim	2009	170x170	150x225	
Youpo Su, et al.	2009		150x300	
Rania Al-Hammoud,	2009		152x254	2000
Mehrdad Sasani, et al	2010	305/170	190	2000
Jun Yu, Kang-Hai				
Tan	2011	250x250	150x250	2750
Forquin, Chen	2014		110x180	900
Forquin, Chen	2014		110x240	900

### 2.3 Numerical simulation analysis

Due to the complexity of the progressive collapse process, the experimental studies have always a number of limitations. As an indispensable approach to study collapse procedure, more and more researches devote to develop numerical calculation method to analyze the mechanical

behavior of structure in progressive collapse, using nonlinear static or nonlinear dynamic approaches.

Typical numerical methods include finite element method and discrete element method. After decades of development, the finite element method itself has been developed in terms of algorithms and meshing grid technology. Various types of elements have been created or developed in order to solve more and more complex problems. A large number of researches [45]–[49] has been devoted to do research in this field. Iribarren [50] proposed a layered beam approach to build the finite element model, followed by the time integration scheme used for the dynamic computation. To simulate dynamic progressive collapse, nonlinear behavior of concrete and steel, material parameters and strain rate effect were considered. However, this simulation work is two-dimensional. The proposed simplified approach might thus lead to conservative results and torsional effects of component are not considered in a 2D formulation.

Bao et al. [51] proposed a simplified simulation model of a beam-column joint to represent essential and critical actions in the floor beams and the transfer of these forces through the joint region to the vertical elements. Two-dimensional models of the frames were subjected to gravity loads and then one or more first-story columns were removed, and the resulting large displacement inelastic dynamic response of each frame was investigated. It was demonstrated that the proposed approach using a validated macro-model was a viable methodology for progressive collapse analysis. The study also found that special RC moment frames detailed and designed in zones of high seismicity perform better and are less vulnerable to progressive collapse than RC frame structures designed for low moderate seismic risk.

Li and Hao [52] presented a new numerical approach that incorporates static condensation into the finite element model to simulate blast load, induced structural response and progressive collapse. Khalid M. et al. [53] presented an analytical formulation of an element removal algorithm, which is based on dynamic equilibrium and the resulting transient change in system kinematics. It was used to calculate a RC 3-bay, 3-story frame test on a shaking table. The computations predicted collapse modes compared to the experimental results revealed the

validity of the developed computational approach. Lu et al. [54] simulated the progressive collapse of the simple RC frames and RC frame-shear wall structures due to earthquake with the fiber-beam-element model and multi-layer-shell-element model. The extreme nonlinear behavior of RC structural was properly simulated by the model including the cycle behavior under coupled axial force-bending moment-shear force.

Some researchers simulated the collapse of frames or substructures by different commercial finite element softwares. Sasani [55] studied the response of a six-story reinforced concrete infilled-frame structure after the removal of two adjacent exterior columns. He used two types of elements to build the model for the infill in the SAP2000 computer program. One is two dimensional shell element and the other is compressive struts. The results show that the infill walls are able to provide the beams with constrains and supports that can help to carry additional loads. The results from the model with shell elements are in good agreement with experimental results. For small deflection, struts do not realistically model beam and column constraints, overestimating vertical displacement. The same year, Sasani [43] reproduced the beam-column assemblages experiment under loss of a middle support by the computer program DIANA. However, the response of the structure beyond bar fracture requires significant and sudden redistribution of stresses and strains which is not carried out in this study. In a following study, the same authors [56] used the computer program OpenSEES to build a model for the whole building with Euler-Bernoulli beam-column elements that are considered to be effective in avoiding a detailed FEM of the whole building and capturing the system response. The results show that even the removal of two adjacent columns from an exterior frame will not result in a collapse of the structure that satisfies the integrity requirements of ACI-318. In addition, the results demonstrated the DCR method can be overly conservative.

Mohamed [57] considered a case study for the progressive collapse analysis of a reinforced concrete building using the Alternate Path method according to the DoD guidelines. The numerical studies based on the linear static analysis show the importance of incorporating 3-dimensional effects, especially in the part of the structure where a column is removed. Shi [58][59] proposed a method that uses P-I (pressure-impulse) diagram to estimate the damage to

structural members by the direct blast load, in which x-axis is the impulse for damage degree and y-axis is the pressure for damage degree (see the Figure 2. 16). The equivalent SDOF approach is used to estimate the velocity and displacement of structure members at the end of the blast-loading phase. The damage on adjacent structural members that might be induced by blast loads and the inevitable non-zero initial conditions when progressive collapse initiates are neglected. It is a big benefit that both non-zero initial conditions and the initial damage of adjacent structural members are considered in this analysis. The authors pointed both the GSA and DoD methods may not give reliable prediction of structural progressive collapse and usually underestimate the stress and strain response.

Kwasniewski [60] carried out progressive collapse dynamic nonlinear analysis for a 8-story steel framed structure by the commercial program LS-DYNA with explicit time integration. The applied solution method allows for taking advantage of parallel processing on multiprocessor computers and makes the computation feasible. However, this approach still requires large computational resources due to the large-scale global model. For the large finite element model, the parallel calculation on 60 processors took 19 days. As a nonlinear dynamic analysis tool, AUTDYN is accurate and a useful tool for progressive collapse assessment of a multi-story building subjected to blast load, but it may take a lot of time to be applied to a progressive collapse simulation of a tall building. How to reduce time cost remains a problem to be solved.

Kim et al. [61] studied on reinforced concrete frame structures using a simplified model with reinforcement Contact technique provided in ANSYS Workbench. With this type of interaction, line body reinforcements are included in solid volumes without sharing any node between volumes elements and beam elements. It is easier to make any kind of shape and size of solid element unit with this method. 1-bay frame model was used to validate the method, including 4m high columns and 6m span beams as shown on Figure 2. 17. The distance between the frame and the explosive was 5m apart and the amount of TNT was 100kg. The study showed the reinforcement contact model graph is close from the detailed model. Reinforcement Contact function is worth to be used in analyses of very large structures. This paper also pointed out

that the resistance performance against the progressive collapse can be improved by reinforced the girders around columns.

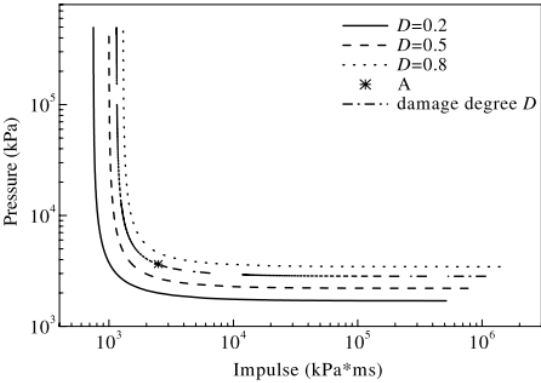


Figure 2. 16 P-I curves for different damage degrees D (Shi et al., 2010)

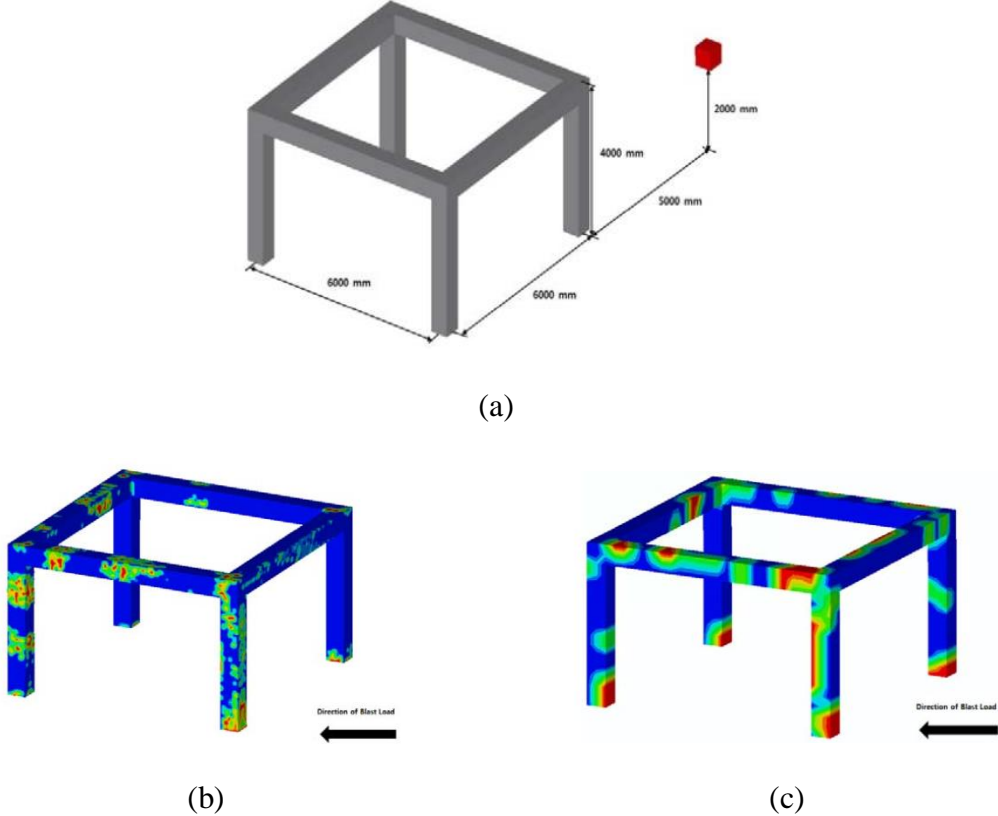


Figure 2. 17 (a) Single story reinforced concrete frame model for blast analysis; (b) Damage contour of the detailed model; (c) Damage contour of the simplified model (Kim et al., 2013)

Apart from finite element method, studies on the progressive collapse behavior of reinforced concrete structure using discrete element method can also be found in recent literatures. Masoero et al.[62] proposed an alternative approach using Discrete Element Method to study the response of 3D framed structures after the removal of one column. The collapse process for

different values of geometrical parameter  $\alpha$  (larger  $\alpha$  enlarges element cross sections, leading to stiffer and stronger structures) was reported in the Figure 2. 18. The study demonstrated that Discrete Element Method can capture the mechanical response as well as the inter-particle contacts. Besides, it also has other advantages such algorithms, computing speed, dealing with mechanical nonlinearities problems. However, difficulties exist in the aspect of simulation of vertical wall and short plasticity model of material. A combined finite-discrete element model for failure and collapse of structural systems is presented in [63]. The paper presents the development of a two-nodes finite element with numerical integration, allowing the capture of the non-linear behavior of both concrete and reinforcements. The numerical results are used to simulate a reinforced concrete beams subjected to a four-point bending test.

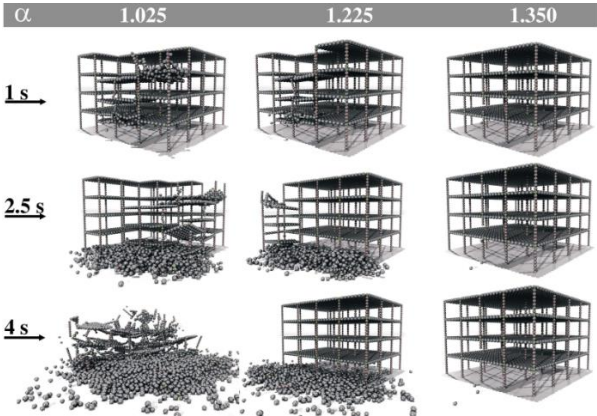


Figure 2. 18 Collapse evolution for structures with increasing  $\alpha$  (Masoero et al. 2010)

A review of these published literatures on numerical studies of progressive collapse behavior shows some clear tendencies. Many commercial codes such as SAP2000, LS-DYNA, ANSYS, OpenSEES, ABAQUS and so on were used by researchers and engineers. The constitutive models of concrete come with the commercial software were often chosen. Most of them generally can be employed in static or earthquake load or other cyclic load, such as concrete smeared cracking model, Johnson-cook model and Drucker-Prager model. Concerning the suitability of the model for the impact load, it still require to be discussed and validated by a great number of calculation cases.

Beam and solid element models dominate, and most of the considerations are confined to 2D frame or 3D substructures. Numerous simplifications applied in the models are justified by the

required limitation of the computational time and resources. In more than half of the mentioned works, a multilevel strategy is applied, where the structure is analyzed first on the subsystem or component level before global analysis is performed on a simplified global model. So far, no perfect tool exists to simulate or predict progressive collapse behavior of concrete buildings with acceptable precision and reliability.

## **2.4 Study of interaction properties between rebars and concrete**

As it was explained previously, large rotation of beam section may occur during progressive collapse, resulting in a catenary action, which means that the reinforcement bars play a major role. Some literatures [64]–[67] also provided evidence to show the important role of concrete-steel bar interface in the response of reinforced concrete structure, especially in their dynamic response. Hence, it is necessary to have better knowledge about the behavior interface between concrete and steel.

Considering all above information to understand well the bond behavior of beam column at the interface with applying a group of spring connectors, a simple case to start with, is the fundamental technique of the pull out test. K. Ahmad et al. [68] carried out an experimental investigation on twisted steel bars in high strength concrete using displacement controlled universal testing machine. It was concluded that by increasing the cover/bar diameter ratio, bond strength increased and slip decreased.

W. Yeih et al. [69] investigated the interface properties by conducting a single rebar pullout test. It was shown that if the confinement of the concrete is strong enough to prevent splitting failure, the dominant failure mode will be a shear pull out failure. The typical load-displacement curve of concrete with and without confinement is shown in Figure 2. 19 and it appears that the confinement effect results in a more ductile mechanical behavior.

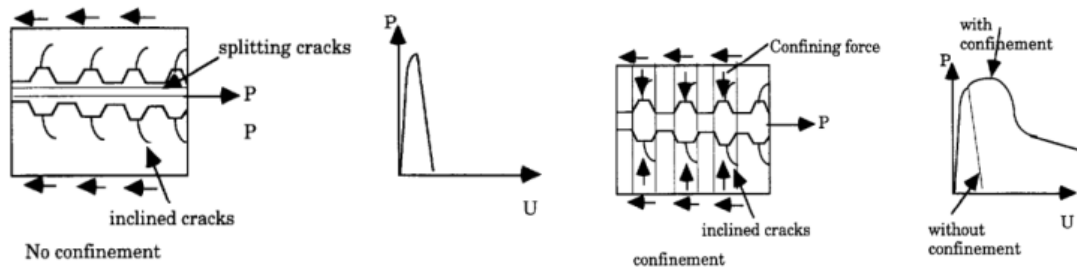


Figure 2. 19 Pull out test: Failure types for concrete specimen with and without confinement (W.Yeih et al. 1997)

The bonding failure mode depends on several other parameters such embedded length, diameter of rebar or speed of loading which causes sliding of rebar from the concrete or break of steel when the steel reached its maximum strength. J. Humbert et al. [70] took into account the uncertainties on materials and on failure modes in the analysis of a pull-out test with variable anchorage length of 8 cm and 32 cm. Two failure modes were observed. In the first case of 8cm of embedding length (see Figure 2. 20 (a)), the steel was sliding out of the concrete. On the contrary, the 32 cm of embedding steel reached the maximal strength and broke (see Figure 2. 20 (b)). Meanwhile, a finite element model was also built from the pull out test, considering the concrete constitutive model based on an elastic law with damage (Mazars' model [71]) to illustrate the probabilistic analysis approach and to reproduce the experimental pull out test.

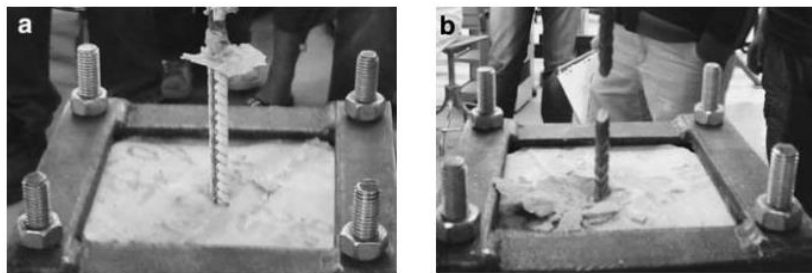


Figure 2. 20 (a) Bond failure at the steel concrete interface; (b) Steel bar failure (J. Humbert et al. 2009)

Tastani and Pantazopoulou [10] did series of tests to see the descending branch of the bond-slip response envelope. The results are depicted in Figure 2. 21, where index 0D refers to specimens without rings, whereas 2D40 and 4D40 refer to specimens with two or four rings, 40mm in diameter, placed along the embedded length of the steel bar. Specimens 0D and 2D40 demonstrated identical responses up to peak load, but different energy dissipation in the post-

peak branch; this implies that the corresponding rings were activated after a significant slip had occurred. Specimen 4D40 showed a 30% increase of bond strength and stiffness due to the improved and more uniform confinement provided by the four rings placed along the anchorage (see Figure 2. 22). As in first group of specimens, failure was marked by a splitting of the cover and slip of the test bar. With the addition of rings toughness increased marked by a reduce steepness of the cover at advanced stages of slip after separation of a concrete cone at the bar front and outwards movement of the upper rings.

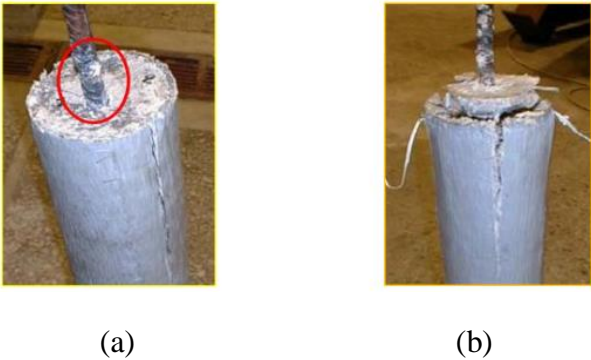


Figure 2. 21 (a) Mode failure of specimen without rings (0D); (b) Mode failure of specimen with rings (4D40) (Tastani and Pantazopoulou, 2002)

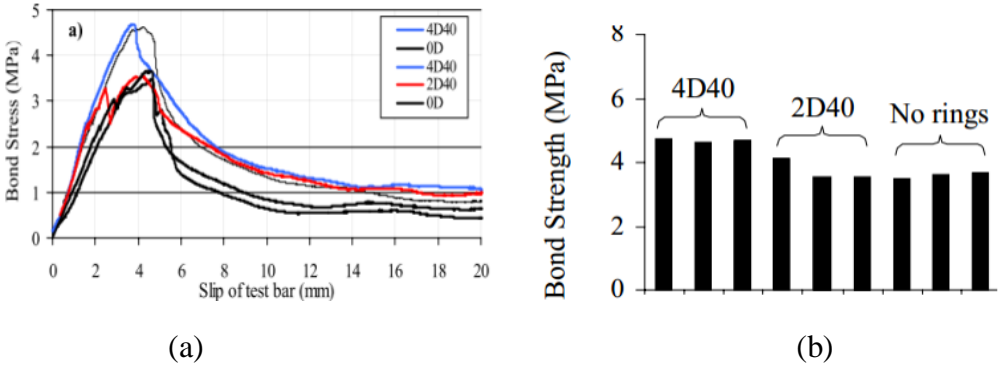


Figure 2. 22 (a) Slip curve of DTP-BT of steel bars with different arrangements of loose metal rings along the anchorage; (b) comparative values of bond strength obtained by two test setups (Tastani and Pantazopoulou, 2002)

The bond between steel and concrete is an important feature of the reinforced concrete. Anchorage of reinforcements depends on the bond between steel and concrete. Crack width and crack spacing are also mainly governed by it. Mahran [72] used special interface elements for the connection of reinforcement steel elements to concrete elements. These interface elements join steel elements and concrete elements together at the bar surface between lugs. Figure 2. 23 (a) shows the stresses distribution in radial and in longitudinal directions in the concrete cylinder.

These stresses indicate that the area of the highest compressive stress concentration is in the front of ribs. A more severe compressive stress concentration is observed at the rib nearest to the applied load. It gradually decreases inwards and the configuration of bond stress distribution along the embedded length reflects the mechanical behavior of bond between steel and concrete. There are several ways to identify and simulate the interface behavior by using special interface elements, defining very small size of mesh around the rebar at the interface or defining a group of spring for the bond behavior. It seem that the most efficient way to simulate the interface behavior and to well model damage at the interface is in applying a connector constitutive damage evolution law for the steel concrete interface and to identify the sliding phenomenon. Therefore, this constitutive law will be applied first for the pull out the test and then for a large calculation in RC beams column sub assemblage.

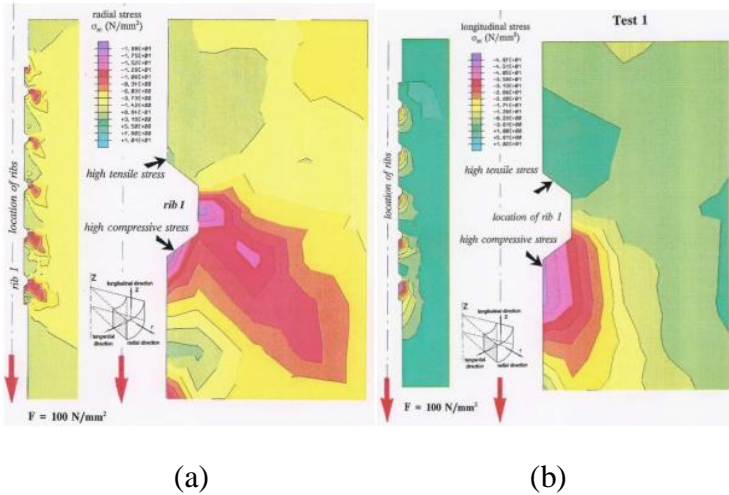


Figure 2. 23 (a) Radial stress; (b) Longitudinal stress (Mahran, 2008)

The whole process of collapse involves a series of complex phenomenon, including damage of concrete, large rotations and large deformation of members, interaction between steel bars and concrete and so on. Several publications covering the subject of progressive collapse under static or quasi-static loading exist in the scientific literature. However the collapse resistance of reinforced concrete structures subjected to complex quasi-static or dynamic loadings remains uncertain and the numerical simulation of the progressive collapse of a whole reinforced concrete beam-column sub-assemblage or structure remains often out or reach.

# **Chapter 3 Experimental and analytical evaluation of response of a RC beam-column sub-assemblages under a removal support**

## **3.1 Introduction**

When local damage of a structure may cause damage to a major part of the overall structure leading to a degree of damage that is disproportionate with the initial damage of the structure, the destruction mode is called progressive collapse. For example, a failure of a column in a frame may result in collapse of the entire frame structure. It emphasizes that the response of local structural elements is especially important. This type of collapse supplies a simple approach for us to study progressive collapse, which is to rely on a sub-structure model with suitable boundary conditions to study the resistance to progressive collapse. It is different from structural earthquake-resistant research. Seismic research generally focuses on the response of the entire structure, while a study on progressive collapse pays more attention to the relationship between the local to the global performance of the structure. Hence, using a local structural element, such as beam-slab or beam-column sub-assemblages, can be very useful in the research field and engineering. Most of research work based upon the GSA and DoD anti-collapse design guidelines carried out static or quasi-static experiments to evaluate the performance of structures in resistance collapse. Few dynamic experiments have been conducted to investigate the performance of the progressive collapse resistance of structures. As mentioned in previous chapter, GSA or DoD design guidelines recommend to use the linear elastic static anti-collapse analysis method despite of some disadvantages and limitations. It is currently recognized as a practical and standardized analysis method for anti-collapse thanks to its simplicity model and fast calculation. However, many researchers believe that it is possibly unsafe for the entire structure [39][40]. Effective analytical methods as well as technical measures against continuous collapse need to be validated with experiments. All kinds of collapse events and accidents can only provide actual information of structure concerning the macro damage form, it is difficult in these events to get details regarding the process of collapse. The details of structural collapse must be achieved with the help of certain test conditions.

Therefore, a good anti-collapse test of the structure can have great significance in the anti-collapse design, analysis and evaluation.

This research, the beam-column sub-assemblages being the research object, neglected the effect of abnormal load such as the impact load or the explosion on the remaining part. Dynamic testing was achieved by removing suddenly a middle support element after a dead load was applied to the structure. This test allows measuring not only the dynamic response of the structure but also a series of important dynamic constants such as the natural frequency and damping.

### **3.2 Specimen design**

In reinforced concrete frame structures, the main means to improve the structural resistance against progressive collapse is to increase the redundancy of structural members and then to improve the robustness of each members. Then, when the initial load transfer path is destroyed due to local failure, the load can be transmitted to other replacement paths. In a reinforced concrete frame structure, the main forced bearing element are the frame beams and frame columns. In practice, the external columns are very vulnerable to attack. Therefore, the effect of the slab on the resistance during the fall is not considered. A two span beam-column sub-assemblages was considered to study force-transferring mechanism and load alternation path under dynamic load.

A public building that is three-story four bay RC frame was used as the prototype of the study. The ground story is 4.0 m high and a typical story is 3 m high. The spans length is 6 m in the both transverse and longitudinal directions, as shown in Figure 3. 1. According to the GSA, removing supporting element should meet the requirement as shown in Figure 3. 2. The periphery middle beam-column system enveloped by red dash lines was picked up as test objective because it most easily suffer from impact and destruction.

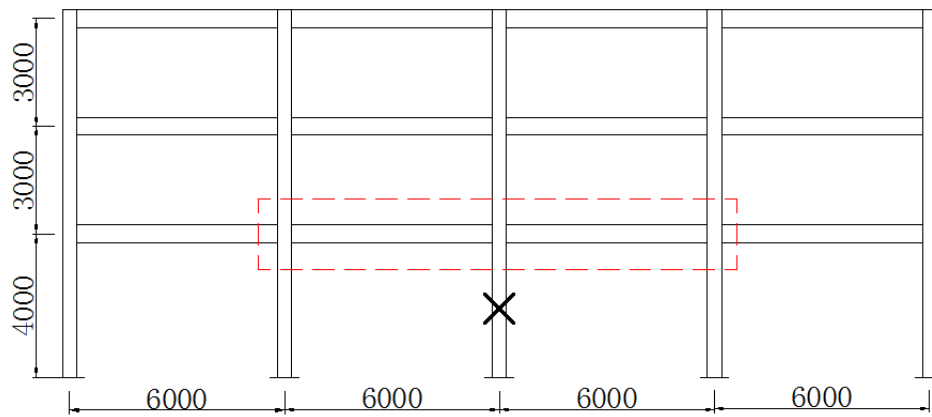


Figure 3. 1 The prototype building and local sub-assembly used for the test

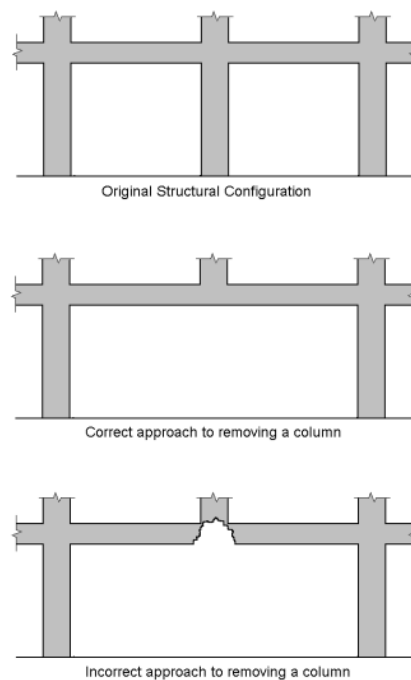


Figure 3. 2 Boundaries of removed elements based on GSA

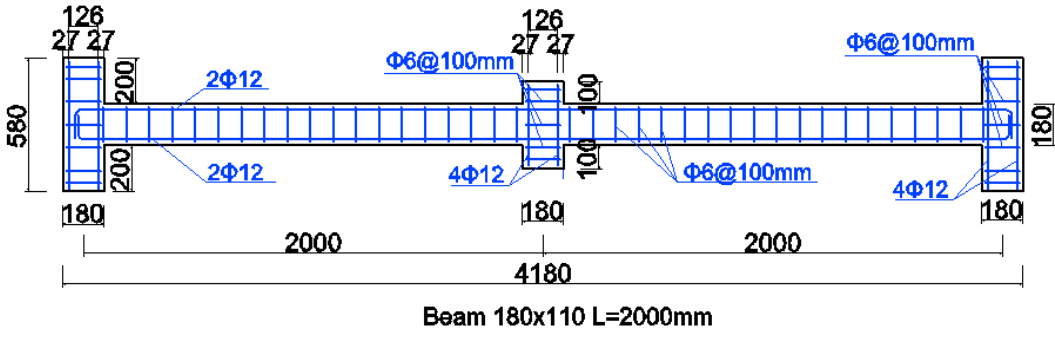
### 3.2.1 Dimensions of specimens

The specimen is composed of two beams, middle column and two enlarged end columns stubs. In accordance with the Eurocode design of concrete structures (Eurocode 2 1-1), one-third scaled specimen (S1) was designed. The span of the beam is 2m and the section is 110mm×180mm; the columns are 180 mm wide by 110 mm deep. The vertical distance from surface of beam to the surface of side column is 200 mm. The dimensions and details are shown in Figure 3. 3.

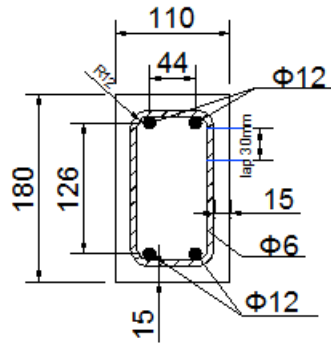
In order to study the effect of span-depth ratio and of the reinforcement ratio on the mechanical

performance, two other different size specimens were also designed. Table 3.1 lists some span-depth ratio with a similar experiment scale that were used in literature in the last two decades [8][10][12][34]. The range of span-depth ratio is 4.1 to 15 and most of them is around 11. To investigate different span-depth ratios, the type of the specimen (S2) keeps the section of beam as the same as the first one. While the span is changed from two meters to three meters (see Figure 3. 4) so that we can study the effect of span and span-depth ratio on the progressive collapse resistance. Besides, another type of specimen (S3) with a beam section of 110mm×270mm is designed with a span of 3 m as well. Compared with the first type specimen, both of them have equal span-depth ratio of 11.1 in order to evaluate the sensitivity of the structure response and bearing capacity due to the section size. The dimensions and details of the specimen are reported in Figure 3. 5.

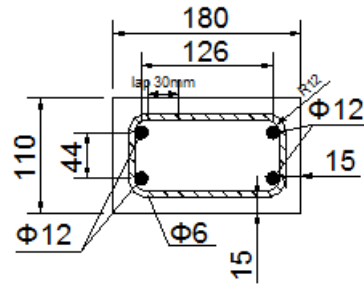
For every beam and column, the thickness of covering layer is set to 15 mm. In real construction, the minimum diameter of reinforcing bar is generally 12 mm. Hence, in all the specimens, four D12 longitudinal steel bars and D6 stirrup bars with spacing 100mm are used. The longitudinal bars extend into the exterior column and are anchored with a tail extension of the hook. The length of the tail of the hook was longer than five times the diameter of rebar like it is required in Eurocode. In that case, both specimen S1 and S2 have the same reinforcement ratio of 2.28%. Basic information of the specimens is listed in table 3.2. Finally, three different sizes of specimen have been considered for the test.



(a). Dimension of specimen S1.

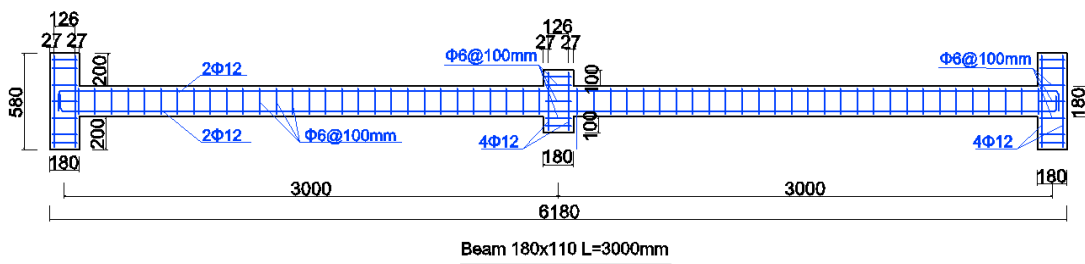


(b) Details of beam cross section S1

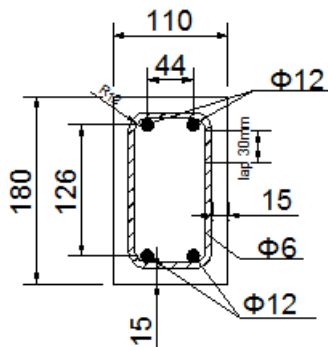


(c) Details of column cross section S1

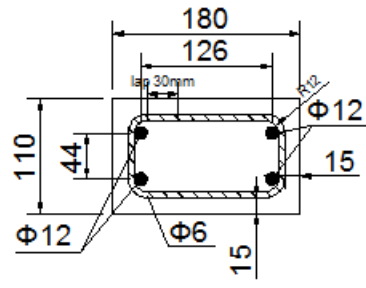
Figure 3. 3 Specimen S1 180x110 L=2000mm



(a) Dimension of specimen S2

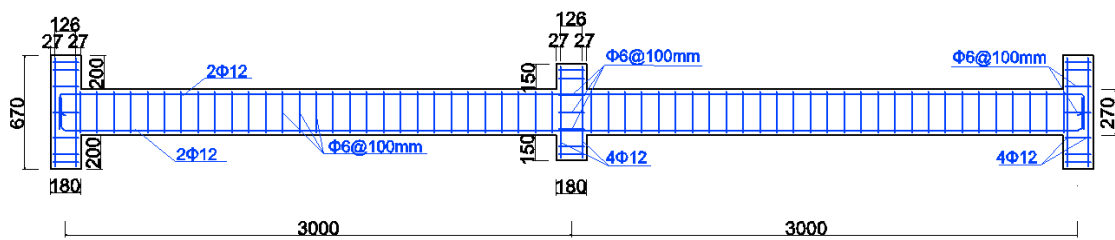


(b) Details of beam cross section

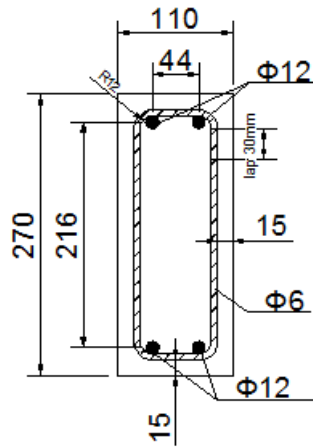


(c) Details of column cross section

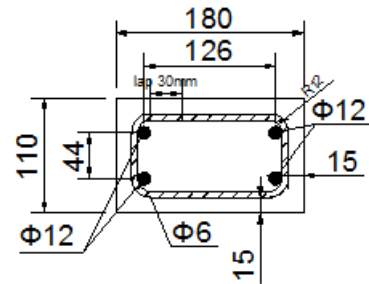
Figure 3. 4 Specimen S2 180x110 L=3000mm



(a). Dimension of specimen S3



(b) Details of beam cross section



(c) Details of column cross section

Figure 3. 5 Specimen S3 270x110 L=3000mm

Table 3. 1 Span-depth ratio of the specimen

Author	Year	L/h	Diameter of bars (mm)
Yanchao Shi,Hong Hao etc.	2007	12	10
Wei—jian yi, etc.	2008	13.3	12
H.Choi, J.Kim	2009	9.1	10
		11.1	10
He Qing-feng etc.	2009	15	12
Youpo Su, Ying Tian etc.	2009	4.1	12
		6.1	12
Mehrdad Sasani, Andre Werner etc.	2010	10.5	9.5
Jun Yu, Kang-Hai Tan	2011	11	10
Forquin, Chen	2014	4	12
		4	8

Table 3. 2 specimen properties

Specimen No.	span	Beam section		L/h	Reinforcement bars	Reinforcement ratio
	L(mm)	h (mm)	b(mm)			
S1	2000	180	110	11.11	4D12	2.28%
S2	3000	180	110	16.67	4D12	2.28%
S3	3000	270	110	11.11	4D12	1.52%

### 3.2.2 Material

A basic low strength concrete named R30A7 was used in this study. It is the same baseline material that was used in laboratory 3SR for several collaboration with CEA-Gramat. The

concrete made of hard siliceous aggregates, sand, cement and water. Table 3.3 gathers the composition and the main mechanical properties. The ratio of water to cement is 0.64 and the maximum grain size is 8mm. The behavior of this concrete has been investigated by a large number of tests such as quasi-static triaxial compression tests under pressures as high as 800 MPa [74]–[76], dynamic tensile loading test [77] [78] and shear loading test [79]. In addition, Dupray et al. [80] and recently Erzar and Forquin [78] have developed a mesoscopic modelling method to simulate the behavior of R30A7 concrete in confined compression and under impact loading.

Table 3. 3 Composition and properties of R30A7 concrete [22] [77]

Composition and properties	R30A7
Aggregates 0.5/8 (kg/m <sup>3</sup> )	1007
Sand(kg/m <sup>3</sup> )	838
Cement CEM I 52.5 (kg/m <sup>3</sup> )	263
Water(kg/m <sup>3</sup> )	169
Water/Cement	0.64
Young modulus (GPa)	42
Uniaxial compression strength (MPa)	30

The stress-strain relationship of longitudinal reinforcement bar D12 can be obtained by quasi-static tensile tests as shown in Figure 3. 6. The average mechanical properties, including the yield stress  $f_y$ , the ultimate stress  $f_u$  and the elastic modulus E of the longitudinal bars are listed in Table 3.4.

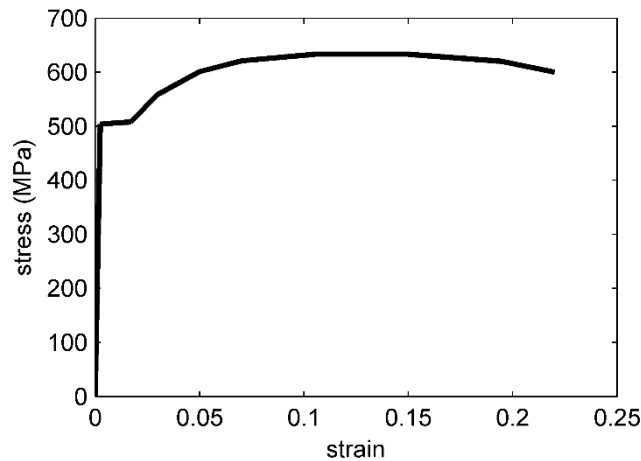


Figure 3. 6 Stress-strain curve of steel rebar

Table 3. 4 Material properties of steel reinforcement [22]

Diameter	$f_y$ (MPa)	$f_u$ (MPa)	E (GPa)	$\epsilon_y$	$\epsilon_u$
D12	504	633	210	0.004	0.22

### 3.2.3 Fabrication of specimen

Two specimens were made for each three types. Making all these specimens in the 3SR laboratory helped to insure a high degree of quality. Production of specimens can be divided into four steps.

- (a) The reinforcement cage is placed in the mould horizontally so that the distance between the rebars and the surface of the mould can be well controlled (see Figure 3. 7 (a)). The volume of concrete for each assemblage was calculated in accordance with composition of R30A7 concrete as shown in table 3.5. According to this volume, the batch of concrete for one specimen was prepared as shown in Figure 3. 7 (b), where each type of material from the concrete composition was separated in two parts before mixing.
- (b) Add the concrete constituents to the mixer following the flowchart of Figure 3. 8 for mixing efficiently and get the good workability of the concrete. The whole mixing time is no more than 6 mins.
- (c) Once the concrete has been adequately mixed, it was placed into the formwork with the reinforcement cage. Then the vibration tube was inserted into the concrete so that the concrete can flow around and fill the mould.
- (d) After the specimen was stored in inside ambience conditions more than 28 days, the surface of the concrete need to be sprayed in white and black paint to meet the requirement of digital image correlation (DIC) technique that is a method to measure

deformation, displacement and strain by tracking the changes of images (see figure 3.7 (d)).

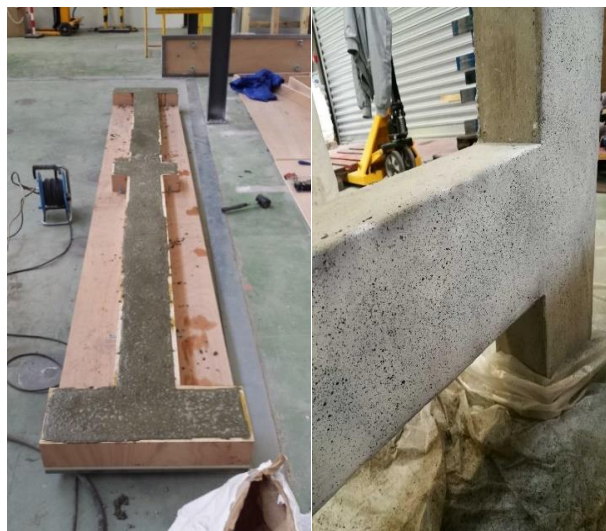
Table 3. 5 Consumption of materials for each type of specimen

		S1	x1. 1	S2	x1. 1	S3	x1. 05
<b>volume</b>	m <sup>3</sup>	0. 1	0. 1	0. 1	0. 2	0. 2	0. 2
<b>D 0, 5/8</b>	kg	103. 3	113. 6	143. 2	157. 5	214. 8	225. 5
<b>D1800 <math>\mu</math> m</b>	kg	85. 9	94. 5	119. 1	131. 0	178. 7	187. 6
<b>CEM</b>	kg	27. 0	29. 7	37. 4	41. 1	56. 1	58. 9
<b>water</b>	kg	17. 3	19. 1	24. 0	26. 4	36. 0	37. 8



(a)

(b)



(c)

(d)

Figure 3. 7 Making of specimens (a) Reinforcement cage and mould; (b) concrete constituents; (c) Casting the specimen; (d) Spraying the specimen

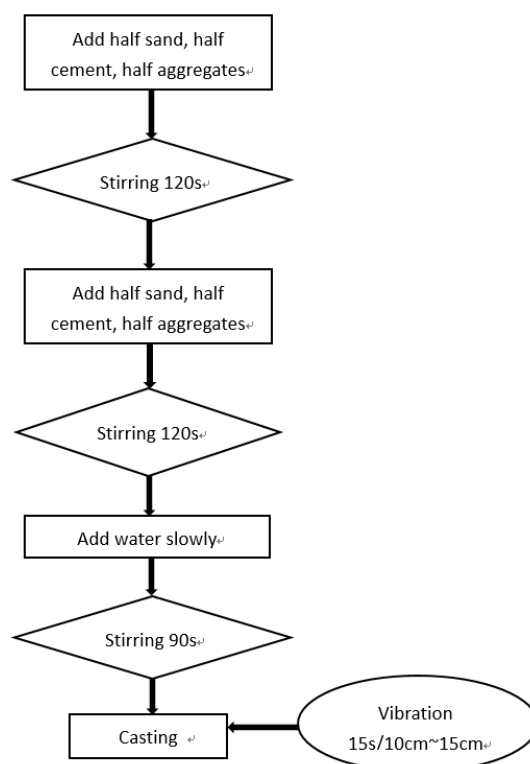


Figure 3. 8 Flowchart of the concrete mixing

### 3.2.4 Estimation of the bearing capacity by traditional design method and identification of the range of failure loads

The objective of this dynamic test is to study the damage behavior of beam-column sub-assemblages under a removal of the middle supporting element. Considering the load provided by the steel plate and the steel transfer frame, it is necessary to estimate the plastic bearing capacity prior to design load. According to engineering design method (Eurocode2 1-1 p34), the resistance of a beam can be estimated with parameters of the material as follows:

For R30A7 concrete, the compressive strength of concrete is  $30MPa$ . The value of design compressive is defined as:

$$f_{cd} = \alpha_{cc} f_{ck} / \gamma_c$$

$$f_{cd} = 1.0 \times \frac{30}{1.5} = 20MPa$$

$\gamma_c$ : is the partial safety factor for concrete.

$\alpha_{cc}$ : is the coefficient taking account of long term effects on the compressive strength and of unfavorable effects resulting from the way the load is applied.

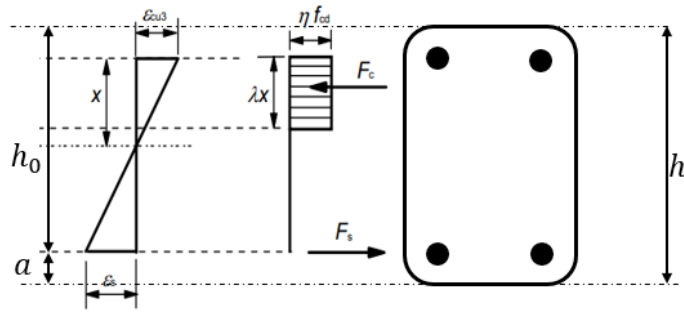


Figure 3. 9 Rectangular stress distribution (Eurocode 1-1)

Due to equilibrium condition as shown on Figure 3. 9, for the specimen  $L=2000\text{mm}$ ,  $h=180\text{mm}$ ,  $b=110\text{mm}$ ,

$$x = \frac{f_y A_s}{\alpha_1 f_c b} = \frac{504 \times 226.2}{1.0 \times 20 \times 110} = 51.82\text{mm}$$

$$h_0 = h - a = 180 - 27 = 153\text{mm}$$

$f_c$ : is the compression strength of concrete;

$f_y$ : is the tension strength of reinforcing steel;

$A_s$ : is the area of the longitudinal reinforcement;

$x$ : is the effective height of compression zone;

$h_0$ : is effective height of the beam;

$a$ : is the distance from the cover to the center of the longitudinal reinforcement.

the max bending moment that the component can sustain is

$$M = f_y A_s \left( h_0 - \frac{x}{2} \right) = 504 \times 226.2 \times \left( 153 - \frac{51.82}{2} \right) = 14489\text{N} \cdot \text{m}$$

This bending moment was produced by a concentrated force  $P$  and a distributed load  $q$  (the self-weight of beam) as shown on Figure 3. 10.

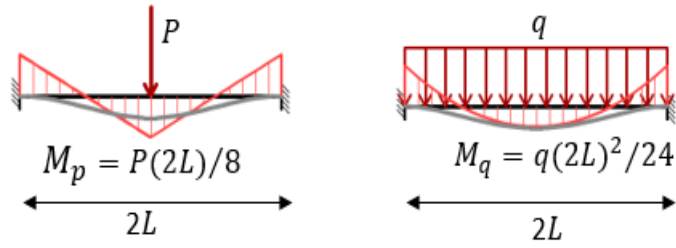


Figure 3. 10 Bending moment diagram

The distributed load can be obtained by the self-weight of beam  $W_s$ ,

$$q = \frac{W_s g}{2L} = \frac{245.21 \times 9.8}{2 \times 2} = 600.76 \text{ N/m}$$

Therefore, the maximum load at the center of the beam can be calculated,

$$M = M_p + M_q = \frac{P(2L)}{8} + \frac{q(2L)^2}{24}$$

$$P = \frac{8}{2L} \left( M - \frac{q(2L)^2}{24} \right)$$

$$P = \frac{8}{2 \times 2} \times \left( 14489 - \frac{600.76 \times (2 \times 2)^2}{24} \right) = 28.18 \text{ kN}$$

That means the maximum load that can be applied to the middle column is 2875kg, which is designed in accordance with the engineering design method when the middle support is removed.

Similarly, for the specimen S2,  $L=3000$  mm,  $h=180$  mm,  $b=110$  mm, the self-weight is 555.10N/m. The maximum load that can be applied to the middle column is equal to

$$p = \frac{8}{2 \times 3} \times \left( 14489 - \frac{555.10 \times (2 \times 3)^2}{24} \right) = 18.20 \text{ kN}$$

That means the maximum load that can be applied to the middle column for the specimen S2 is 1857kg.

For the specimen S3,  $L=3000$  mm,  $h=270$  mm,  $b=110$  mm, the self-weight is 801.97N/m. the

effective height of compression zone is

$$x = \frac{f_y A_s}{\alpha_1 f_c b} = \frac{504 \times 226.2}{1.0 \times 20 \times 110} = 51.82 \text{ mm}$$

$$h_0 = h - a = 270 - 27 = 243 \text{ mm}$$

Similarly, the maximum bending moment that the section of beam can sustain is

$$M = f_y A_s \left( h_0 - \frac{x}{2} \right) = 504 \times 226.2 \times \left( 243 - \frac{51.82}{2} \right) = 24749 \text{ N} \cdot \text{m}$$

The maximum load that can be applied to the middle column for the specimen S3 is

$$p = \frac{8}{2 \times 3} \times \left( 24749 - \frac{801.97 \times (2 \times 3)^2}{24} \right) = 31.4 \text{ kN}$$

Therefore, the maximum load that can be applied to the middle column for the specimen S3 is 3204kg.

For each type of specimen, geometric and physical properties of sub-assemblages specimen is shown in table 3.6. According to practical engineering design method, the maximum load that can be applied to the middle column is 2875kg, 1857kg, 3204kg, respectively for every type of specimen. We will not use loads beyond this value.

Table 3. 6 Basic configuration of specimens and bearing capacity

NO.	L (mm)	h (mm)	b (mm)	L/h	V (m3)	W (kg)	Plastic hinge	reinforcement ratio	Max Load (kg)
S1	2000	180	110	11.11	0.1026	245	4	2.28%	2875
S2	3000	180	110	16.67	0.1422	340	4	2.28%	1857
S3	3000	270	110	11.11	0.2053	491	4	1.52%	3204

### 3.3 Experimental set up

#### 3.3.1 The loading system

The experimental [21] system has two parts including the loading system and the supports, as

shown in Figure 3. 11. The loading system consists of two standing columns, two girder, four bracing tubes and a loading transfer frame. The central mass is composed of steel plates that are fixed by four long screws on the steel transfer frame as shown in Figure 3. 12. Six wheels were set on the each side of the transfer frame so that it can slide up and down along the standing columns. The load transfer frame is connected with two adjustments (see Figure 3. 12 (b)) by means of two cables passing through the pulleys that were set on the top of the standing columns. In this way, the height of the transfer frame can be adjusted easily to the height of the middle column load by adjusting the length of the cable.

The height of the whole loading system is 3.2m, and floor space 8m<sup>2</sup>. It can provide a maximum load of 3.3 tons. The design load of the equipment is 3 tons considering a safety factor. It can meet the test requirements.

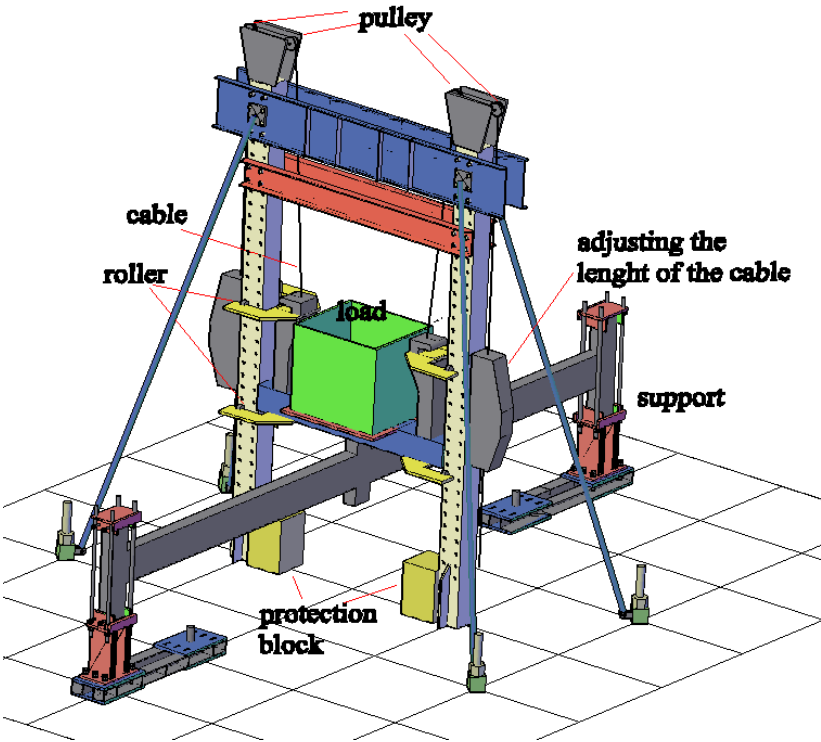


Figure 3. 11 Layout of test set-up



(a)



(b)

Figure 3. 12 (a) front elevation of the loading system; (b) lateral view of the loading system

### 3.3.2 Design of the support for the side columns

For this beam-column assemblages test, one of the most important thing are the boundary conditions, which are crucial to reproduce a realistic sub-assembly collapse of a whole frame. During the conceptual design of the test equipment, the intent was to develop a type of support that can supply restraint mode like real columns.

In real situations, when a middle column fails, side columns may accept horizontal motion while the rotation is restrained by the lower and upper floors. Hence, the support should both have a controlled rigidity in horizontal direction and be able to avoid rotation in the plane of beam-column. The preliminary design plan is shown on Figure 3. 13. This support is made of an upper case, a bottom case, and four connector bars. The upper case and the bottom case connected by four steel bars are used to restrain the rotation of the side column. The horizontal displacement is controlled by the connector plates. The whole support is totally fixed on the ground by two steel beams screwed to the DESSIS testing slab as shown in Figure 3. 11. The height of the upper case can be changed in order to fit the different size of columns stub.

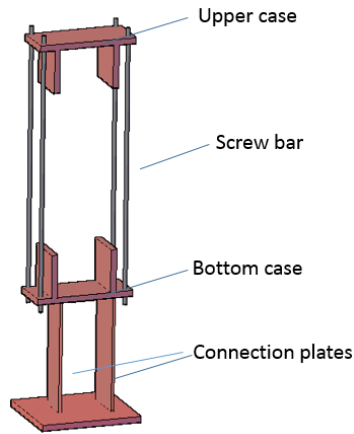


Figure 3. 13 The support for side columns

### Identification of the dimension of the steel connection plates

The state of stress and strain in the support need to be checked in order to make sure that the dimension of connection plates and their position can meet the requirement of our experiment. Considering the largest specimen that is supposed to be the worst situation of testing, when the middle support is removed, we must confirm that both sides support have deformation in the range of elasticity and that it can recover after test.

As mentioned above in several references, most of tests conducted with the beam-column sub-assemblages can active catenary action and basically lose the bearing when the vertical displacement of middle column reaches the height of the beam. According to the geometry condition as shown in Figure 3. 14, the corresponding horizontal displacement that the support of the side column can carry on can be calculated as follows.

$$u = \sqrt{l + h^2} - l = l \left[ \left( 1 + (h/l)^2 \right)^{\frac{1}{2}} - 1 \right] \approx \frac{1}{2} l \left( \frac{h}{l} \right)^2 = \frac{h^2}{2l}$$

$u$ : is the horizontal displacement of the support;

$l$ : is the clear span of the beam;

$h$ : is the height of the beam.

For the specimen S1,  $u = 8.9\text{mm}$ ; For the specimen S3,  $u = 13\text{mm}$ . Hence, the largest horizontal displacement of the support is 13mm.

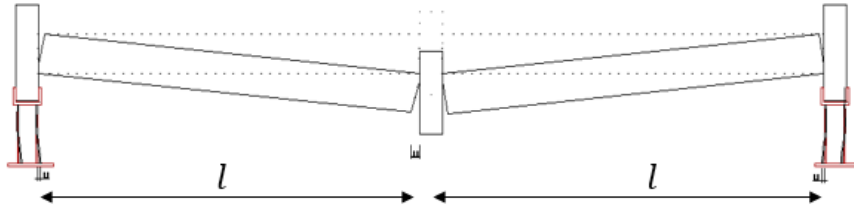


Figure 3. 14 Deformation of structure after the removal of the middle support

The bottom support can be calculated according to the simplified model as shown in Figure 3. 15. In this model, the rotation angle ( $\theta_a, \theta_b$ ) at both ends of the connector steel plates is supposed to be zero. The case only takes place lateral displacement under the load applied to the middle column.

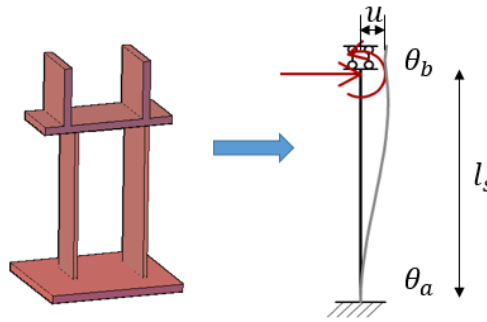


Figure 3. 15 Simplified diagram of the deformed shape of the support connector plate

$$\theta_a = \theta_b = 0 \quad (3.1)$$

According to mechanical structure theory, moment  $M_b$  at the point b in the beam is

$$M_b = 2i\theta_a + 4i\theta_b - 6i \frac{u}{l_s} \quad (3.2)$$

where  $i$  is the line stiffness of the steel plates;  $l_s$  is the length of the steel plate which is designed to 40cm;  $u$  is horizontal displacement of the support.

The stress of the steel plate can be calculated by the following formula

$$\sigma = \frac{My}{I_z} \quad (3.3)$$

where  $M$  is the bending moment;  $I_z$  is the rotational inertia. The equations 3.1 and 3.2 were

introduced into the formula 3.3, the stress is equal to

$$\sigma = 3E \frac{ub}{l_s^2} \quad (3.4)$$

Therefore, the thickness of the plate can be calculated

$$b = \frac{\sigma l_s^2}{3Eu} \quad (3.5)$$

Substituting value of the constants,  $b$  should be at least equal to 4.88mm when the  $l_s$  is 40cm.

Besides, in order to avoid to occur buckling failure and plate fracture, it is also necessary to check the critical buckling load of the steel slice. According to stability theory, the critical buckling load is given by:

$$N_{cr} = \frac{\pi^2 EI}{4l_s^2} \quad (3.6)$$

For the largest specimen, the vertical load of the each support is approximately 32 kN (see table 3.6) after removal of the middle support. The critical load of each slice is 3.8 kN. Considering the requirement of the stiffness and stability, six pieces of steel plates were set in each support. A stress analysis will be presented in the chapter about numerical simulation. Finally, the support for the side column was designed as shown in Figure 3. 16. The length of the steel plates is 400mm; the thickness is 4 mm with a space of 20 mm between each plate.

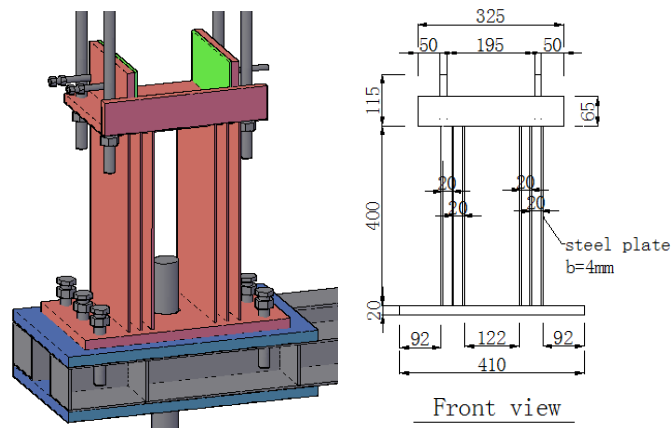


Figure 3. 16 designed support for side columns

### 3.3.3 Unloading device under the middle column

This experiment is carried out by removing the support of the middle column, hence, there are some requirements for the middle column support. Firstly, it should have quite high rigidity. When the maximum load, about 3 tons, is applied to the top surface of the middle column, it has to act a fixed support to avoid any vertical displacement of the specimen. Secondly, the device should be easily removed from the middle column to generate the dynamic loading. Thirdly, the operation should be done by keeping a safe distance between the testing specimen and the operator because the specimen may drop at a high-speed due to the upper load after removing the support. To meet the requirements above, an unloading device was designed as shown in Figure 3. 17. This device consists of four pieces made of steel rods. Three of them are fixed and, one of them can rotated around a bolt. The pin bolt that is circled in red line on Figure 3. 17 is connected to a steel strand. When it is put out, the steel rod in the middle may occur a rotation that simulates the middle supporting component failure. In order to remove it effortlessly, it is necessary to smear some lubricating oil on the pin.

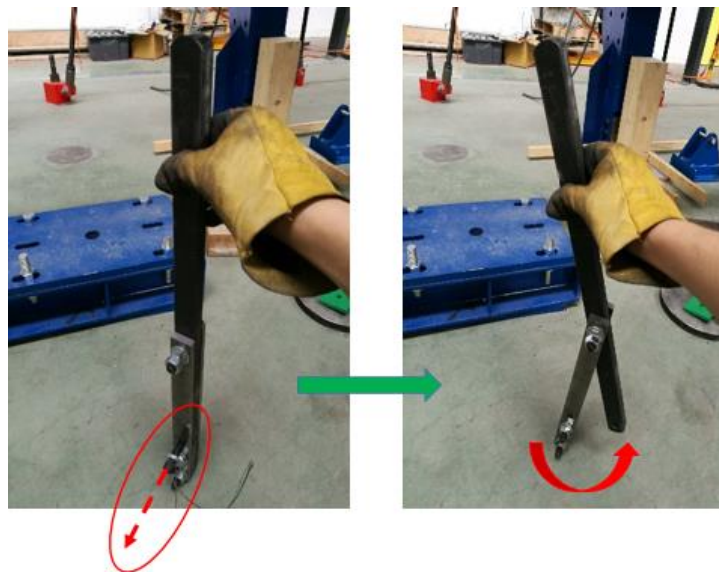


Figure 3. 17 Unloading device

### 3.3.4 Instrumentation

The measuring device includes a Phantom Miro M310 high-speed camera with a 50 mm Nikon lens and a laser interferometer. The high-speed camera is directed towards the middle of the specimen as shown in Figure 3. 18. It is a 1 megapixel camera with 3.2 Gigapixels/second (Gpx/s) throughput. This translates to over 3,200 frames-per-second (fps) at full 1280 x 800

resolution. The minimum exposure time is 1  $\mu$ s and is available in both color and monochrome versions. In this test, the camera is set to take 500 to 1000 frames per second to record pictures of the specimen during the test. Then, the images are processed by DIC software to get the corresponding displacement and strain field. This technology has been adopted in experimental mechanics by many researchers and has obtained good results [21] [22] [78] [81]. Meanwhile, the development of cracking and the level of damage can be observed on the surface of the sample by the video from the camera.

A laser interferometer (Polytec OFV-551) was installed under the middle column to measure the falling velocity. It was connected to the oscilloscope (YOKOGAWA DLM 4038 model) to display and save the data.

Noted that in few tests several strain gauges were stuck to the longitudinal rebar in the concrete to obtain strain data of reinforcing bars as in previous literature [24] [27]. However, these strain measurements were not very usable. It was assumed that casting and vibrating of concrete caused strain gauges damage or peeling off, resulting in poor credibility of the data. It should be noted that most of the previous experiments were static experiments that lasted for a longer time. The experimental results were generally regular without much noise. On contrary, in a dynamic test, the duration time of the test is extremely short. The strain itself fluctuates violently. The experimental results show a strong discreteness with much more noise [37]. In addition, due to the strain gauges, the adhesion of steel and concrete may become locally weakened, and may affect the mechanical properties of reinforced concrete components. Therefore, the strain gauges were not used in next dynamic experiments.



Figure 3. 18 Measurement device

### 3.4 Experimental procedure

The experiment is generally divided into three stages:

The first, is the experimental preparation. After the installation of the test specimen, the middle support, unloading device, is immediately placed under the middle column. And then the load transfer frame with the steel plates is lay down slowly on the top of the middle column by means of the loading system. During this period, the whole specimen should avoid to undergo vertical displacement. After the load is stable, the cables are completely released to insure that they will not remain transferring any load to the frame when it will be in its lowest position. In order to ensure the safety of personnel and equipment, two wood protection blocks were put beside the stand column of the load system. They are used to protect the loading system from impact and prevent cable from breaking. The camera and light positions are adjusted until the screen can be clearly displayed. From then, preparing work is ready, as shown in Figure 3. 19.

In the second stage, at the beginning of the experiment, the pin bolt was pulled out of the unloading device quickly to simulate the sudden loss of bearing capacity of the vertical supporting member. The dead load was applied dynamically to the beam-column assemblage. The middle column started to move downward until a new stable equilibrium was reached or the specimen lost its carrying capacity totally.

The third stage consists in saving the test data. The load transfer frame is lifted up to unload the beam-column assemblage. If the specimen need to be tested two or more times with different load level, the middle support is reinstalled after unloading. To reload, step two and three are just repeated until the specimen is damaged enough to stop the test.

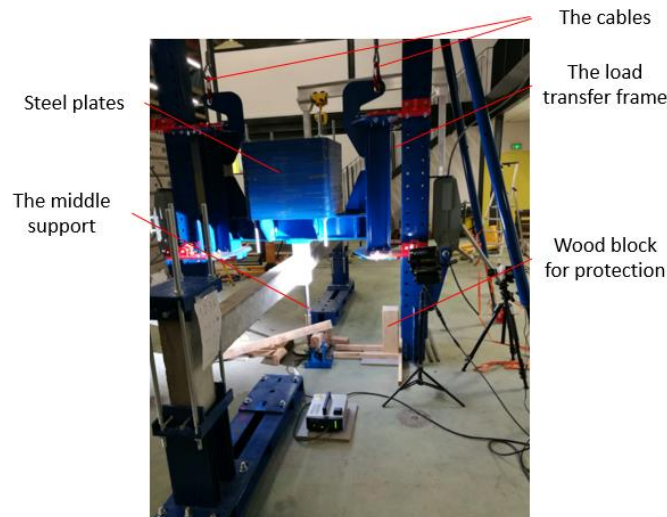


Figure 3. 19 Layout of set-up before the test

### 3.5 Test results

#### 3.5.1 Specimen 1-1 L=2m 110mm×180mm

##### Loading

According to engineering design approach, the maximum bearing capacity of this structure is 2875kg (see Table 3.6). In this case, a load of 2662 kg was applied directly to the top of the middle column.

##### Test data

According to measured data, the curve of velocity-time can be plotted as shown in Figure 3. 21. At the beginning of the test, the specimen had a quite large acceleration in a very short time. At about 0.1 s, the middle column reaches a maximum velocity of 0.43m/s. After the velocity passed the max value, the acceleration changed from positive to negative. The velocity started to decrease quickly until the specimen stopped moving downwards. Just before the end of the test, the value of velocity was changing rapidly. It is because the load transfer frame was in connect with the wood protection blocks that were put beside the stand column of the load system.

Figure 3. 22 shows the vertical displacement of middle column. The middle column initially moved downwards of 2.2 mm within 25 ms whereas the displacement of the middle column reached to 10mm after second 25 ms. Between 50 ms to 150 ms, the displacement grows more and more rapidly; after 150ms, the displacement gradually slows down. The maximum displacement of the middle column was 76mm.

Figure 3. 23 gives the damage level when the middle column reached to different displacements. There was no crack on the concrete surface of the specimen arriving the first 150 ms. When the middle joint fell down about 40 mm, the cracks began to develop and, the velocity decreased significantly. In the tension zone, there are three dominant cracks due to tension forces and few fine cracks along axis subjected to interaction between reinforcement bar and concrete. In the compression zone around middle column, the concrete at the corner of the joint was damaged and flaked away. It is noted that no important damage took place on the side column but several cracks were visible due to rotation and tension.

Generally speaking, this dynamic load can caused more serious damage on the specimen 1-1 than the static load of the same value. However, the total displacement was not very large and the structure has not completely loss its bearing capacity under the applied load of 2662kg. After removing the middle support, the test structure become a simply supported beam. Hence, the resistance force  $F_R$  is easy to calculate. A calculation sketch is drawn as Figure 3. 20.

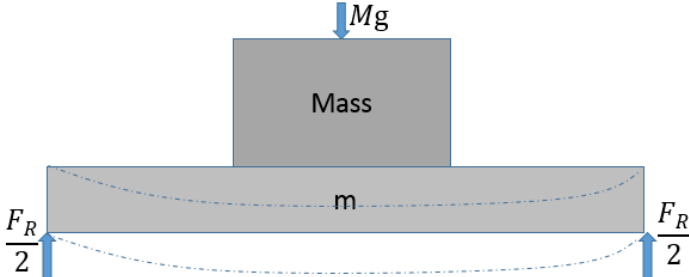


Figure 3. 20 Calculation sketch of the resistance force

we can have a formula as following

$$Mg - F_R = Ma \tag{3.7}$$

$$a = \frac{dv}{dt} \quad (3.8)$$

$M$ : is the weight of the load (steel plates);

$g$ : is gravity;

$a$ : is the acceleration.

Thanks to the test data,  $dv/dt$  can be known. Here the weight of the beam is neglected since a larger part of it that remains fixed. And the quality of beam is much less than the load.

Figure 3. 24 (a) shows the variation of the resistance force versus the vertical displacement of the middle column. Figure 3. 24 (b) illustrated the strain field near the middle joint in the longitudinal direction. It was obtained by processing a large amount of images by GOM correlate that is a free digital image correlation and evaluation software for materials and component testing.

Before the vertical displacement of 4.3 cm, the resistance force increased continually with the cracking development in the vicinity of the middle joint. Three domain cracks were observed on the surface of concrete (see Figure 3. 24 (b)). Beyond this point, the concrete in the compressive zone started to seriously damage. The resistance of the beam is due to the plastic behavior of the rebar and the resistance did not show an obvious increase. Till to the end of test, the concrete at the corner of the joint was damaged and flaked away. Under dynamic load, the maximum bearing capacity was 35.53KN, which is 36.2% more than the applied load and beyond the designed maximum load (2875kg) under static condition.

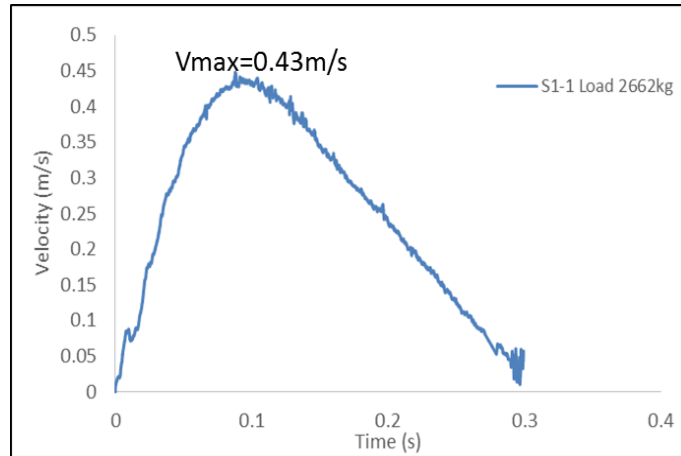


Figure 3. 21 Velocity of the middle column of the specimen 1-1 under the dynamic load 2662kg. The maximum velocity is 0.43m/s.

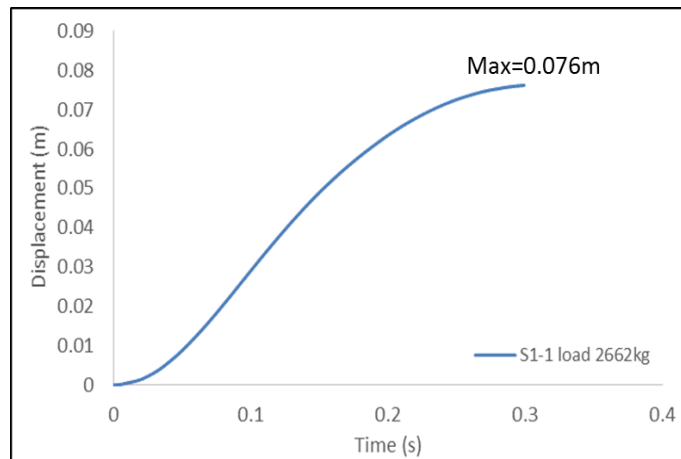


Figure 3. 22 Time history of vertical displacement of the middle column and the strain field under the load 2662kg

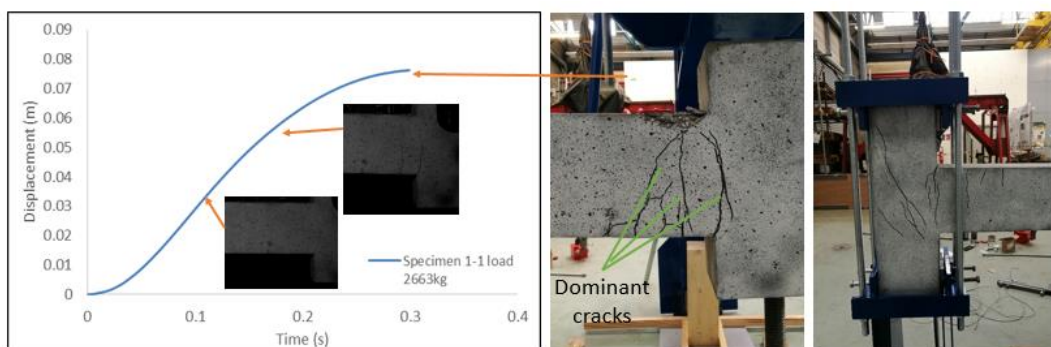
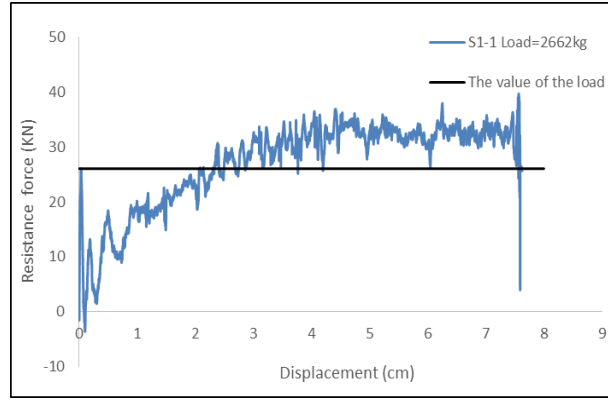
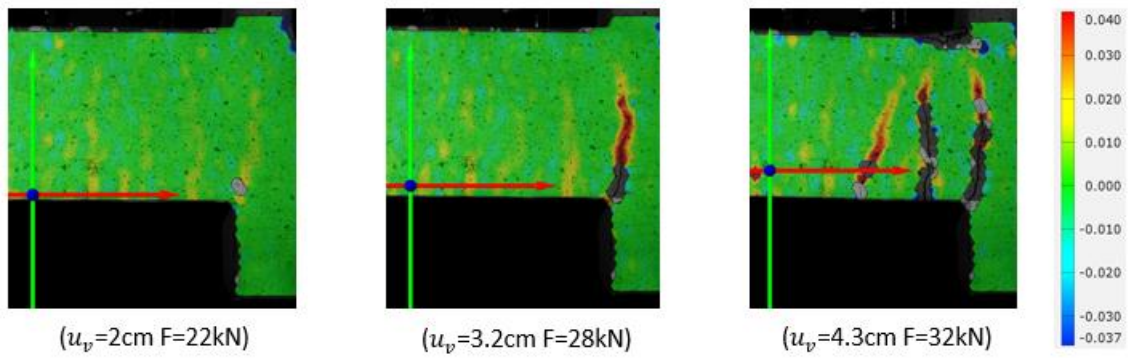


Figure 3. 23 The vertical displacement of the middle column versus time and the damage under the load 2662kg



(a)



(b)

Figure 3. 24 (a) Resistance force versus vertical displacement of middle column; (b) The stain field near the middle joint by the DIC (S1-1 Load=2662kg)

### Validation the horizontal displacement of the support

In this experiment, a significant difference from other beam-column assemblage tests is that the elastic supports were used for the side columns. We expected that it can offer a fine horizontal displacement so that the specimens have a more real boundary condition. In this part, we will check the horizontal displacement of the side support to verify our method.

After loss the middle support, the middle stub go down some distance. The form of beam-column is drawn as Figure 3. 25. If the side support has no horizontal displacement, the length of hypotenuse is  $l'$ . The horizontal displacement of the support can be roughly estimated by the formula as following:

$$U_{sl} \approx l + C_l - l' \quad (3.9)$$

Where the displacement of the lift support  $U_{sl}$  is equal to the clear span of the beam  $l$  plus the total width of the cracks  $C_l$  and minus  $l'$ .

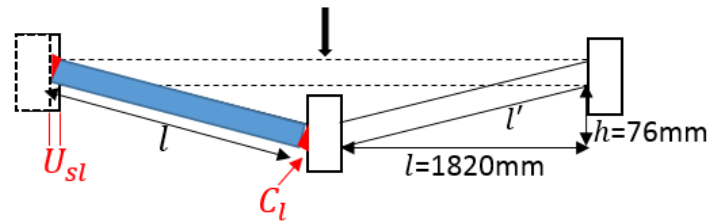


Figure 3. 25 Calculation diagram of the displacement of the support

For this test, the width of each crack is illustrated in Figure 3. 26. There is no obvious crack near the side columns. Four cracks distributed in the vicinity of the middle joint, in which  $C_1$ ,  $C_2$ ,  $C_3$  can be obtained by GOM correlate software and  $C_4$  was measured by vernier caliper. All the values was introduced into the formula 3.9. the horizontal displacement of the supports can be known. The lift support was 5.8mm; the right supports was -1.1mm. That means the life support had an outward displacement of 5.8mm, the right support had an inward displacement of 1.1mm. These results are in accordance with the practice and indicates that the boundary condition used in the test is reasonable and right.

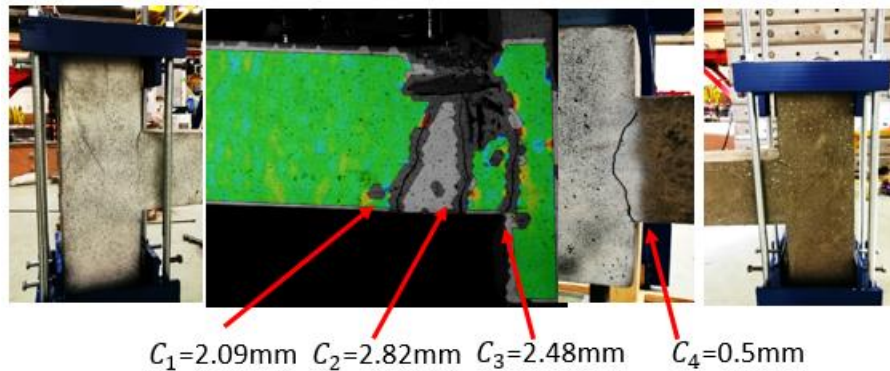


Figure 3. 26 Concrete crack pattern on the specimen (S1-1 Load=2662kg)

### 3.5.2 Specimen 2-1 L=3m 110mm×180mm

#### Loading

In the case of specimen S2-1, three different loading levels were applied, 675kg, 994kg and 2063kg, respectively. The first one was repeated four times. Subsequently, the second load was applied three times and the last one, 2063kg was applied one time. The specimen was initially placed on its supports as shown in Figure 3. 27.



Figure 3. 27 Set up of the specimen S 2-1

### Test data

During the test, the laser measured the velocity profile of the middle column as shown in Figure 3. 28. A damped pseudo periodic response was observed under the load of 675 kg with a max velocity of 0.194 m/s and time period of 0.167 s. However, the velocity and the vibrating period was a significantly increased with the some load applied a second time. This second time, the velocity was 0.41m/s and the vibration period was 0.337s, respectively. Hereafter, the maximum velocity and the vibrating period were kept constant during several tests at the same load of 675kg.

The displacement can be easily obtained by a velocity-time integration. At first load of 675kg, the max displacement is merely 19 mm. Repeating the rest at the same level load, the max displacement extends to 44 mm. At the end of the test, the amplitude of vibration decrease till zero. Meanwhile, by the digital image correlation processing, the images can be processed to get the strain field in the visualized part of the structure as shown in Figure 3. 29 and Figure 3. 30. We can observe that the strain field is smooth in the compression zone under the load of 675kg. All over the body of the specimen there is not appeared visible crack or damage. After each loading and unloading, the middle column of specimen is recovering its original height. The performance of the beam seems to be in pseudo elastic state during the test.

Figure 3. 31 shows the falling velocity of the middle column under the load 994 kg. Changes

are quite small when repeating the same load. The max velocity reaches 0.58 m/s and the time period is about 0.39 s. Compared to the behavior of the beam under the applied load of 675kg, the max velocity is increased of about 38% while the load was increased of 47%. On the left of the Figure 3. 32, we can also observe that larger strains started to appear when the beam is far away from the balance position, the maximum displacement reaching 6.6 cm. In looking carefully, a visible crack can be found in the tensile zone in the vicinity of the middle column, as shown in Figure 3. 33. At this moment, the structure entered into plastic state. Some unrecoverable deformation appeared on the beam even after complete unloading. For example, when the middle column stopped moving (no unloading), the static displacement was 45mm; after unloading, the middle column came back up of about 20mm.

For the third test the load was set to 994 kg, Figure 3. 34 shows the strain near the side column where several obvious cracks appeared around the joint. It is noted that one of the cracks was growing from the upper part of the side column as shown in Figure 3. 35. It demonstrates two points: on the one hand, the stub column did not experience very large rotation. It means that this support is able to restraint rotation under this dynamic load level. On the other hand, the joint undergoes both longitudinal tensile force and the vertical compression force. Both two forces lead to an extended damage of the side column. The joint damage can become a crucial element for the evaluation of the capacity of resisting to progressive collapse of the structure.

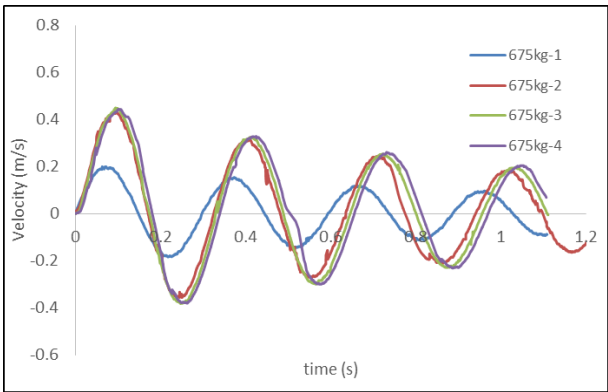


Figure 3. 28 Velocity versus time under several successive loadings of 675kg

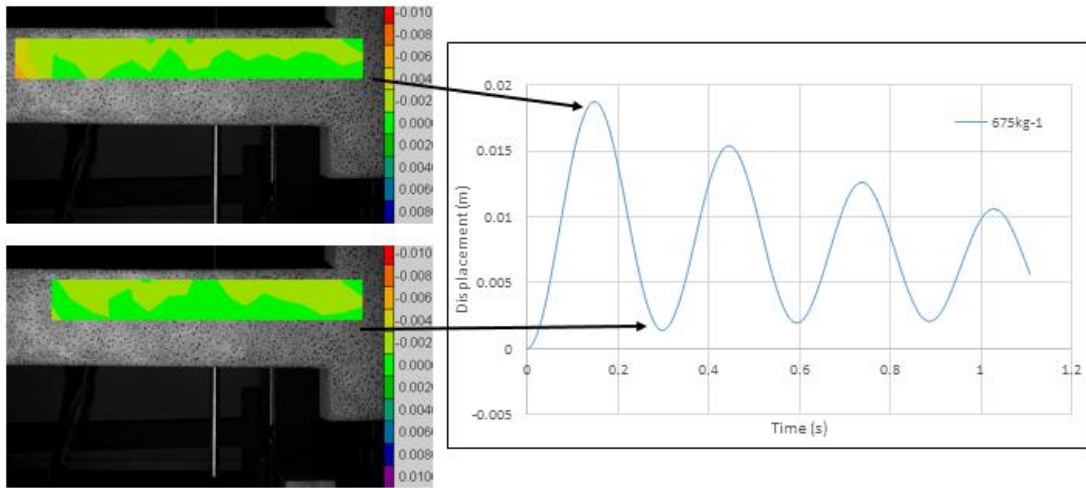


Figure 3. 29 Vertical displacement of the middle column versus time for the first loading at 675kg and strain fields in the horizontal direction

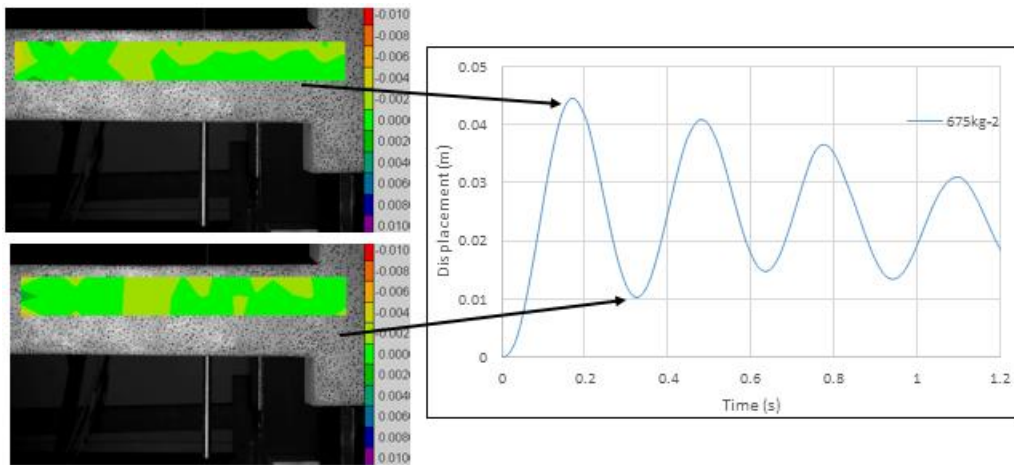


Figure 3. 30 Vertical displacement of the middle column versus time under the load of 675kg for the second time and the strain in the horizontal direction

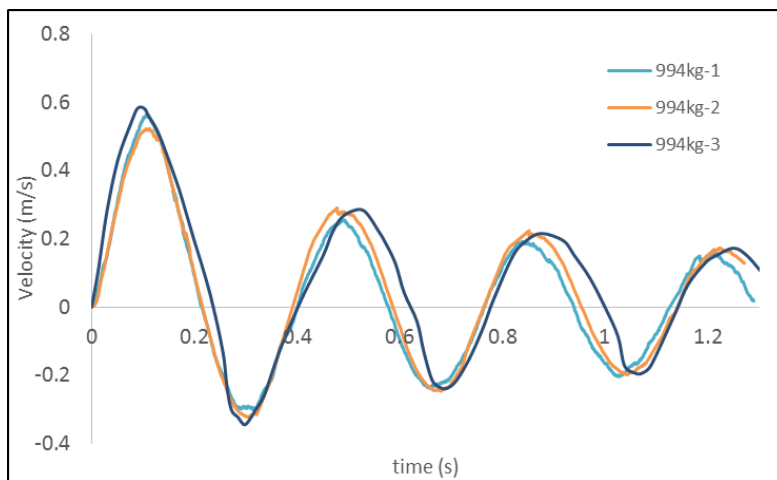


Figure 3. 31 Velocity versus time under the load of 994kg

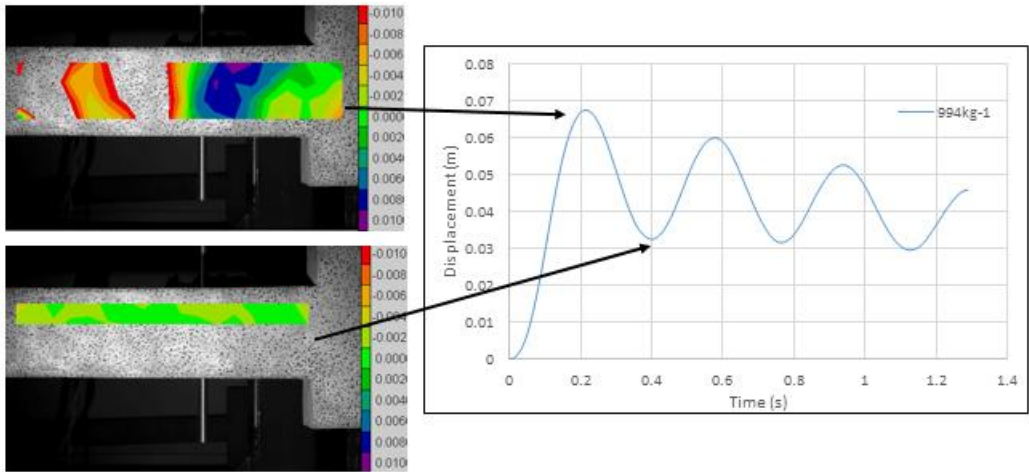


Figure 3. 32 Vertical displacement of the middle column versus time under the load of 994kg for the first time and the strain field in the horizontal direction



Figure 3. 33 Crack development after the first loading at 994kg

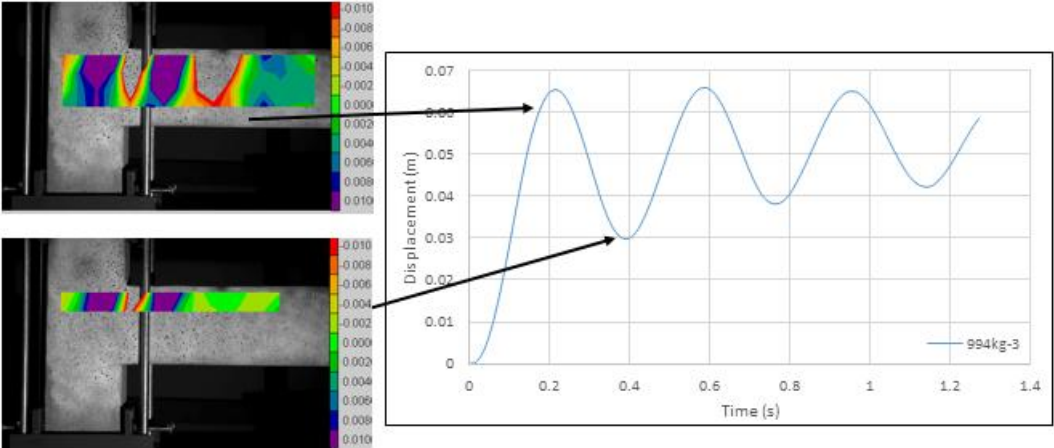


Figure 3. 34 Vertical displacement of the middle column versus time under the third loading at 994 kg and the strain of the side column in the horizontal direction



Figure 3. 35 Crack development under the third loading at 994 kg

The maximum theoretical bearing capacity of the specimen 2-1 is supposed to be 3080kg. That can be verified by finite element method considering in the quasi-static loading. Herein, the load of 2063 kg was chosen to be applied to the structure. This value is 1.5 times smaller than the max design value of bearing capacity.

The test results were reported in Figure 3. 36 and Figure 3. 37. The velocity of middle column is significantly different from the cases with preliminary loads. Under this level of load, the beam had no longer vibration with damping at the beginning. The velocity continuously increased to 0.86 m/s. Then, the speed increased slowly. When the vertical displacement was 168 mm that is almost equal to the height of the beam, the concrete in the compression zone is damaged (see Figure 3. 37). The velocity grows rapidly until the maximum velocity arrived at 1.44 m/s. Subsequently, the velocity fell down sharply from maximum value to zero. Meanwhile, the middle column arrived to maximum vertical displacement 350 mm. Tiny vibrations took place in the structure until the test stopped.

From 0.14 seconds to 0.24 seconds, a small plateau is noted in the velocity curve. Due to previous several loadings, cracks in the tension zone of the concrete around the middle column appeared. In addition, the concrete in the compression zone has also been damage. Hence, when the vertical displacement excesses 168 mm, the load carrying mechanism transformed from rotation to tension. The side column subjected to axial tensile stresses and vertical compression

started to damage (see the right of Figure 3. 37 and Figure 3. 38). That is why the velocity rose sharply again (see the red circle in Figure 3. 36) .

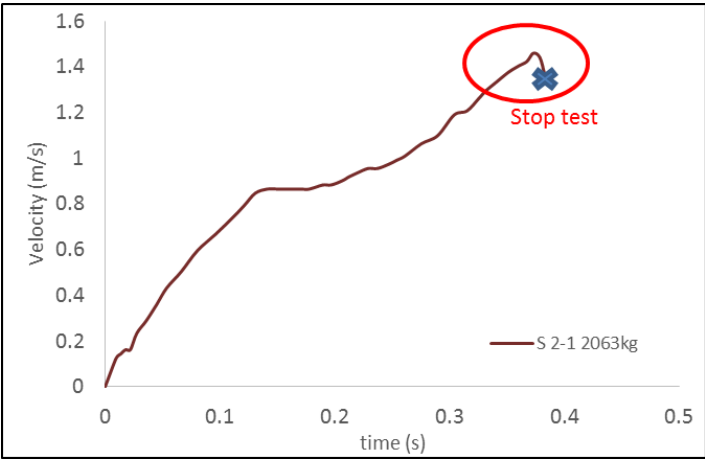


Figure 3. 36 Velocity versus time under a loading of 2063kg and after undergoing previous loading of 675kg and 994kg

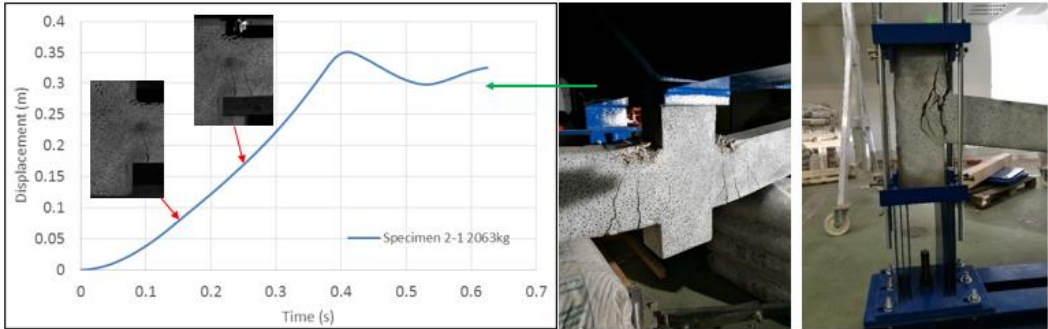


Figure 3. 37 Vertical displacement of the middle column versus time under the load of 2063kg



Figure 3. 38 Failure mode of the structure under the load of 2063kg

### 3.5.3 Specimen 2-2 L=3m 110mm×180mm

#### Loading

For this specimen, only the load of 2063 kg will be applied to the structure in order to compare its response with the previous case for which the same load of 2063kg was applied after undergoing loads of 675kg and 994kg.

#### Test data

Figure 3. 39 shows the response of the two specimens 2-1 and 2-2 supporting a loading of 2063kg. The comparison shows several differences. First, the maximum velocity was 1.11 m/s for specimen 2-2, which is much lower than the former. Second, the period of time from the beginning of test to velocity of the middle column equivalent to zero (end of the test) is a bit longer than the former case (S2-1 is 0.412 s, and S2-2 is 0.498 s). The undamaged beam seems more ductile. Third, at about 0.14s, in both cases the velocity increase very slowly even decrease a little (S2-1: from 0.141s to 0.237 s; S2-2: from 0.14s to 0.356 s). It showing a “velocity plateau”. In this phase, the cracks develops in the plastic zone and the strain in the compression zone exceeds the ultimate strain value, while plastic hinges are produced at that moment. Without repeating loads, the velocity profile shows a more flat slope and a longer time duration. On the other hand, if the structure undergoes preliminary smaller dynamic loads, the velocity plateau becomes shorter and more tilted depending on the damage degree of the structure.

The vertical displacement of the middle column is given in Figure 3. 40. The maximum displacement was 362 mm. Although it shows an obvious difference of speed between these two cases, yet there is no large gap in the total displacement. Moreover, we can observe that most of damage on the stub side column and beam occurred after a vertical displacement about 200 mm as shown in the right of the Figure 3. 40. Before the vertical displacement 200mm, the beam had only few cracks. It shows that in this case if the middle column fell down less than the height of the beam no important damage may occur. If the middle column has undergone large vertical displacement, beyond the height of the beam, the stub side column is damaged a lot as shown in the red circle on Figure 3. 40.

Figure 3. 41 shows the resisting force for tests (S2-1 and S2-2). Firstly, at the beginning of S2-1 test the first peak value was just equal to the applied load. The bending resistance of the beam was smaller probably due to preliminary loads. Specimen 2-2 did not show this phenomenon. Secondly, we see that the maximum bearing capacity of the specimen that has not undergone many loadings (S2-2) showed a much higher maximum resistance force of 30kN. It suggests that once the components are damaged, the bearing capacity under dynamic conditions is significantly reduced.

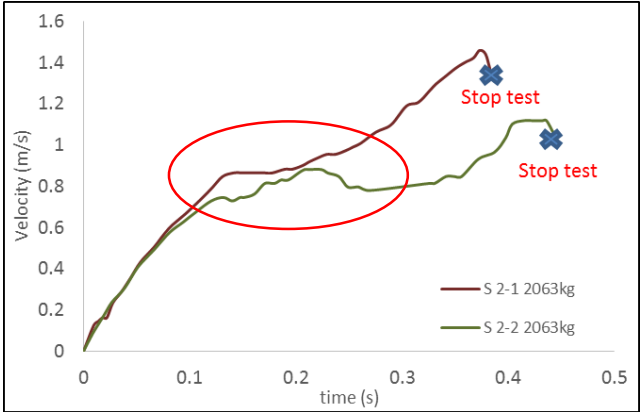


Figure 3. 39 Velocity versus time under a loading of 2063kg (the specimen 2-1 was previously loaded with multiple smaller loading; the specimen 2-2 was loaded with a unique load of 2063kg.)

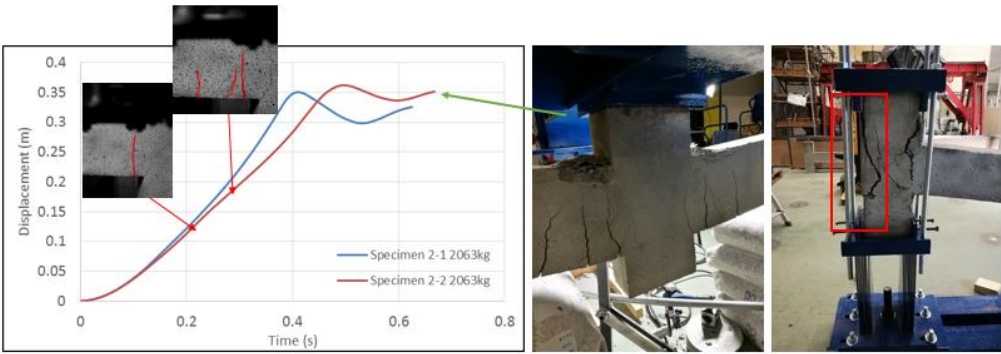


Figure 3. 40 Vertical displacement of the middle column versus time under a load of 2063kg

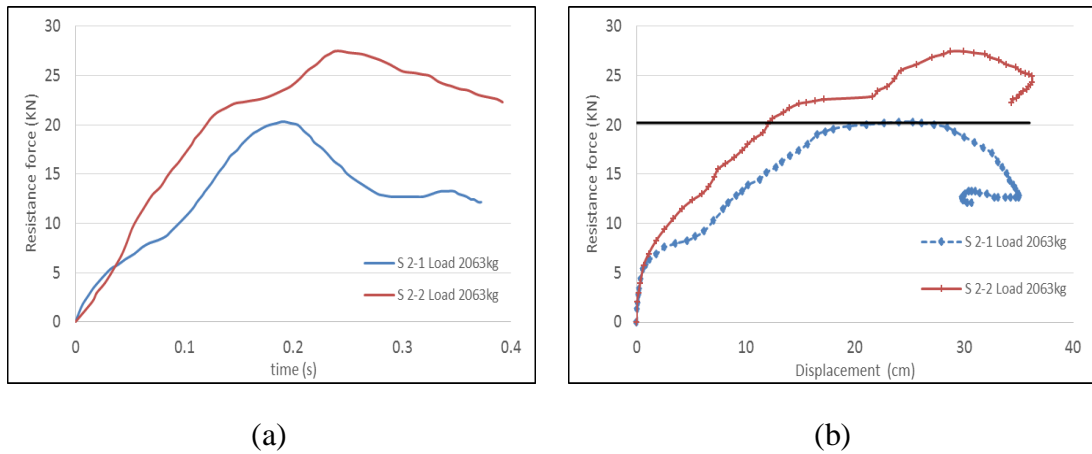


Figure 3. 41 (a) Time history of vertical resistance force; (b) Resistance force versus vertical displacement of middle column (S2-1 Load=2063kg, S2-2 Load=2063kg)

### 3.5.4 Specimen 3-1 L=3m 110mmx270mm

#### Loading

Two load levels were applied to this specimen: 994kg and 2737kg. The former was mainly used to test the dynamic elasticity of the beam. The latter was applied to the structure to characterize the collapse behavior of beam-column assemblages.

#### Test data

Figure 3. 42 shows the velocity of the middle column under the load 994 kg. The response of structure is different repeating the same loading. At the first time loading 994 kg, the falling speed of the middle column was 0.385 m/s. At the second loading 994 kg, the speed increases to 0.527 m/s. We can also observe in this test, after two cycles, the period of time became longer. It demonstrates the beam-column has almost no damage in the first test. But when the load 994kg was applied a second time to the structure, it may already exist slight damage (larger period and larger amplitude).

Under the load 994 kg for the first time, the maximum vertical displacement reached 0.04m. At that moment, the strain field shown in Figure 3. 43. Large strains are observed in certain position. It indicates the deformation is elastic and restorable. However, if repeated the same load, the maximum vertical displacement increased to 0.052m and the period of time became longer (see Figure 3. 44). In the seismic study, the degradation of stiffness of beam-column joint often occurs after four to five cycles [82] [83], while under impact load, the stiffness can degrade more rapidly even if the load applied is only forty percent of the maximum load (Engineering

design value).

It is obvious that the case with the load 2737kg shows a quite different response from previous cases with low-level preliminary loads. We can observe in the Figure 3. 45, vibration with damping is not occurring as in previous two tests. From beginning to 0.09 seconds, the velocity increased linearly. From 0.09 seconds to 0.42 seconds, the velocity entered into the velocity plateau as mentioned above. At this period of time, the cracks in the tension zone successively increased. Once passed this phase, the concrete in the compression zone started failing so the velocity rose up again, up to a maximum of 0.932 m/s. Finally, the velocity decreased sharply due to the side column failure.

Figure 3. 46 shows the strain of the beam and the vertical displacement of the middle column. The strain measurements processed by the DIC method is not very good. It only shows parts of results. The reason is that the spot quality of the specimen may be not meet our requirement completely or the position of measurement equipment is not reasonable. However, we can observe the change of strain from the first crack inception to the compressive concrete failure. The purple zone represents exiting cracks. The first crack appeared when the middle column fell down to 80mm. When the vertical displacement of middle column is equal to half height of the beam, three dominant cracks were generated. When the vertical displacement increased to about 270 mm, which is equal to the height of the beam, the compressive concrete started to crush and fell out. Finally, the maximum displacement arrived to 434 mm for this case. After that, the structure had almost no obvious vibration until it stopped. The stub column came out serious damage due to tension force as shown in Figure 3. 47.

Figure 3. 48 gives the resistance (support force) of the structure over time. The test results are basically the same as those in the previous test. At the instant of removing the middle support, the resistance had a big jump. Then, the bearing capacity increased gradually, and slowly dropt after reaching the peak value. We observe that for this test the resistance force did not increase due to dynamic effects. The maximum value was basically equal to the applied load (2737kg). Table 3.7 reported the key value from a series of dynamic tests.

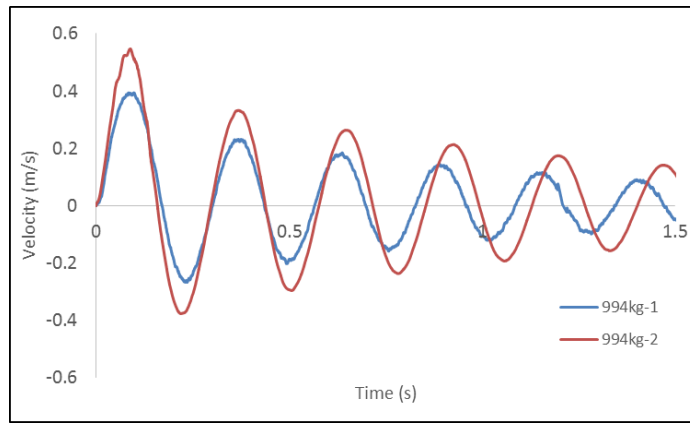


Figure 3. 42 Velocity versus time under successive loads of 994kg

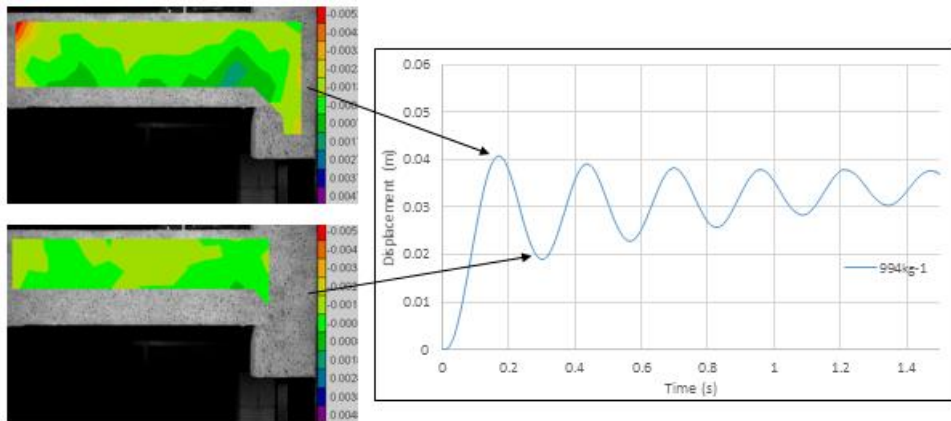


Figure 3. 43 Vertical displacement of the middle column versus time and strain field under the load of 994kg (first loading time)

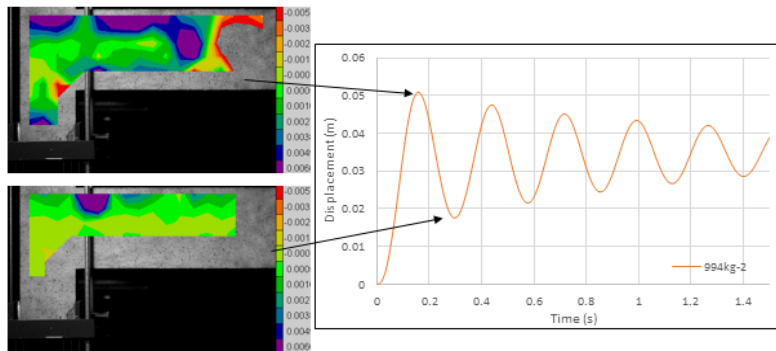


Figure 3. 44 Vertical displacement of the middle column versus time and the strain under the load of 994kg (second loading time)

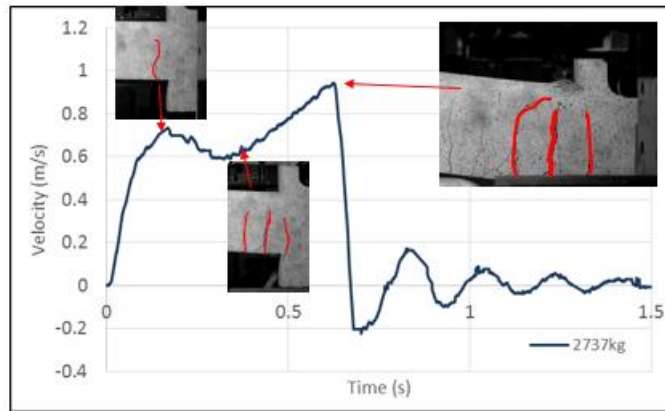


Figure 3. 45 Velocity versus time under the load 2737kg (third loading time)

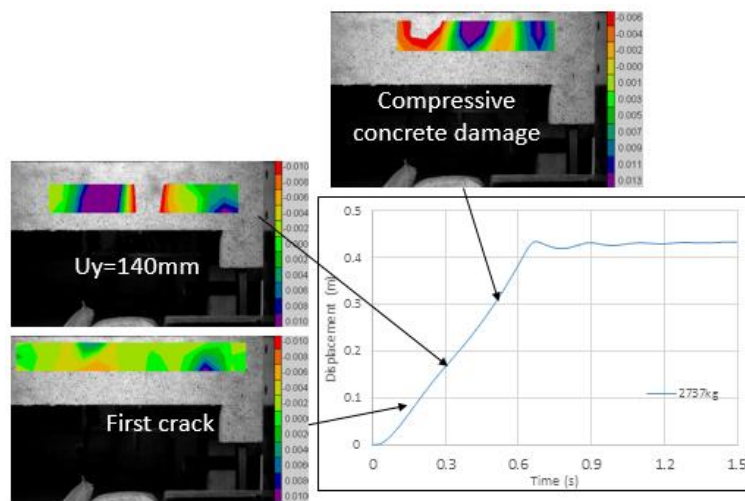
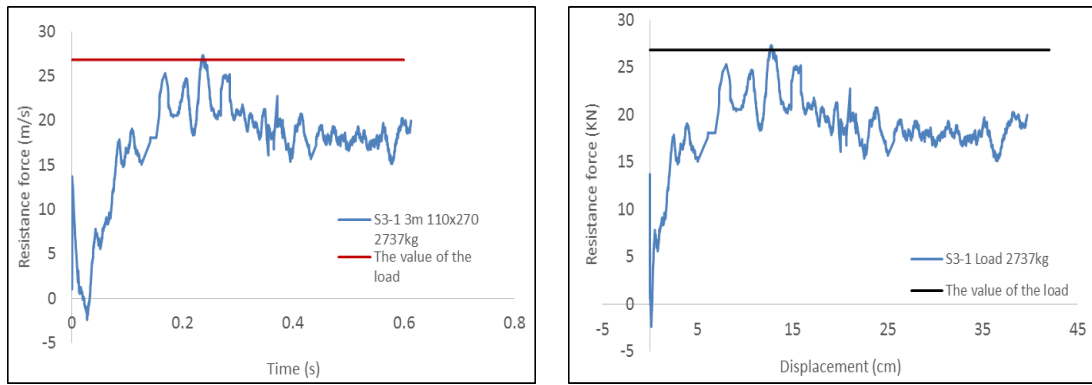


Figure 3. 46 Vertical displacement of the middle column versus time and strain field under the load 2737kg (third loading time)



Figure 3. 47 Damage of structure under the load of 2737kg at the end of the test



(a)

(b)

Figure 3. 48 (a) Time history of vertical resistance force; (b) Resistance force versus vertical displacement of middle column (S3-1 Load=2737kg)

Table 3. 7 The summary of experimental results

No.	Specimen dimension	L/h	Reinforcement ratio	Applied load (kg)	Design load (kg)	Max V (m/s)	Max displ (mm)
S1-1	L=2000mm bxh 110x180	11.11	2.28%	2662	2875	0.433	76.2
S2-1	L=3000mm bxh 110x180	16.67	2.28%	675-1	1592	0.194	18.4
				675-2	1592	0.413	44.3
				675-3	1592	0.429	44.8
				675-4	1592	0.431	45.5
				994-1	1592	0.55	66.6
				994-2	1592	0.515	64.4
				994-3	1592	0.561	64.5
				2063	1592	1.44	-
S2-2	L=3000mm bxh 110x180	16.67	2.28%	2063	1592	1.12	-
S3-1	L=3000mm bxh 110x270	11.11	1.52%	994-1	2790	0.387	40.3
				994-2	2790	0.532	50.2
				2737	2790	0.916	-

### 3.6 The dynamic analysis of the beam-column assemblages

#### 3.6.1 Calculation of vibration properties $\zeta$ , $\omega_D$ , $T_D$

As described earlier, few dynamic testing results were presented in recent literatures. Study on

the dynamic response is very important for a structure that is losing a support. Herein this part focuses on the analytical evaluation of dynamic characteristic of the beam column assemblages. This test system, including two supports, a specimen and the upper mass, can be considered as a single-degree-of-freedom (SDF) system by supporting that the mass is concentrated at one location as shown in Figure 3. 49. The lateral displacement is supposed to be small that it can be neglected.

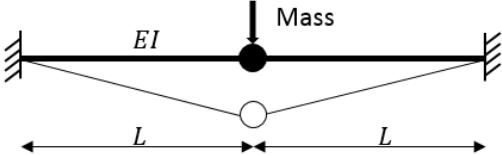


Figure 3. 49 Dynamic analysis diagram

Considering the section of the beam, its material elastic modulus  $E$ , rotational inertia  $I_z$  and the span  $L$  of the assemblages; the end column stubs are fixed on the supports. The stiffness of the beam is given by [84] [85]

$$k = \frac{192EI_z}{(2L)^3} \tag{3.9}$$

The parameters of each specimens being known, the stiffness of the beam are calculated as shown in Table 3. 8.

Table 3. 8 The stiffness of the beam

Specimen	Span (mm)	Beam section (mm)	The stiffness of the beam $k$ (N/m)
S1	2000	110×180	1.54e6
S2	3000	110×180	4.35e5
S3	3000	110×270	1.08e6

According to structural dynamics theory, it is easy to know the natural circular frequency of vibration [84]

$$\omega_n = \sqrt{\frac{k}{m}} \tag{3.10}$$

$m$  being the applied mass plus the equivalent self-mass of the specimen. The natural period of vibration is then equal to

$$T_n = \frac{2\pi}{\omega_n} \quad (3.11)$$

According formula (3.18) and (3.19), the period of vibration can be known in the idealized boundary condition of Figure 3. 49 without damping.

As it is known, the building, bridges, dam and so on are restricted to underdamped systems. However, as typically, their damping ratio is less than 0.1. In this dynamic test, after removing the steel middle support, the system starts free vibrating with damping. The differential equation of motion governing the beam deflection is

$$m\ddot{u} + c\dot{u} + ku = Mg \quad (3.12)$$

where  $\dot{u}$  denotes the velocity of the mass;  $\ddot{u}$  denotes its acceleration; the constant  $c$  being the damping coefficient.

The initial conditions, the displacement of the mass and the velocity at time zero, can be defined as

$$u(0) = 0 \quad \dot{u}(0) = 0 \quad (3.13)$$

Subject to these initial conditions, the solution to the differential equation is obtained

$$u(t) = e^{-\zeta\omega_n t} \left[ \frac{u(0) + \zeta\omega_D u(0)}{\omega_D} \sin\omega_D t + u(0)\cos\omega_D t \right] \quad (3.14)$$

Where

$$\omega_D = \omega_n \sqrt{1 - \zeta^2}, \quad \zeta \ll 1 \quad (3.15)$$

And

$$\zeta = \frac{c}{2m\omega_n} \quad (3.16)$$

$\zeta$  is the damping ratio. The natural period of damped vibration,  $T_D = 2\pi/\omega_D$ , is related to the

natural period  $T_n$  without damping by

$$T_D = \frac{T_n}{\sqrt{1-\zeta^2}}, \quad \zeta \ll 1 \quad (3.17)$$

The displacement amplitude of the undamped system is the same in all vibration cycles, but the damped system oscillates with amplitude, decreasing at each cycle of vibration. Equation (3.14) indicates that the displacement amplitude decays exponentially with time. Derived from equation (3.14), the ratio  $u_i/u_{i+1}$  of two successive peaks of damped free vibration is given by

$$\frac{u_i}{u_{i+1}} = e^{\zeta\omega_n T_D} = e^{\frac{2\pi\zeta}{\sqrt{1-\zeta^2}}}, \quad i = 1,2,3 \dots \quad (3.18)$$

The logarithm of this ratio, called the logarithmic decrement, can be calculated by knowing  $\zeta$ :

$$\delta = \ln \frac{u_i}{u_{i+1}} = \frac{2\pi\zeta}{\sqrt{1-\zeta^2}}, \quad i = 1,2,3 \dots \quad (3.19)$$

To be more precise, several cycles would be used, for example 5, equation (3.20) can be written as

$$\delta = \frac{1}{5} \ln \frac{u_i}{u_{i+5}} = \frac{2\pi\zeta}{\sqrt{1-\zeta^2}}, \quad i = 1,2,3 \dots \quad (3.20)$$

So far now, the natural circular frequency of vibration and the period of vibration without damping can be known from equation (3.15) and (3.17). Meanwhile based on the dynamic test data,  $\delta$  can be measured and  $\zeta$  can be calculated by equation (3.20). Furtherly, the natural frequency of damped vibration and the period of damped vibration can be obtained from equation (3.15) and (3.17). Since large loads were applied to the specimen 1-1 and 2-2, harmonic vibration response of the specimen were not observed except at the end of the experiment. Hence, the natural frequency and the period of vibration of the system with damping were not studied for both of these two cases. The calculation results of the other tests were reported in Table 3. 9. From this table, we can observe some features as following:

a. First, seeing the calculated damping ratio, the damping ratio of beam-column structure is quite small, about 0.01 to 0.03. That means that little energy is dissipated by the damping for the reinforced concrete structure which is already a well-known results. The damping ratio for the typical reinforced concrete structure is 0.01 to 0.08.

b. For the same specimen, repeating the same load makes the damping ratio decrease. It indicated that the original beam-column structure occurred in varying degrees of damage due to the repetitive load, which may result in the reduction of stiffness of the beam-column structure. The lower stiffness the structure has, the smaller the damping ratio. It shows a positive correlation between stiffness and damping ratio. In addition, for the specimen S2-1, when the load was increased from 675 kg to 994 kg, the damping ratio was enhanced even if the specimen had undergone several times loading as well as an indication of the stiffness degradation had been shown. It illustrates the quality of the structure has a signification effect on the damping. With greater mass, higher the damping ratio are obtained. Noted that with specimens 2-1 and 3-1 the loads were applied at the first time, but with specimen 3-1 which has a larger mass and stronger stiffness than specimen 2-1, a lower damping ratio was obtained than with the specimen 2-1. This may be because the specimen 3-1 subjected to the load of 994 kg leads to inelastic deformation. This result manifested in the displacement curve where the gap between the first peak and the second peak narrowed. Thus the damping ratio is also reduced.

c. The natural period  $T_n$  are 0.303 s and 0.348 s for the specimen 2-1 under different load. For the specimen 3-1 with the load of 994 kg, the natural period is 0.233 s. From equation (3.10) and (3.11), it can deduce that  $T_n$  is related to the mass and stiffness. The natural period is extended with increasing the mass, and the natural period is shorten with stronger stiffness of the structure since  $T = 2\pi\sqrt{m/k}$ . The natural period of damped vibration is about 0.304s and 0.348s for the specimen 2-1 under the load of 675 kg and 994 kg. For the specimen 3-1, the natural period of damped vibration is 0.233 s. Duo to the small damping ratio of the assemblages, the natural frequency and period of the structure with damping is very close to that the structure without damping. Damping has the effect of lowering the natural frequency from  $\omega_n$  to  $\omega_D$  and lengthening the natural period from  $T_n$  to  $T_D$ . Through calculation and comparison, these

effects are negligible when the damping ratio is below 20% [84].

From the comparison of the analytical values with experimental values, it can be found that the experimental value is close to the analytical values. Especially for the first load applied to the specimen 2-1, the error between the experimental values and analytical value was only 1.87%. After repeating the load, the gap between the experimental value and analytical value was increased, which is also due to changes in the stiffness of the specimen. The maximum error was 15.57% when the second load was applied to the specimen 3-1. By comparison analysis and experimental feedback, the experiment is successful and feasible. It is important that the entire system, including specimen, supports and loading device, is suitable for simulating the collapse process of beam-column assemblages.

Table 3. 9 The frequency and period of damped vibration

Specimen	Load	$\omega_n$ (rad/s)	$T_n$ (s)	$\zeta$	$\omega_D$ (rad/s)	$T_D$ (s)	$T_{test}$	Error (%)
S2-1 l=3000mm 180x110	675kg-1	20.7	0.303	0.029	20.70	0.301	0.298	1.01
	675kg-2	20.7	0.303	0.016	20.70	0.303	0.314	3.34
	675kg-3	20.7	0.303	0.017	20.70	0.304	0.321	5.45
	675kg-4	20.7	0.303	0.013	20.70	0.303	0.325	6.62
	994kg-1	18.1	0.348	0.017	18.06	0.348	0.375	7.22
	994kg-2	18.1	0.348	-	-	-	0.377	
S3-1 l=3000mm 270x110	994kg-1	27.0	0.233	0.019	26.96	0.233	0.257	9.32
	994kg-2	27.0	0.233	0.011	26.96	0.233	0.276	15.57

### 3.5.2 Evaluation of the damage state of the sub-assemblages under dynamic loads

Through discussed above, we know the basic vibration characteristics of the beam-column assemblages subjected to accidental loads. It can be used to evaluate their damage degree after applied loads of different levels. According to the test data, we can know the experimental value of the frequency of vibration  $\omega_t = 2\pi/T_t$ ; As above mentioned, the effect of the damping ratio can be neglected. That means  $\omega_D \approx \omega_n$  as well as

$$\omega_t \approx \omega_n \quad (3.20)$$

Substituting equation (3.9) and (3.20) into equation (3.10), we can have

$$\omega_t = \sqrt{\frac{192EDl}{m(2L)^3}} \quad (3.21)$$

Arranging the equation (3.21), the Young' modulus of damage concrete  $E_D$  is given by

$$E_D = \frac{m\omega_t^2(2L)^3}{192I} \quad (3.22)$$

Here the damage degree of the beam-column assemblages, described by a scalar damage variable  $d_c$ , can be defined as

$$d_c = 1 - \frac{E_D}{E} \quad (3.23)$$

By equations (3.21), (3.22), (3.23), Table 3. 10 calculated the elastic moduli and damage factors of the specimens under different loads. As can be seen, even in the case of small loads, the components are subject to varying degrees of damage. After the repeated load of 675 kg for the S2-1, the damage factor increases to 0.128. After the repeated load of 994 kg, the damage factor reach 0.171. If applied a larger load at the first time, the damage is more serious (see S3-1 in the Table 3. 10).

This dynamic analysis may be used to improve the numerical simulation in term of natural period (t) and damage of the beam on boundary conditions (fixed, sliding, rotation).

Table 3. 10 Damage factor of the structure under different level loads

Specimen	Load	$\omega_t$ (rad/s)	$E_D$ (GPa)	$d_c$
S2-1 l=3000mm 180x110	675kg-1	21.1	31.1	-
	675kg-2	20.0	28.0	0.066
	675kg-3	19.6	26.8	0.106
	675kg-4	19.3	26.2	0.128
	994kg-1	16.8	25.8	0.139
	994kg-2	16.7	25.5	0.149
	994kg-3	16.4	24.9	0.171
S3-1 l=3000mm 270x110	994kg-1	24.4	24.7	0.178
	994kg-2	22.8	21.4	0.287

# Chapter 4 Application of connector in simulating bond-slip behavior

## 4.1 Introduction

To simulate the behavior of beam-column assemblages under removal of the middle support scenario, the problem has two difficulties: one is that the concrete members suffer from brittle failure. Therefore, an efficient constitutive model of concrete is imperative to describe the strength reduction of concrete after cracking and damage. Another difficult point is how to deal with the interaction between steel bars and concrete, especially in the post-stage where the steel bar is going to play an important role for resistance overload after the concrete in the compression or tension zone has been suffering from serious damage.

According to above circumstances, the concrete damage model, named DFH-KST model, was used in this numerical calculations. The objective of this chapter is to present an approach for capturing the bond-slip behavior between steel bar and concrete with a type of spring wire connector, that will be used in the numerical model with the commercial finite element code ABAQUS. Contrary to other methods that rely on two springs in two directions (longitudinal and transverse) [47][86]–[89], this approach only need to build a connector with a model for describing the relationship between steel bar and concrete. Previously, a few research papers referred to this function in ABAQUS due to difficulties to identify the model and the corresponding parameters of connector. Herein a reasonable model is identified and then validated from pull-out tests.

## 4.2 The concrete constitutive model

DFH model is based on the concept of probability of non-obscuration, and predicts the tensile damage and the crack density in a loaded volume subjected to tensile loading for any size, shape of the loaded volume, stress gradients, and stress-rates [77][90]. It was demonstrated to be suitable for brittle materials such as concrete ultra-high strength, limestone rock, soda-limet silicate glass. In this model, three damage variables are used associated to each cracking directions ( $d_i$ ) assumed to be orthogonal. The strain tensor  $\varepsilon$  is related to the stress tensor  $\Sigma$  by

[90]

$$\varepsilon = K(D_1, D_2, D_3)\Sigma \quad (4.1)$$

The compliance tensor K is defined by

$$K(D_1, D_2, D_3) = \frac{1}{E} \begin{bmatrix} \frac{1}{1-D_1} & -\nu & -\nu \\ -\nu & \frac{1}{1-D_2} & -\nu \\ -\nu & -\nu & \frac{1}{1-D_3} \end{bmatrix}_{(d_1, d_2, d_3)} \quad (4.2)$$

where E is the Young's modulus and  $\nu$  the Poisson's ratio of the undamaged material. The growth of each obscuration probability variable  $P_{oi}$  associated to each principal microscopic stress is computed according to equation (4.3)

$$\frac{d^{n-1}}{dt^{n-1}} \left( \frac{1}{1-D_i} \frac{dP_{oi}}{dt} \right) = n! S(kC_0)^n \lambda_t[\sigma_i(t)] \quad \text{when } \frac{d\sigma_i}{dt} > 0 \text{ and } \sigma_i < 0 \quad (4.3)$$

Assuming a constant stress rate ( $\sigma_i(t) = \dot{\sigma}_i t$ ),  $kC$  is the velocity of a propagating crack, S is a shape parameter, the power  $n=1,2,3$  is the space dimension. All these characteristic parameters can be identified [91].

The macroscopic strength is related to the obscuration probability according to:

$$\Sigma_i = (1 - P_0^i)\sigma_i + (P_{oi})^{\alpha_D} \sigma_i^{coh} = (1 - D_i)\sigma_i \quad (4.4)$$

where  $P_0^i$  is obscuration probability. The cohesion strength in obscured zones  $\sigma_i^{coh}$  is expressed as

$$\sigma^{coh}(\varepsilon, \dot{\varepsilon}) = \sigma_0^{coh} \cdot \exp\left(-\left(\frac{\varepsilon}{\varepsilon_0^{coh}}\right)^{n_{coh}}\right) \cdot \left(\frac{\dot{\varepsilon}}{\varepsilon_0^{coh}}\right)^{\frac{m}{m+n}} \quad (4.5)$$

where  $\sigma^{coh}$ ,  $\varepsilon_0^{coh}$ ,  $n_{coh}$  are parameters to be fitted from experimental data of quasi-static and dynamic tensile tests. The present model has been implemented as a VUMAT routine in ABAQUS.

### 4.3 Connector technology

#### 4.3.1 Connector elements

Connectors allow to model the mechanical relationships between two points in an assembly. The connection can be simple, such as a link, or the connection can impose more complicated constraints, such as constant velocity joints. The connector geometry is modeled using an assembly-level wire feature that contains one or more wires. The wires may connect two points in an assembly or connect a point to ground. A connector section needs to be created that specifies the type of connection and connector behaviors, such as spring-like elasticity behavior. One connector is completed after creating a connector section assignment that associates a connector section with the wires. In this study, the type of connector element CONN3D2 was adopted, which could be used to deal with three dimensional problems.

#### 4.3.2 Connector behavior

The behavior of wire connector is related to a damage evolution law. The non-linear model of spring wire is showed in Figure 4. 1. The behavior of connectors is controlled by five parameters, which are the spring stiffness, the yield force, damage initiation displacement, ultimate failure displacement and exponential parameter, corresponding to these three phases, elasticity, plasticity and damage. Whereas some parameters have not been subjected of extensive research, in this study, we try to combine the experimental work to find a series of parameters for describing the slip and damage at the interface.

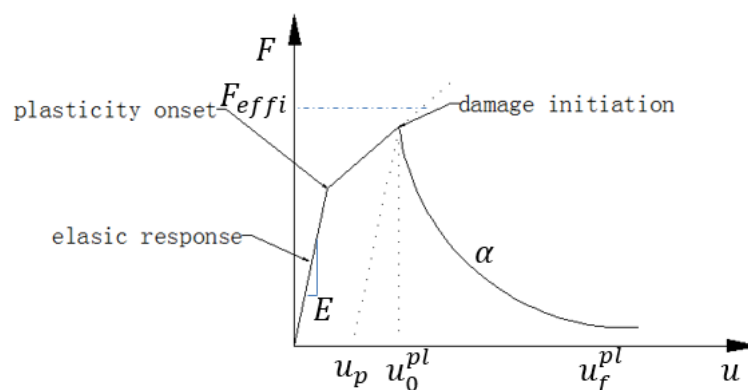


Figure 4. 1 Connector damage evolution

#### Definition of linear uncoupled elastic behavior of connector

In the simplest case of linear uncoupled elasticity (see ABAQUS Analysis User's Manual

31.2.2) [92], the spring stiffness is defined for the selected components. It can be expressed according to the equation

$$F_i = D_i u_i \quad (4.6)$$

where  $F_i$  is the force in the elastic range and  $u_i$  is the connector displacement.

### **Definition of plasticity behavior**

To define connector plasticity behavior, it is necessary to defined yield function upon which plastic flow is initiated as well as hardening behavior to define the initial yield value and, optionally, the yield value evolution after plastic motion initiation. The yield function  $\emptyset$  is defined as

$$\emptyset(f, \bar{u}^{pl}) = P(f) - F^0 \quad (4.7)$$

where  $f$  is the collection of forces and moments in the available components of relative motion that ultimately contribute to the yield function; the connector potential  $P(f)$ , defines a magnitude of connector tractions similarly to defining an equivalent state of stress in Mises plasticity.  $F^0$  is the yield force. The connector relative motion  $u$ , remain elastic as long as  $\emptyset < 0$ ; and when  $\emptyset = 0$ , plastic flow occurs (see ABAQUS Analysis User's Manual 31.2.6).

### **Damage formulation in connectors**

If relative forces or motions in a connection exceed critical values, the connector starts undergoing irreversible damage. In ABAQUS, it offer two damage models, linear damage evolution law and exponential damage evolution law. The former is for a truly linear damaged force response, only in the case of linear elastic or rigid behavior with optional perfect plasticity; the latter is for a truly exponential damaged behavior. Obviously, the latter can meet our requirements.

The force response in the connector component is changed according to the following general form

$$F_i = (1 - d_i) F_{effi} \quad 0 \ll d_i < 1 \quad (4.8)$$

where  $d_i$  is a scalar damage variable;  $F_{effi}$  is the response in the available connector component of relative motion  $i$  if damage is not present. The damage initiation criterion can be specified in terms of an equivalent relative plastic motion in the connector. When the equivalent relative plastic motion as defined by the associated plasticity definition is greater than the specified limit value  $u_0^{pl}$ , damage is initiated. A damage variable evolution  $d$  is given by the following equation

$$d = \frac{1 - e^{-\alpha(u^{pl} - u_0^{pl}) / (u_f^{pl} - u_0^{pl})}}{1 - e^{-\alpha}} \quad (4.9)$$

where  $\alpha$  is an exponential coefficient,  $u_f^{pl}$  is the ultimate plastic motion at failure and  $u_0^{pl}$  is the plastic motion at damage initiation.

#### **4.4 Identification and validation of parameters from pull-out tests**

##### **4.4.1 Identification of parameters**

Pull-out tests with steel bar of diameter 12 mm have been carried out by P. Forquin and W. Chen [93]. The height of specimen is 240 mm and the diameter of concrete is 160 mm with a steel bar standing at the center of the specimen. The rebar anchorage length is 50 mm. One end of the sample was fixed; on the other side, the steel bar is loaded, by applying a quasi-static displacement. Thanks to this test, we can obtain a relationship between the pull-out force and the displacement as shown in Figure 4. 2. The modelling parameters used in the connector element can be identified by the test results. They are shown in Table 4. 1 for reinforcement bars D12mm.

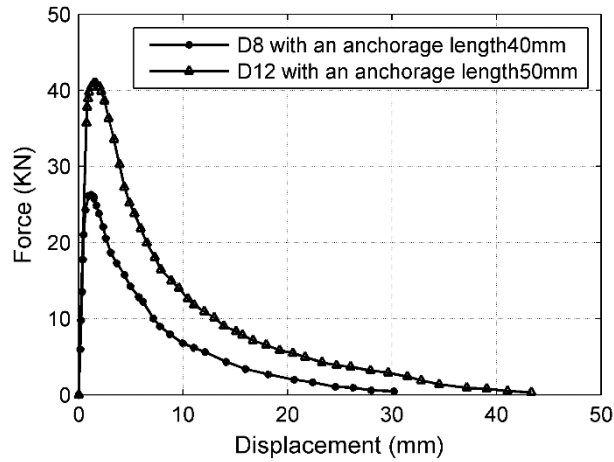


Figure 4. 2 Evolution of force versus displacement for the pull out tests

Table 4. 1 Parameters of connector law (with hardening) for D12mm

elastic behavior	$D_i$ Spring stiffness (N/m)	4.263e7	
Plastic behavior	$F_y$ the yield force (N)	7778	
	Plastic hardening	Force (N)	Motion (m)
		7778	0
		7956	8.69e-5
		8095	3.04e-4
8194	5.65e-4		
Damage evaluation	$U_i$ damage initiation (m)	5.65e-4	
	$U_f$ ultimate failure (m)	0.0433	
	$\alpha$ exponential parameter	5	

When the spring-wire connectors are created, a nonlinear damage behavior is assigned at the interface of steel rebar and concrete numerical specimen. A mesh was constructed in such a manner that nodes of the rebar coincide with the nodes of the specimen.

#### 4.4.2 Numerical model of pull-out test

A 3D symmetric finite element formulation in ABAQUS is used to simulate the pull out test where a single rebar is pulled out from a quarter cylindrical concrete specimen as shown in Figure 4. 3. Linear hexahedron elements of type C3D8R of size 10 mm, were used for concrete and a linear line T3D2 elements were used for the rebar. The interface is characterized by the spring-like connectors using element type CONN3D2 with damage behavior. They were set along the rebar as shown in Figure 4. 4. The nodes on the steel bar were connected with the corresponding nodes of the concrete element along the wire. According to the anchorage length,

four or five connectors were set with in the numerical model with reinforcement bar diameter 12 mm. The boundary condition and load are illustrated in Figure 4. 3. The top surface of the specimen was fixed. Other lateral surfaces were set with appropriate constraint as symmetric planes. The pull out load was applied at the top node of the rebar.

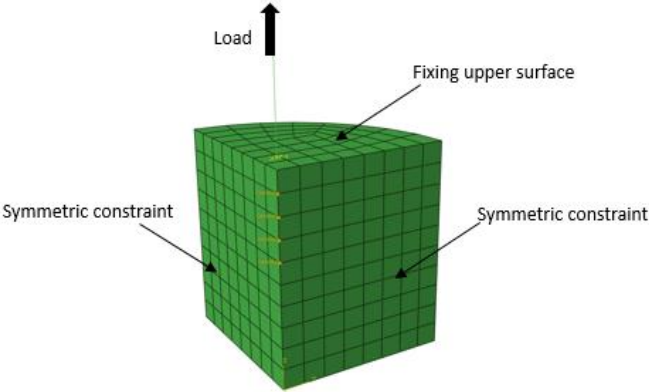


Figure 4. 3 Boundary and loading conditions for the FE model

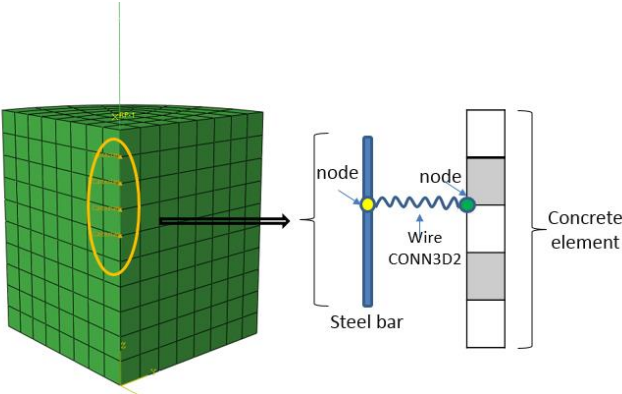


Figure 4. 4 Schematic representation of connector in FE model

**4.4.3 Identification the connector parameters (D12mm)**

Figure 4. 5 (a) shows the force and displacement data obtained numerically from both elastic model and concrete damage model. The response is initially linear with the stiffness which represents the spring-like connector that has not undergone any plasticity or damage. Then the spring wire develops forwards its plastic behavior. Force increases and reaches the peak value 40.3kN when the displacement is almost 2 mm and then connector starts undergoing irreversible damage and the force is decreasing exponentially. From the comparison, it can be concluded that the DFH-KST damage model combined with the connector behavior law give reasonable result with the values obtained from the pull out experiment. Indeed, force-displacement curve

of the case with damage concrete model is quite well correlated with the experimental curve. It works better than the case with the elastic concrete model. However, the peak is not well in good agreement, perhaps because the concrete element that was connected with the node of rebar was damage so that the force did not reach the value of the peak of the experiment. The effect of confinement or of sliding phenomenon could also be different from the actual failure mode in the experiment. Figure 4. 5 (b) shows the response of the single connector that illustrates a weak disparity of the peak value between using elastic model and damage model for the concrete. The bond stress is weakened in the latter due to some location of damage in concrete.

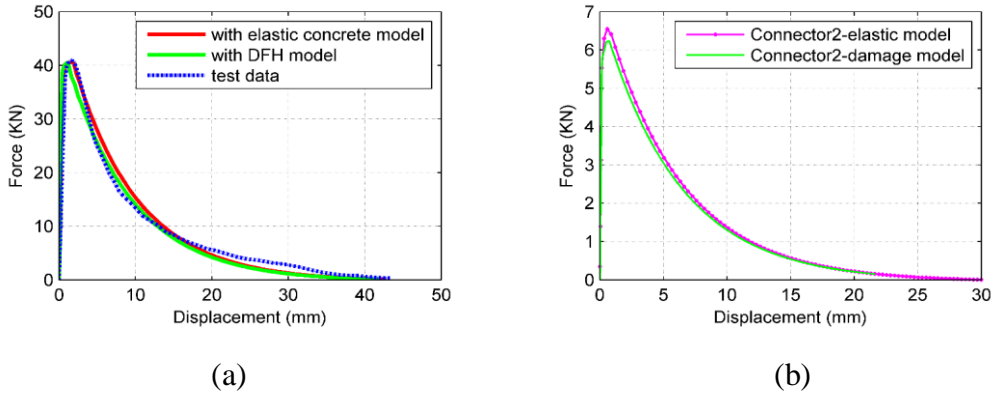


Figure 4. 5 (a) Pull out force versus displacement of steel bar; (b) The response of the single connector (D12mm)

As above mentioned, the calculation results with D12mm rebar are matching well with test data. The model describes accurately the interaction behavior between reinforcement bar and concrete. The parameters obtained from pull-out test have been validated. Next, the connector function and all these parameters were introduced into the beam-column subassemblies to study the influence of connection mode of reinforcement bar in the behavior of RC beam.

**4.4.4 The effect of different restrain modes on the beam**

In this section, three different constraint reinforcement bar modes were set in the concrete model in order to study the effect of interaction between steel bar and concrete on the structure. A 3D symmetric numerical model of beam-column was built in the ABAQUS software as shown in Figure 4. 6. Two sides of the beam had no vertical displacement ( $U_2=0$ ) and neither rotation as boundary conditions. A displacement load was applied to the top of the middle column.

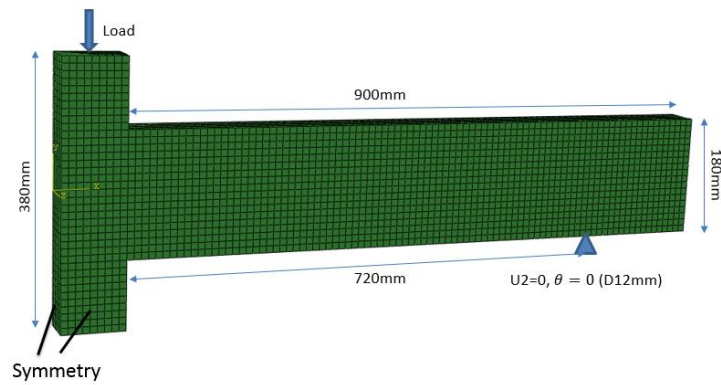
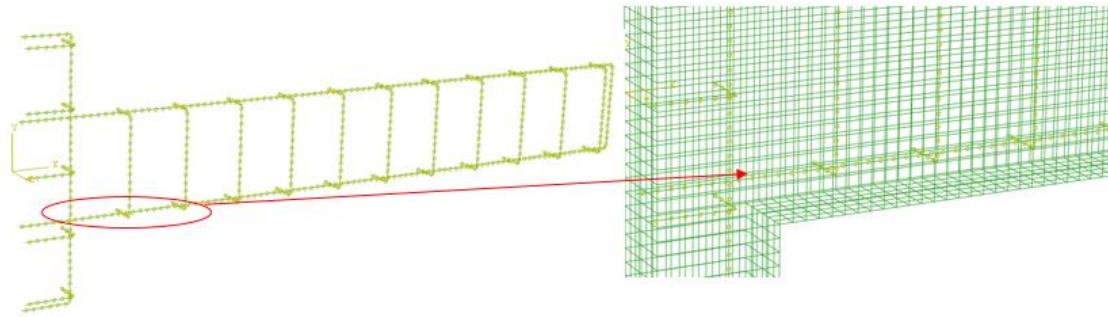


Figure 4. 6 The numerical model of the beam-column assemblage

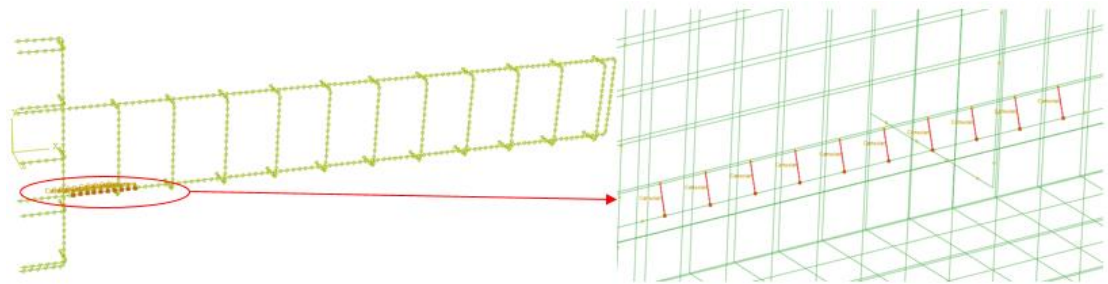
Three different constraint reinforcement bar modes were considered:

- a. Fully embedded reinforcement in concrete.
- b. Embedded reinforcement except in the plastic hinge region where connectors are used.
- c. Embedded reinforcement but no use of connector and embedded in the plastic zone.

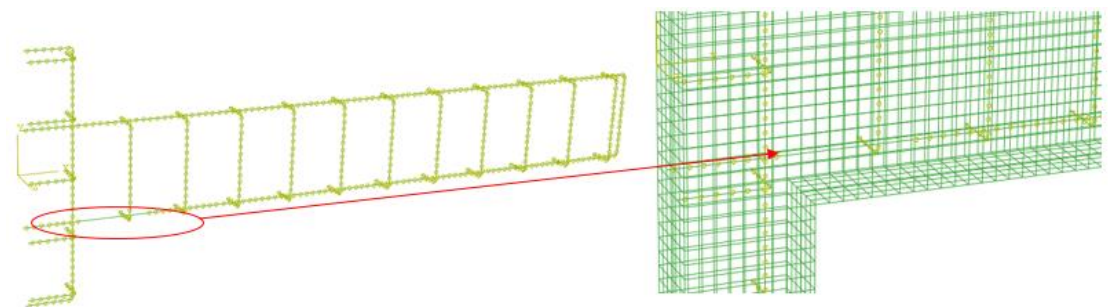
Figure 4. 7 shows the three different restraint modes of reinforcement bars in the concrete. The first (a) is a very common method to set the reinforcement bars in the concrete and is widely used in various kinds of commercial softwares. It is used to specify that an element or group of elements is embedded in “host” elements. ABAQUS searches for the geometric relationships between nodes of the embedded elements and the host elements. If a node of an embedded element lies within a host element, the translational degrees of freedom at the node are eliminated and the node becomes an “embedded node.” The translational degrees of freedom relative displacement of the embedded node are constrained to the interpolated values of the corresponding degrees of freedom of the host element. The second approach (b) is proposed in this section. The CONN3D2 type of element is used for the spring-wire connector. Ten connectors nodes are used in the plastic hinge zone (on a length of 100mm) to observe the influence of connector links and eventually to compare with other two calculations.



(a) Embedded all the steel bars in the concrete



(b) Addition connectors between steel bars and concrete in the plastic zone



(c) Without connector or embedded restraint on the rebar in the plastic zone

Figure 4. 7 Numerical model of reinforcement cage for the three studied cases

Figure 4. 8 compares the calculation results with experimental data. There is a significant influence on the bearing capacity of the beam-column sub-assemblages when comparing overall embedded reinforcement and use of connectors. It is the same if we compare the case with connector and with no restraint on the reinforcement bars, the component can still support bearing capacity at later stage (after the vertical displacement reaching 30mm). It illustrates the reinforcement bar played its role effectively after concrete damaged gradually. On the contrary, the bearing capacity of structure with embedded reinforcing steel bars was decreasing at later time, especially after the vertical displacement exceeded 28mm.

In addition, it is noted that there is a jump in the force-displacement results when the vertical displacement of middle column reached about 18mm. At the left of Figure 4. 8, two images of concrete damage are pinned. We can observe that in the compression zone, the concrete was crushed and a crack ran through the beam. A great number of local element had failed at the same time leading to a significant fall of the carrying capacity.

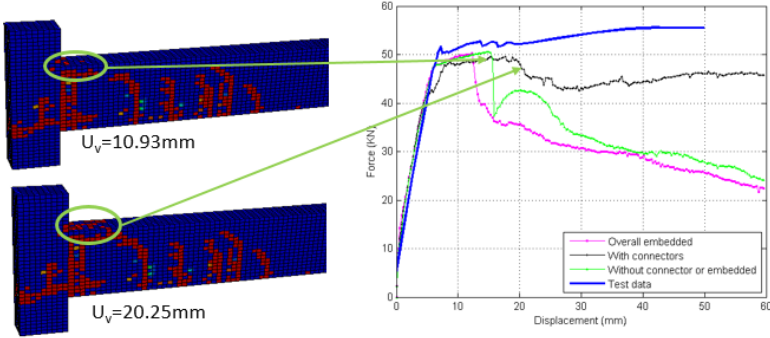
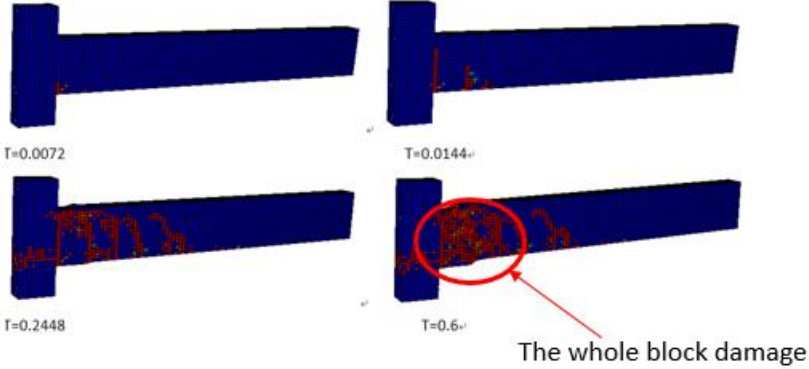


Figure 4. 8 Effect of different constraint modes of rebars on bearing capacity (D12mm) of beams

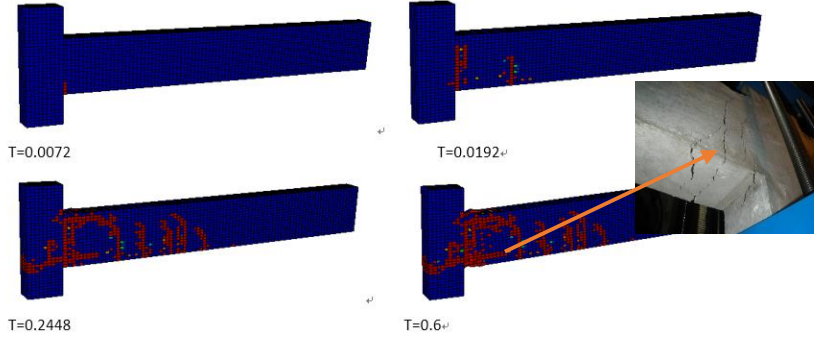
According to the comparison above, it is also found that there is no significant influence on the bearing capacity of beam-column for the cases (b) and (c). However, it could affect the cracking development and damage failure mode.

Figure 4. 9 shows the failure process of the concrete beam for the three cases (a), (b), (c) during the whole test. About initial development of cracks, the cases (a) and (b), both of them match with the experiment. The damage of the beam is controlled by two main cracks. The main difference is the damage mode. In the first case (a), entire embedded, we can see damage concentration at the position of the joint. In fact, this method just increases the stiffness of the element that contains the reinforcement bar. Hence, the load had to be undertaken by the concrete elements. However, in the second case (b), there are still several dominant cracks in the plastic zone at final failure mode. And it is noted that the steel bar boundary point from embedded part to connector part is damage earlier than connector part. Because it started to play a role when the bond stress reach a certain level. That means once the force applied on the concrete, it could be transferred to the reinforcement bars. That is why we often see some horizontal fine cracks on the surface of the beam. About the last case as shown in Figure 4. 9

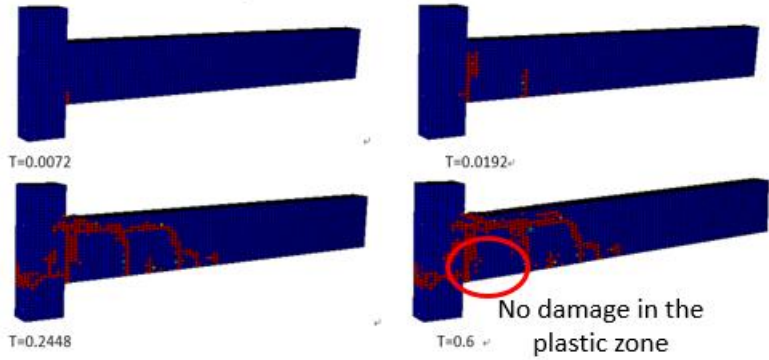
(c), the damage of beam was also characterize by two main cracks. However, unlike with connectors, the bottom of the beam that is under tension did not show any damage. To sum up, the case using connectors is closest to reality.



(a) Entire embedded



(b) With connectors



(c) Without connector or embedded

Figure 4. 9 Cracking development

In this chapter, the model and the corresponding parameters of connector were validated. The results demonstrated that the simulation of bond-slip between steel bar and concrete by means of connector skill within ABAQUS is feasible and available approach. The parameters of

connector can be identified from pull-out test data. This modeling technique can improve the accuracy of simulation. Relatively speaking, the function of embedded reinforcing steel bar in concrete is not suitable to calculate large deformation in the beam-column structure or models where relative displacement between steel bar and concrete occurs. Otherwise, the influence of steel bar cannot be observed by this method.

# Chapter 5 Numerical investigation of reinforced concrete structure in progressive collapse

## 5.1 Design support for the side stub columns

### 5.1.1 Assessment of the design of the support for the side columns

In order to capture the realistic response of a real beam-column assemblages subjected to a progressive collapse scenario, it is very important to define adequate boundary conditions for the specimen used as sub-assembly. The third chapter has determined the approximate shape and design of the support and the thickness of the steel plates used for this support. Actually, in the pre-design stage, we also designed kinds of configuration of the support by means of numerical simulation. This design process will be introduced in this section.

An important thing to do is to estimate the maximum force that the side columns may transfer to the supports. Considering the worst-case, the support will bear the maximum force from the specimen S3 for which the cross section is 110mm×270mm, the span is 3000mm and; the self-weight is 491kg; the max load is 2063kg. Both ends of the specimen are assumed to be fixed. From this, a simple calculation diagram can be drawn as shown on Figure 5. 1.

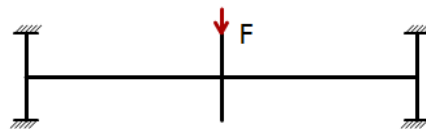


Figure 5. 1 Calculation sketch diagram

Based on structural mechanics theory and the assumption that the materials are elastic, the maximum internal force in the stub side column and the support reaction can be known. The force diagrams of the beam-column assemblages are shown in Figure 5. 2, the force of the support in the horizontal direction is 38.9kN, and the vertical force is about 8kN. In fact, the force that the supports may bear in the test should be less than the calculation results due to the concrete damage and the deformation of the structure. Here we just consider the worst conditions.

To simplify the calculation, the forces (horizontal force and vertical force) and the bending moment are applied on the support directly in order to insure that the support can work without

cracks or damage. It is not necessary to build a beam-column model in finite element software when we only analyze the supports.

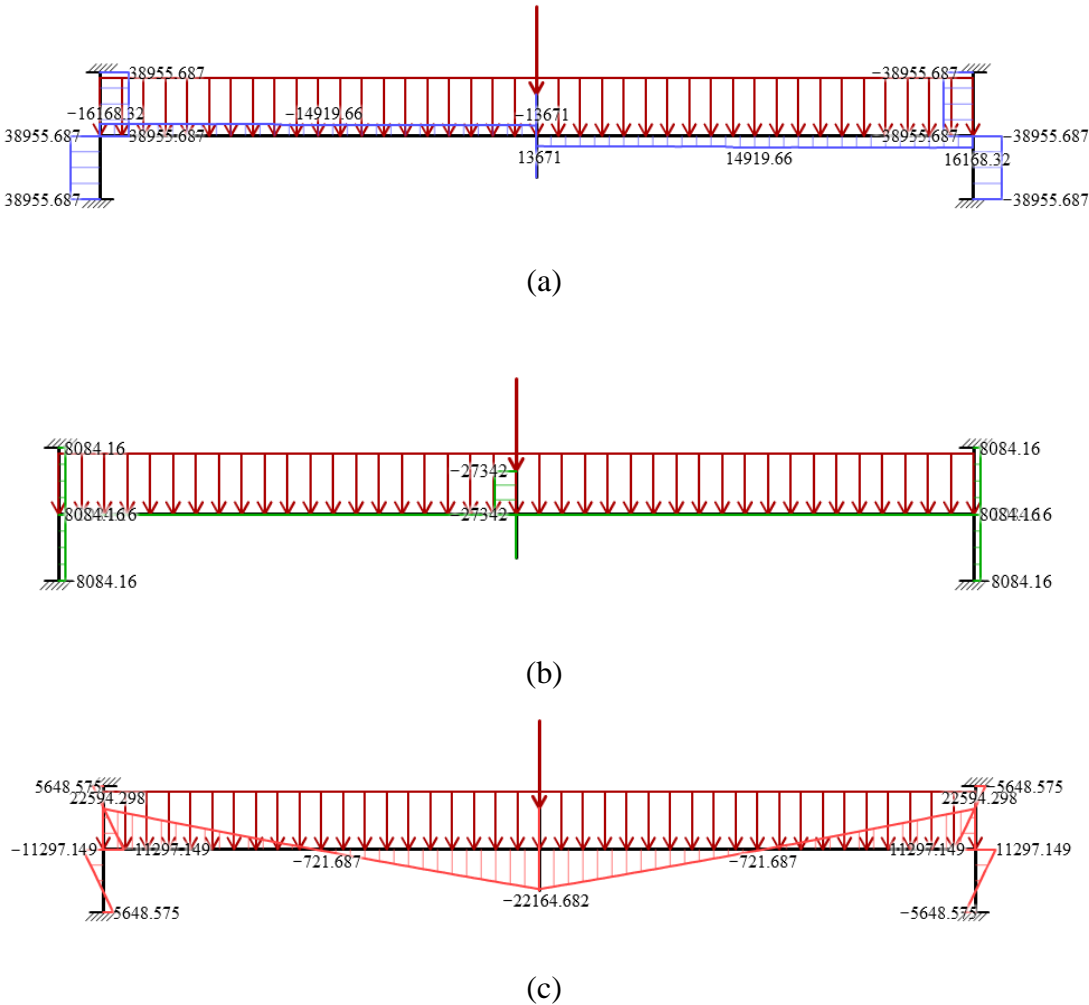


Figure 5. 2 Force diagram of beam-column assemblage in elastic state (a) shear force; (b) axial force; (c) bending moment

**5.1.2 Analysis of the stress and strain of the supports**

As mentioned in chapter 3, the supports that we need have to authorize a horizontal displacement but rotation. And it should have a larger rigidity in vertical direction so that it can support the specimen. The first plan designed is shown in Figure 5. 3. The bottom support is made of an upper case, a bottom plate, and connector steel slices. The connector steel slice cannot be too thin in order to prevent rupture. And they cannot be too thick so that the horizontal displacement is permitted. To sum up, three types of configuration of supports are designed as follows:



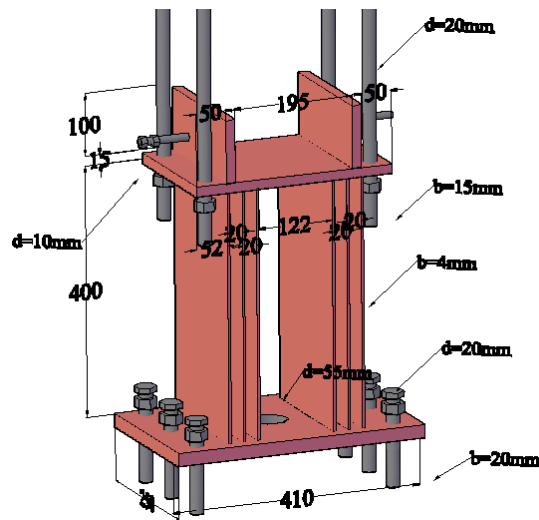


Figure 5. 5 Details of the support (thickness=4mm, 6 slices)

The three types of model of the support were built with commercial software ABAQUS. The finite element models of the support were made of solid element C3D8R. The bottom plates of the support were fully fixed. Two forces, a vertical force and a horizontal force that were obtained in last section, were applied along the direction of the arrows (see Figure 5. 3). The connector steel slices in the middle of the support were meshed with four elements in the thickness in order to have results precise enough.

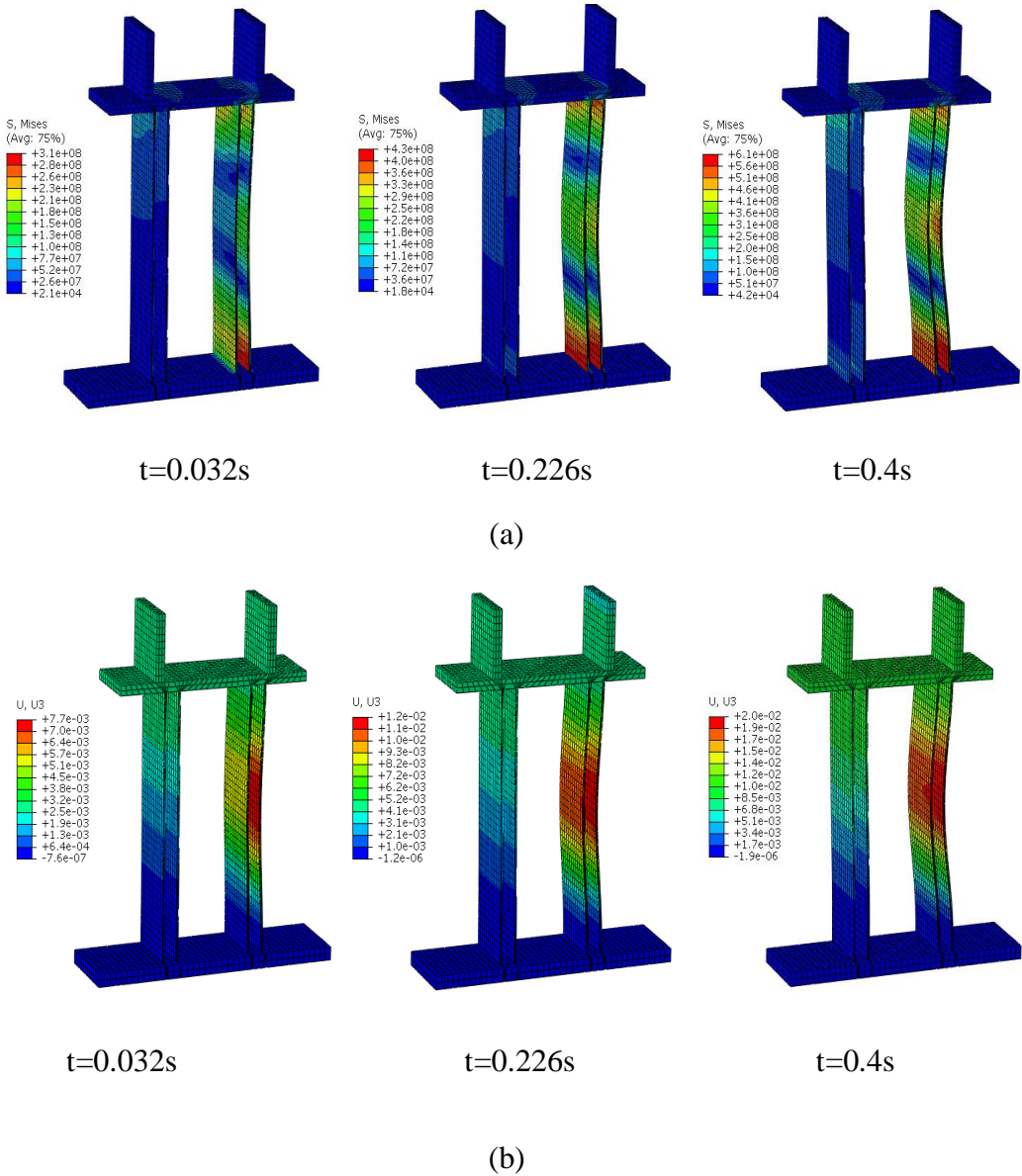
We used a 3D model for the support, because it can be imported into the entire model that included the beam-column assemblage and supports. This 3D model will be used in the subsequent calculation work.

The calculation results (thickness=5mm, 4 slices) are shown in Figure 5. 6. The maximum Mises stress was 644 MPa when the lateral displacement reached 16 mm, which was beyond the yield strength of steel of 500MPa. Figure 5. 6 (b) shows a large deformation in the middle of the connector steel plate when the time was from 0.226 seconds to 0.4 seconds. These results are not safe enough for the test equipment.

Figure 5. 7 shows the results of the support with six connector steel slices with a thickness of 5mm. It can be seen the displacement value of the support with six connector steel slices is smaller than that one with four steel slices. The max Mises stress was 306 MPa, which is lower than the yield strength of steel. However, the support need get enough safety margin. Thus, the

thickness of plate was reduced to 4 mm in order to try to get a lower stress.

Figure 5. 8 shows the results of the support with six connector steel slices with a thickness of 4mm. The max Mises stress was 274 MPa while the horizontal displacement reached 12 mm. Compared to the yield of the steel plate of 500 MPa, the safety factor is about 1.8. Then compared to the three types of support, the third one is the best choice.



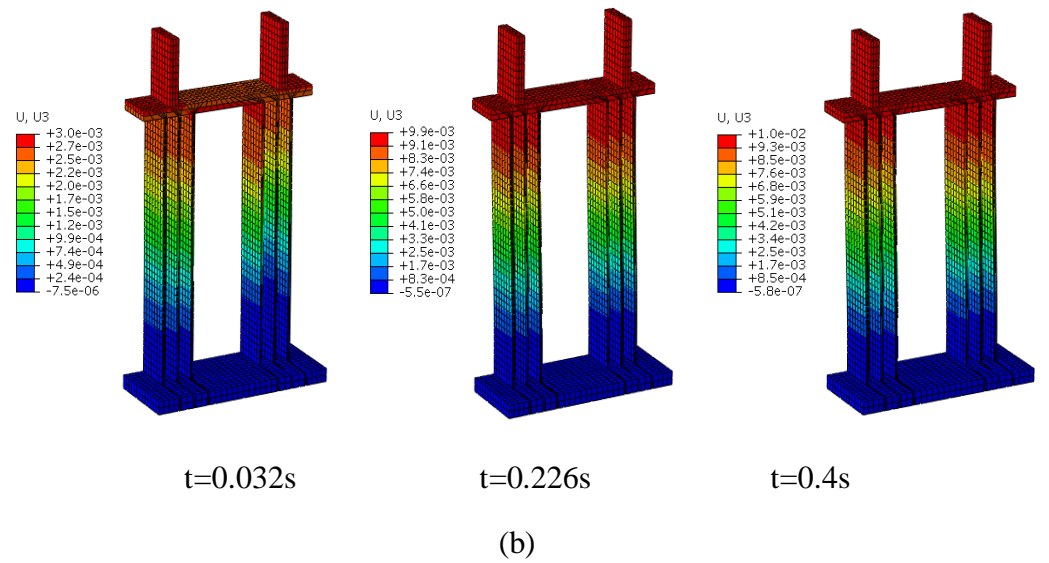
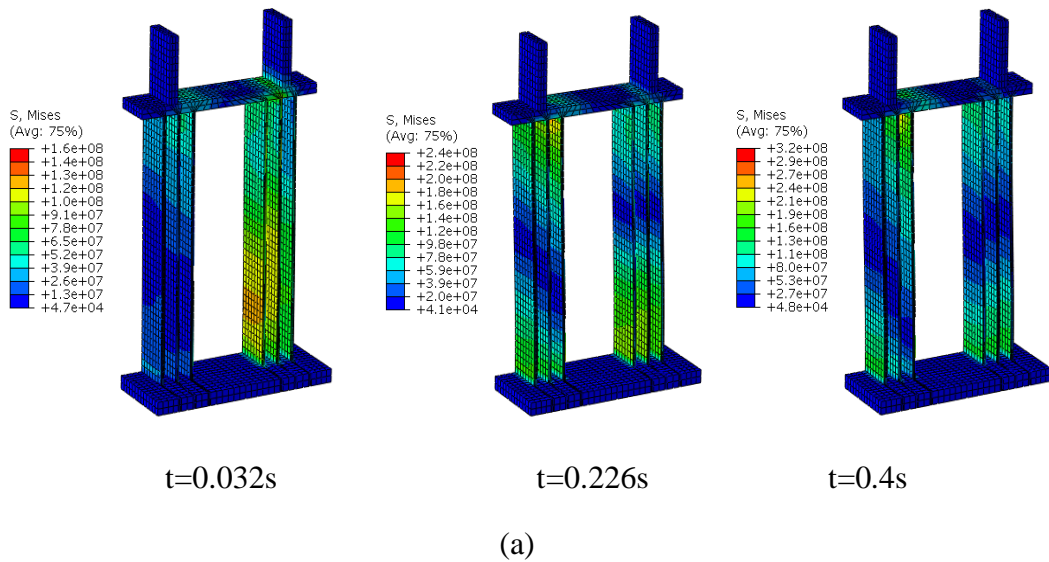
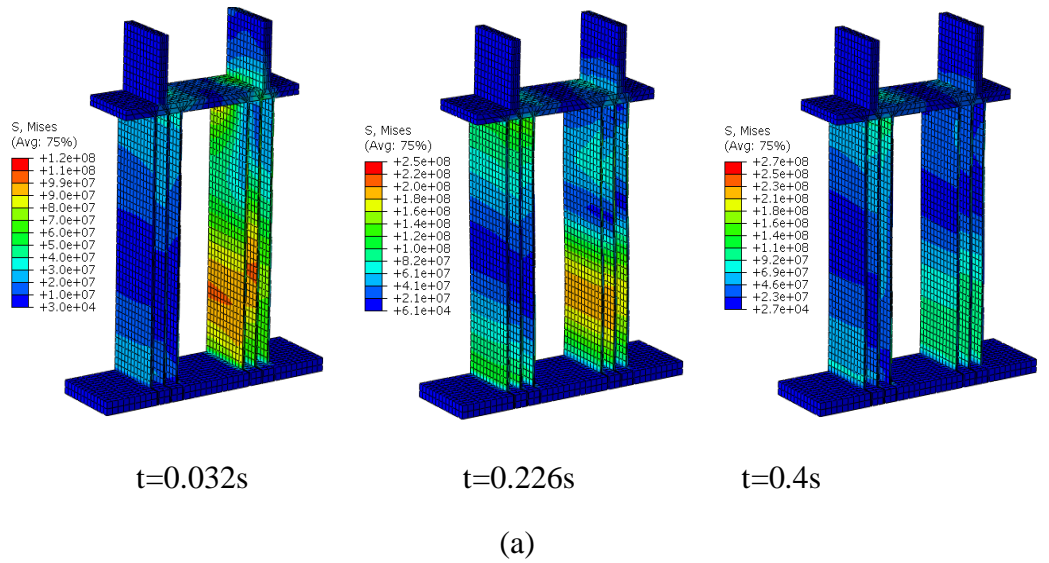


Figure 5. 7 (a) Mises stress in the support; (b) Lateral displacement of the support (thickness=5mm, 6 slices)



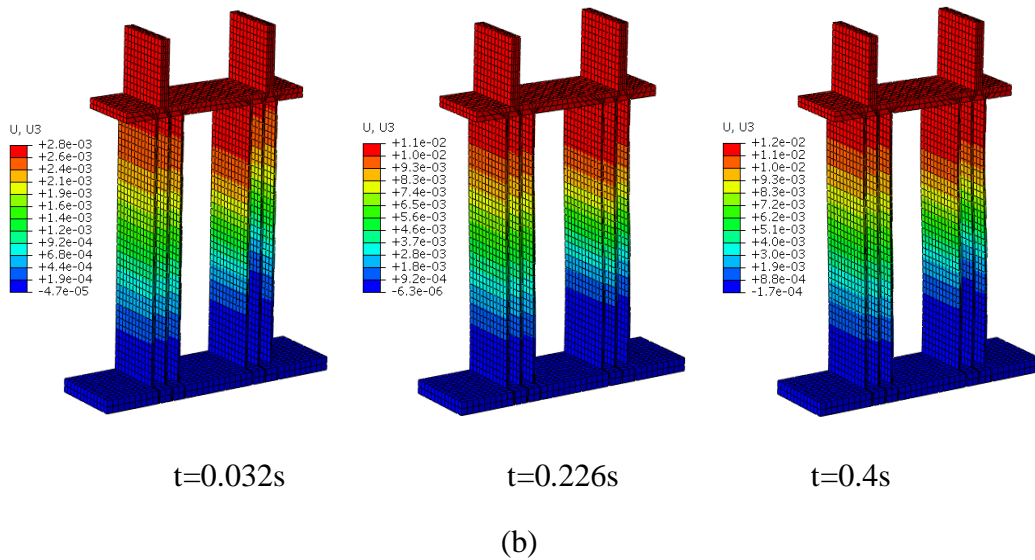


Figure 5. 8 (a) Mises stress in the support; (b) Lateral displacement of the support (thickness=4mm, 6 slices)

## 5.2 Numerical simulation the beam-column assemblages under the removal of the middle support

In order to comprehensively understand and study the progressive collapse behavior of reinforced concrete structure, in parallel to the experimental program, numerical simulations were conducted with the finite element code ABAQUS.

As mentioned in chapter 4, there are two difficult points for simulating progressive collapse of reinforced concrete structures. One is that an efficient constitutive model is needed. Another is simulation the interaction between steel bars and concrete. In this section, the DFH concrete damage model and connector skill that have been validated in chapter 4 will be used together to reproduce the test process. This nonlinear analysis that used concrete damage model and added nonlinear springs for concrete-rebars interface was often found in seismic analysis [47][86]–[89]. But a few instances in the literature used this way to investigate progressive collapse of reinforced concrete structure, especially for dynamic state. This study is innovative in this aspect.

In our experimental work, no quasi-static tests were performed. Therefore, it is interesting to reproduce it in numerical simulation work. On one hand, some information of beam-column in the quasi-static state such as the ultimate bearing capacity can be obtained. On the other hand, the behavior of beam-column in quasi-static can be compared with the behavior in dynamic

state.

Therefore, this section will be divided into two parts. The first part presents numerical simulation in the quasi-static state. The second part is dedicated to dynamic tests.

## **5.2.1 Evaluation the resistance of beam-column assemblages subjected to the middle support removal in the quasi-static state loading**

### **5.2.1.1 Modeling**

A numerical model representing the quarter of a beam was created in the commercial code ABAQUS. The model consists of both beam-column assemblages and the support. The different parts that constitutes the support such as stock and connection steel plates were merged. The whole model was meshed finely as shown in Figure 5. 9. The size of elements for the concrete beam specimen was 15mm, which is quite small so that it can display the development of damage and provides more precise results in terms of stress and strain in concrete. The beam-column and the support were made of C3D8R solid element and the steel reinforcement bars were built with T3D2 truss element. In some literatures[43][54][55], it is shown that beam elements can be used to simulate steel reinforcements. By comparing the results between these two types of element that are often used to model steel reinforcement bars, we observed no obvious difference in simulating progressive collapse of reinforced concrete structure, especially at the post-stage of collapse. But one benefits of using the truss elements is that the computing time can be reduced.

In this model, the truss elements were finally chosen to build reinforcement bars. Symmetrical boundary conditions are applied to mid-plane of the structure. The bottom of the support was totally fixed. The whole model is shown in Figure 5. 9. Ten connectors were set in the tension zone and compression zone respectively. The other parts of the reinforcement bars were embedded in the concrete element. It can be seen in Figure 5. 10.

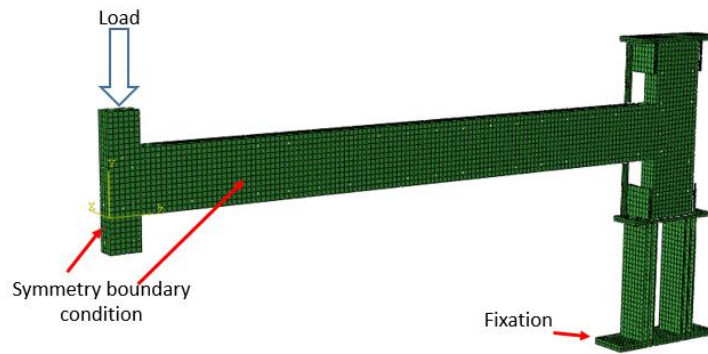


Figure 5. 9 Numerical model used in ABAQUS representing the quarter of a beam

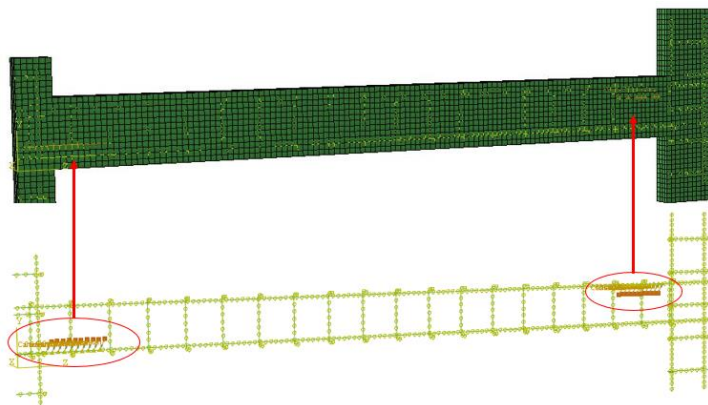


Figure 5. 10 Additional connectors in the plastic zone

### 5.2.1.2 Loading path

In this numerical model, a vertical velocity field set to 10cm/s was applied to the top surface of the middle column. A study performed by P. Forquin and W. Chen [21][22] concluded that the structure is in the quasi-static state in this range of applied velocity.

### 5.2.1.3 Results

#### Reaction force-displacement response

Figure 5. 11 shows the variation of the applied forces with the middle column vertical displacement. As it can be seen from the figure, the span-depth ratio has a significant effect on the mechanical properties. The specimens S1 and S3 have the same span-depth ratio (both span-depth ratio are 11.1) but with different cross section. They have almost same behavior before the vertical displacement of the middle column dropped of 200mm. The ultimate bearing capacity is also almost the same, which is about 41kN.

After the vertical displacement reach about 200 mm, their force-displacement curves began to

evolve differently. The bearing capacity of the specimen S1 with a small span started to exceed that of the specimen S3 with a larger span, even though both of them decrease. Another difference is that the specimen S1 failed earlier than the specimen S3, S1 lost its carrying capacity when the vertical displacement reached 346 mm; while S2 failed totally when the vertical displacement arrived to 383 mm.

Compared with specimen S1 and S3, the ultimate bearing capacity of the specimen S2 with a larger span-depth ratio is only 30.5kN. And the mechanical performance is different from specimen S1 and S3. We observe a continuous increase in the bearing capacity of the specimen S2 was kept before it totally failed, while the bearing capacity of specimen S1 and S3 began to decrease gradually after the vertical displacement reached 220 mm.

Comparing the values of bearing capacity and failure time, indicates that a larger span and a larger span-depth ratio are not good for better resisting the accident and abnormal load that is caused by the failure of a local component.

It is observed from the experiment and numerical calculation results that the failure process of the beam-column assemblages under removal middle support can be divided into several phases. Currently, the failure process according to the state of material can be divided into four phases, elastic, elastoplastic, plastic and damage stages. Such a classification can be found in the literatures [20][24]. Another way is to divide into three phases according to mechanical mechanism of the structure, successively flexural action (FA), compressive arch action (CAA) and catenary action (CA). Such a classification can also be found in other literatures [29][31].

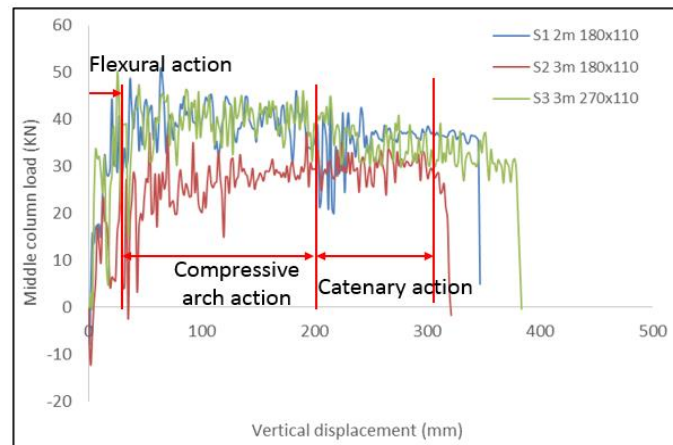


Figure 5. 11 Middle column load versus vertical displacement of failed middle column

Through the horizontal displacement variation of the stub, as shown in Figure 5. 12, the transition between the structural mechanisms can be observed. A negative value of horizontal displacement indicated that the stubs of beam was away from the middle column. When the horizontal displacement is positive value, the ends of beam was close to the middle column. At the beginning, a small negative horizontal displacement linear like is associated with flexural action. Then, this negative horizontal displacement first went up and decreased to zero, which is representative of compressive arch action. Finally, the horizontal displacement continually increases revealing the structure entered in a catenary action phase.

The results given by Figure 5. 12 show that the specimen of S1 and S3 with the same span-depth ratio reach at the same point the change of horizontal displacement from negative to positive. On the contrary, although the specimen S2 has the same section than the beam as S1, the horizontal displacement evolution is different; the beginning of catenary action phase begin later than that of specimen S1 and S3. It demonstrates that the failure are classified mechanisms of the structure are mainly controlled by the span-depth ratio. This observation is different from other literatures [24][29] where mechanism phases by the depth of the beam and the vertical displacement of the middle column.

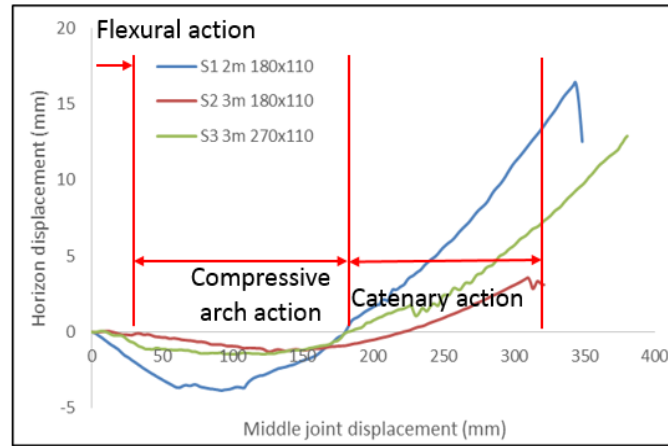


Figure 5. 12 Effect of downward displacement of middle column on horizontal displacement  
Based on conventional plastic mechanisms and nominal moment capacity at critical sections, the capacity of flexural action, compressive arch action and catenary action can be calculated.

**(a) Capacity of flexural action (FA)**

Although the reinforcements at the beam-column joint regions are designed for sustaining negative bending moments, due to the requirements of integrity specified by ACI 318-05, the sections within these regions still have certain capacities to resist to positive bending moments. As a result, after a middle column is removed and the bending moment above the removed column changes its direction, flexural action can sustain external loads. The capacity of flexural action is determined by the yielding moments at critical sections without considering the existence of beam axial forces. In this case, plastic hinges occurred at the middle beam-column joint interfaces and at the beam-end column stub interface. The positive bending moment of the middle beam-column joint interface is denoted as  $M_{nm}$ , and the negative bending moment of the beam-end column stub interface is denoted as  $M_{ne}$ . Then the capacity of flexural action can be computed as [27]:

$$P_f = 2(M_{nm} + M_{ne})/L \tag{5.1}$$

where  $L$  is shown in Figure 3. 3, Figure 3. 4 and Figure 3. 5;  $M_{nm}$  and  $M_{ne}$  are nominal bending moments of specified sections without considering the strength reduction factors specified by building codes.

**(b) Capacity of compressive arch action (CAA)**

Park's model [82] proposed for one-way slabs longitudinally restrained at the slab boundaries can be modified for axially restrained beams. The capacity of compressive arch action of RC beam-column sub-assemblages subjected to a concentrated load at the middle joint is determined as follows:

$$F_p = \frac{2}{L_n} \left\{ 0.85f'_c\beta_1bh \left[ \frac{h}{2} \left( 1 - \frac{\beta_1}{2} \right) + \frac{\delta}{4} (\beta_1 - 3) + \frac{L_n^2}{2\delta} (\beta_1 - 1) \varepsilon_t + \frac{L_n^2}{2h} \left( 1 - \frac{\beta_1}{2} \right) \varepsilon_t + \frac{\delta^2}{8h} \left( 2 - \frac{\beta_1}{2} \right) - \frac{\beta_1 L_n^4}{4\delta^2 h} \varepsilon_t^2 \right] - \frac{T' - T - C'_s + C_s}{3.4f'_c b} + (C'_s + C_s) \left( \frac{h}{2} - d' - \frac{\delta}{2} \right) + (T' + T) \left( d - \frac{h}{2} + \frac{\delta}{2} \right) \right\} \quad (5.2)$$

where  $L_n$  is the net span length of beams;  $b$  and  $h$  are the beam width and depth, respectively;  $f'_c$  is the concrete compressive strength determined from concrete cylinder tests;  $\beta_1$  is the ratio of the depth of concrete equivalent stress block to the depth of section neutral axis (according to ACI 318-05);  $T$  and  $T'$  are tensile resultant forces of reinforcing steel of sections at the interface of middle joints and beam-end column stubs, respectively;  $C_s$  and  $C'_s$  are compressive resultant forces of reinforcing steel of sections at the interface of middle joints and beam-end column stubs, respectively;  $d'$  is the distance from the centroid of compressive reinforcement to the extreme compressive concrete;  $d$  is the beam effective depth;  $\delta$  is middle joint displacement; and  $\varepsilon_t$  is total strain due to beam axial deformation and movement of beam end supporters. It can be computed as [27]

$$\varepsilon_t = \frac{\left( \frac{1}{bhE_c} + \frac{1}{L_n S} \right) \left[ 0.85f'_c\beta_1bh \left( \frac{h}{2} - \frac{\delta}{4} - \frac{T' - T - C'_s + C_s}{1.7f'_c\beta_1b} \right) + C_s - T \right]}{1 + \frac{0.425f'_c\beta_1bL_n^2}{\delta} \left( \frac{1}{bhE_c} + \frac{1}{L_n S} \right)} \quad (5.3)$$

where  $S$  is the stiffness of horizontal restraints, and  $E_c$  is elastic modulus of concrete.

### (c) Catenary action (CA)

Yi [20] gave the formula to estimate the load-carrying capability due to catenary action as follows

$$P_{ca} = 2\Psi N \sin\alpha \quad (5.4)$$

where  $N$  is the total tension force in the cross section provided by the steel when it reaches its tensile strength;  $\alpha$  is the rotational angle of the frame beam; and  $\Psi$  is a strain adjustment

coefficient. This formula only considered the tensile steel bar. But in fact, it is difficult to identify the value of  $\Psi$  for the structure, relying on more experience choose. Here it was supposed equal to 1.0 considering a simple beam-column structure.

To sum up, the capacity of the three mechanisms can be obtained. The results are shown in table 5.1. The numerical simulation results show the ultimate capacity of the three type specimens are 41.5kN, 30.5kN, 40.8kN, respectively. The calculation results are larger than the numerical simulation results in different phases. While according to the conventional engineering design method, the design load are 28kN, 18kN and 31kN (see Table 3. 6), respectively. Compared with the numerical simulation results and theoretical value, the conventional design method may be conservative in resisting progressive collapse.

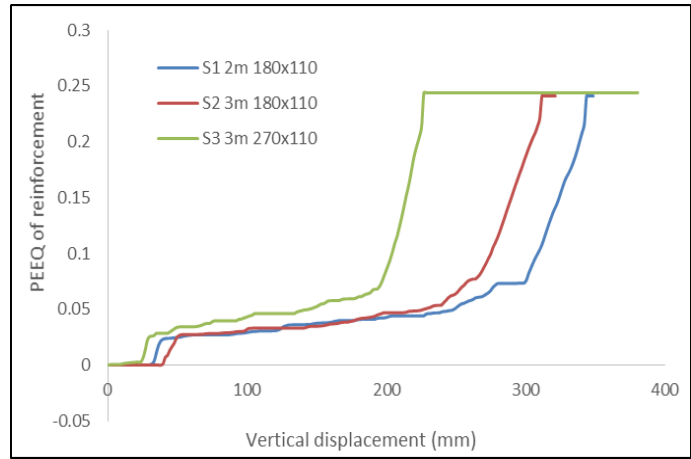
Table 5. 1 Force at critical point of reaction force-displacement curves

Specimen	FA (kN)	CAA (kN)	CA (kN)
S1 2m 180x110	20.6	27.33	54.7
S2 3m 180x110	15.77	18.46	32.4
S3 3m 270x110	25.65	34.15	38.45

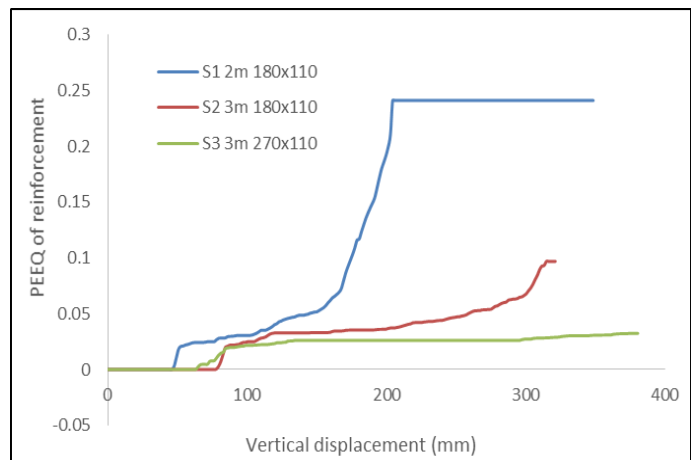
**Strains in the reinforcing bars and concrete**

Figure 5. 13 shows the plastic strain of the reinforcing bars at the middle section and at the end section of the beam, respectively. At the middle section, the first plastic strain appeared in the specimen S3 with the largest depth of the beam; then, the reinforcing bar in the specimen S1 and S2 entered into plastic stage when the corresponding vertical displacement of the middle column reached 23.7 mm, 34.9 mm, and 39.7 mm, respectively.

At the section of the side column, the earliest plastic strain in the reinforcing bar happened in the specimen S1, when the vertical displacement was 49.3mm. Then plastic strains appeared successively in the specimen S3 and S2, corresponding vertical displacement of the middle column of 65.3mm and 72.5mm, respectively. These results show that the activation of plastic strain in reinforcing bars mainly relays on the span-depth ratio. The smaller ratio, the earlier the reinforcing bars will enter into plastic phase and provide bearing capacity.



(a) At middle section



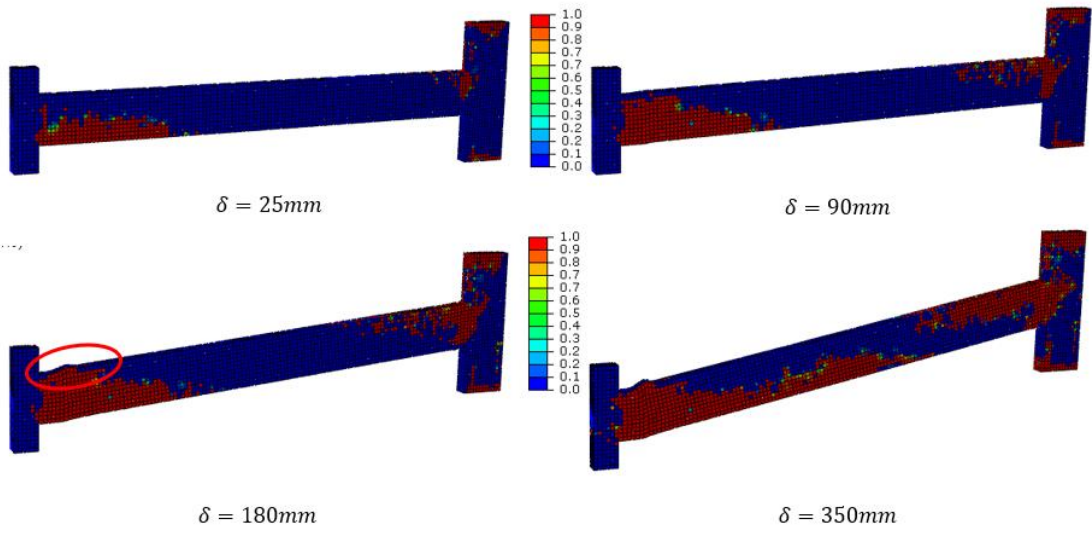
(b) At the beam end section

Figure 5. 13 PEEQ of tension reinforcement at middle and end sections

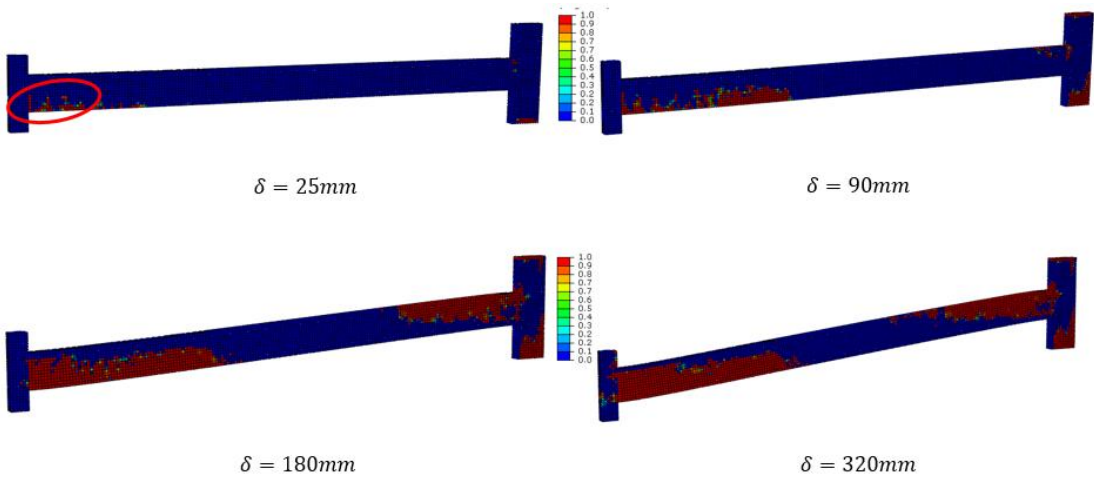
### Damage patterns

To study the failure mechanisms of the beam under external loads, the development of the damage of the structure for vertical displacements of the middle column of 25 mm, 90 mm (one-half beam depth), 180 mm (beam depth) and at the end of the experiment were extracted (see Figure 5. 14). The results show a similar development of cracks for the specimen S1 and S3 with an equal span-depth ratios. In the tension zone near the middle column and the side columns, the cracks appeared simultaneously and expanded rapidly. At the same time, the concrete in the compression zone close to the middle column show obvious damage from the vertical displacement of 90mm. When the vertical displacement reached 180mm, the concrete started to fall. Due to constrain on the side column, concrete damage also appears at both ends of the side columns.

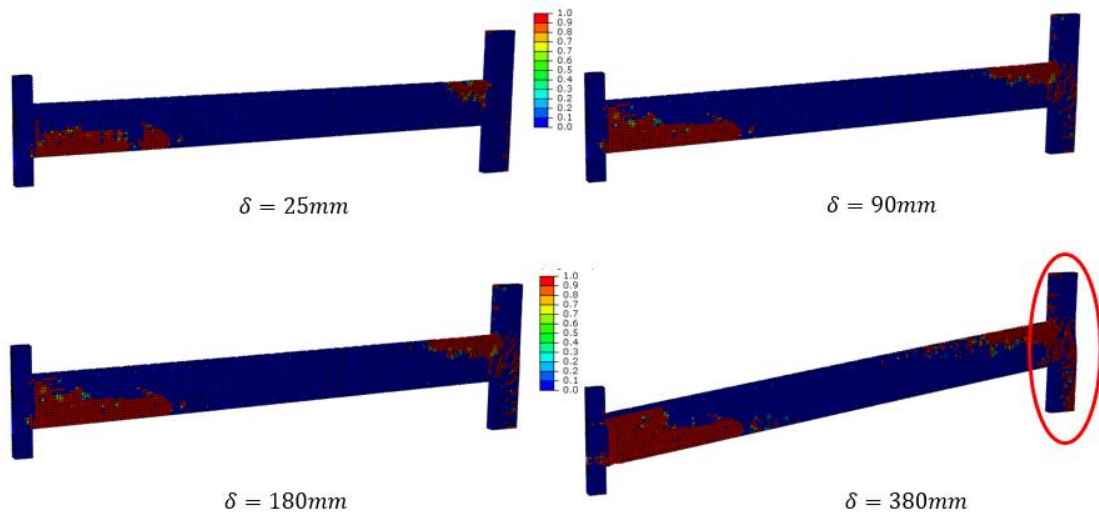
The behavior of S2 is different from the S1 and S3. S2 only shows several growth of tension cracks before the vertical displacement reach 25 mm. After the vertical displacement reached 90 mm, the failure of concrete in the compression zone is still weak, only tensile cracks developed along the beam. When the vertical displacement reached 180mm, the tensile zone at both ends of the beam is importantly damage, but the damage in the compression zone is not serious. At the end of the simulation, the concrete at the bottom of the side column began to damage. These results demonstrated that under large displacement of the middle column, tension effect on the failure of the component is significant if the span of the beam is larger.



(a) Specimen S1-1 2m 180x110



(b) Specimen S2 3m 180x110



(c) Specimen S3 3m 270x110

Figure 5. 14 Damage development in the specimen

## 5.2.2 Numerical simulation study of the dynamic behavior of beam-column assemblages subjected to middle support removal

### 5.2.2.1 Modeling

In accordance with test conditions, a numerical model representing the quarter of a beam was built in ABAQUS. The mesh and boundary conditions are the same as previous model in quasi-static state. Different from previous model, a dead load was applied by gravitational field in this model. Initially, a mass was defined on the top surface of the middle column depending on the applied load. In this period, the gravitational field is zero; the structure was free from any force. Suddenly, the gravitational field rose to normal level as shown in Figure 5. 15. The middle column got a downward force suddenly under gravitational field. Thereby, the test process was achieved.

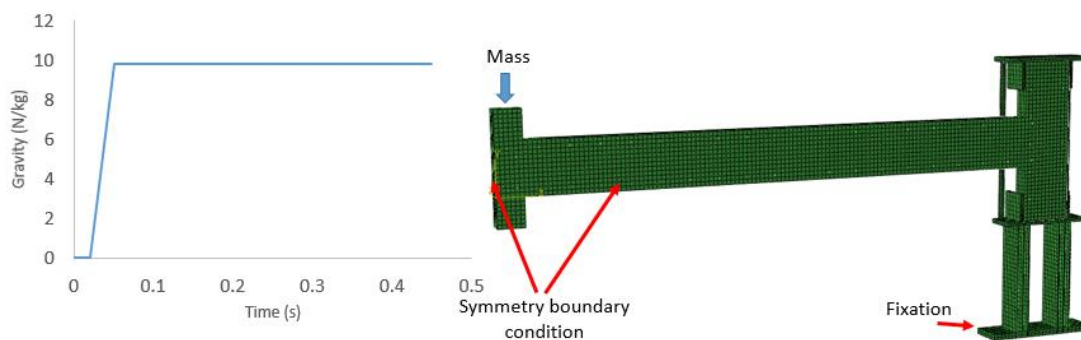


Figure 5. 15 Numerical model used in ABAQUS and gravitational field

### 5.2.2.2 Results and comparisons with dynamic tests

#### Reaction force

Figure 5. 16 shows the applied load at the middle column history for the three types of specimens. It can be seen that the numerical predicted trend of applied force at the middle column are very similar to test results, especially before around 0.13s, which is the time in the flexural action and compressive action phases.

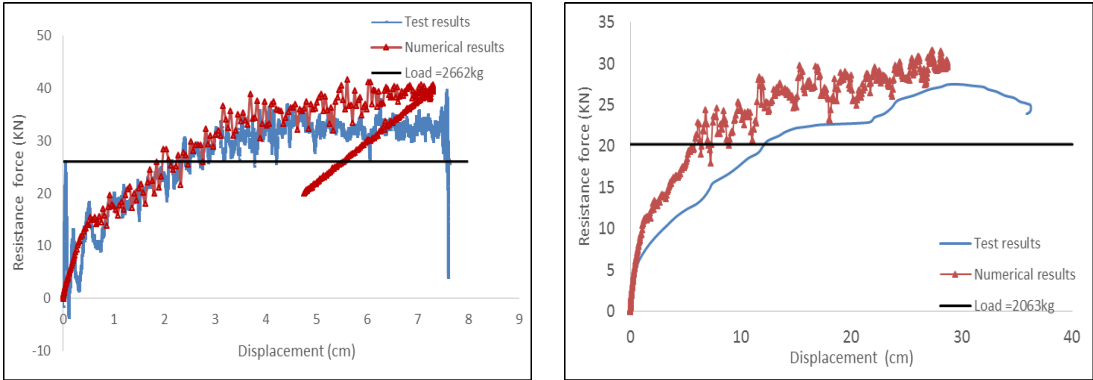
Figure 5. 16 (a) shows the response of the specimen S1-1 under the load of 2662kg. The calculation results is in good agreement with the test results before the vertical displacement of 4cm. The calculation peak of the applied force is 8% larger than the test results. Compared to the load mass, the numerical calculation peak of the applied force is 18.5% beyond, which shows the effect of inertial forces on the structure.

Figure 5. 16 (b) compares the experimental and numerical results of the specimen S2-2 under the load of 2063kg. We observe that experimental and numerical results almost coincide at the beginning of the test. Beyond the vertical displacement of 3cm, the curve of calculation results went up continuously, which makes a gap between numerical and experimental results. The calculation peak of the applied force was 29.4KN, which is also larger than experimental result. The reason may be a perfect model used in numerical calculation while a true specimen could be initially damage.

Figure 5. 16 (c) compares the experimental and numerical results of the specimen S3-1 under the load of 2737kg. The value of numerical simulation is smaller than the test results in the earlier stage. After the vertical displacement reach 18 cm, the numerical results start to close to the test results.

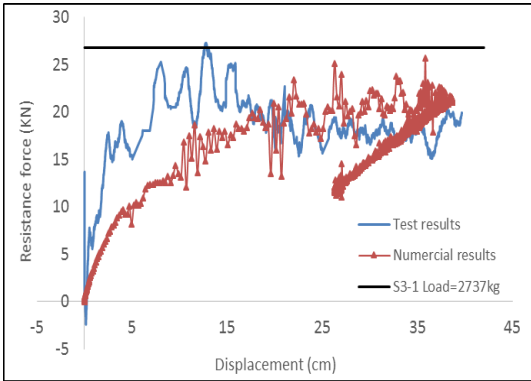
One can note that for the specimen S1-1 and S2-2, both experimental and calculation results are larger than the load mass due to inertial forces. However, in the third case (S3-1) it is observed that the experimental and calculation results are lower than the load mass. Because the specimen S3-1 is difficult to provide all bearing capacity after undergone twice tests with the load of 994kg. See the Table 3. 10, the damage factor is 0.287. We can also know the damage

of the beam is relatively important after the twice tests.



(a) Specimen S1-1 2m 180x110

(b) Specimen S2-2 3m 180x110



(c) Specimen S3-1 3m 270x110

Figure 5. 16 Resistance force versus vertical displacement of middle column

**Middle joint displacement**

Figure 5. 17 shows the displacement results of the middle column for the three specimens. As can be seen in Figure 5. 17 (a) and (b), the numerical calculation results is in good agreement with the experimental results, especially in earlier stages of case S1-1 and S2-2. In the middle and last period, the calculation results have a bit more difference but the error is not beyond 20%.

However, the results of third case (S3-1) is not in very good agreement with the test results. The calculation results is much larger than the test results even in the earlier stage.

The calculation results of the displacement field are not as good as the results obtained for the applied force. The reason may be related to the stiffness of the entire system. It is well known that in the numerical calculation, there is a relationship between the nodal forces and the

displacements [94]

$$[K_e] \{u_e\} = \{F_e\} \tag{5.5}$$

Where the matrix  $\{u_e\}$  is the vector of nodal displacements;  $[K_e]$  is the stiffness matrix, which relates the nodal displacements to the nodal forces. As shown in Figure 5. 16, the resistance force obtained from numerical simulation are in good agreement with the experimental results. However, Figure 5. 17 (c) shows the displacement results are much larger than the experimental results. It demonstrates that the stiffness of the numerical model is too small. In this case, the specimen S3-1 underwent repeated load. That means the numerical model needs to be carried out multi-step calculation. So the stiffness of the structure is not very accurate after several times calculations. Meanwhile, there are other factors that affect the calculation results. For example, the defects and subtle damage already exists in the real concrete beam-column, and the contact patterns between each part in the numerical model (screw bar and bottom case, reinforced concrete stub and bottom case). These may cause both the calculation and experimental errors in terms of displacement.

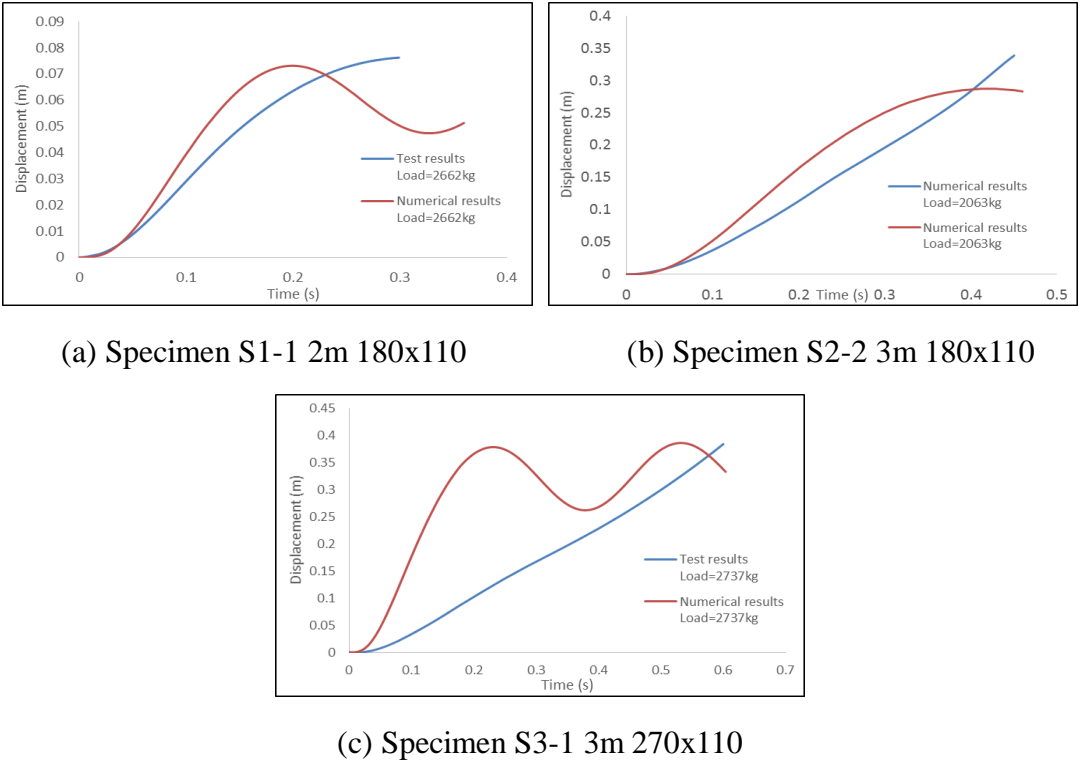


Figure 5. 17 Comparison of experimental and numerical results for the vertical displacement history of the middle joint

## **Damage patterns**

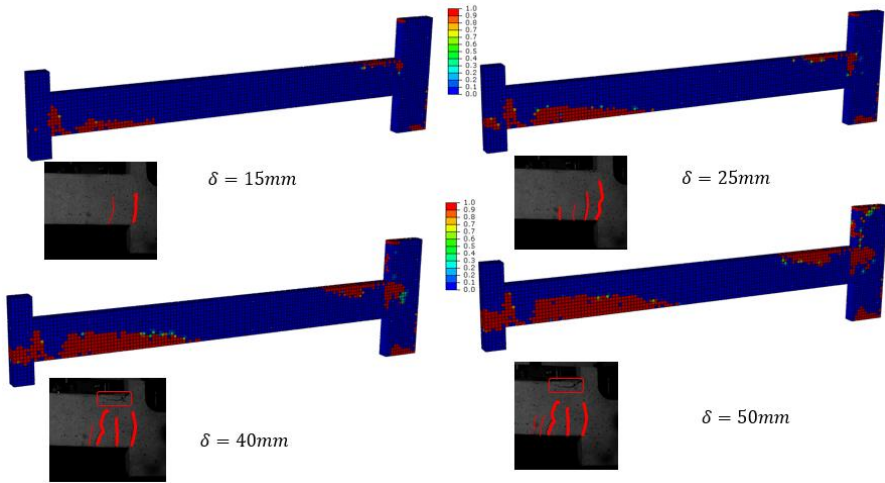
Figure 5. 18 shows the development of cracks and the damage of concrete under dynamic loading. For specimen S1-1 (see Figure 5. 18 (a)), when the vertical displacement of the middle column reached 15mm, one dominant crack can be observed near the middle column. When the vertical displacement reached 25mm, tensile cracks began to develop at the side joint. The width of the cracks was extended after the vertical displacement of the middle column reached 40mm. Increasing at the middle column up to a vertical displacement of 50 mm, concrete damage is also observed at the fixed end of the side column. Compared with the photos from experiments by the high-speed camera, the numerical simulation results are basically consistent with the experimental results. However, in the experiment, the concrete damage of the middle joint in the compression zone was more severe; the numerical simulation did not show such phenomena.

Compared to specimen S1-1 with a small span, specimen S2-2 did not show significant tensile cracks until the vertical displacement reached 50mm (see Figure 5. 18 (b)). There are two main differences between numerical simulation and experimental results. The first is that the damage of the middle column was serious in the numerical simulation, but longitudinal cracking was not observed in the actual middle column. Second, the damage of the beam in the tensile zone in numerical simulation is relatively large, whereas, in the experiments, the real damage zone of the beam is not so important.

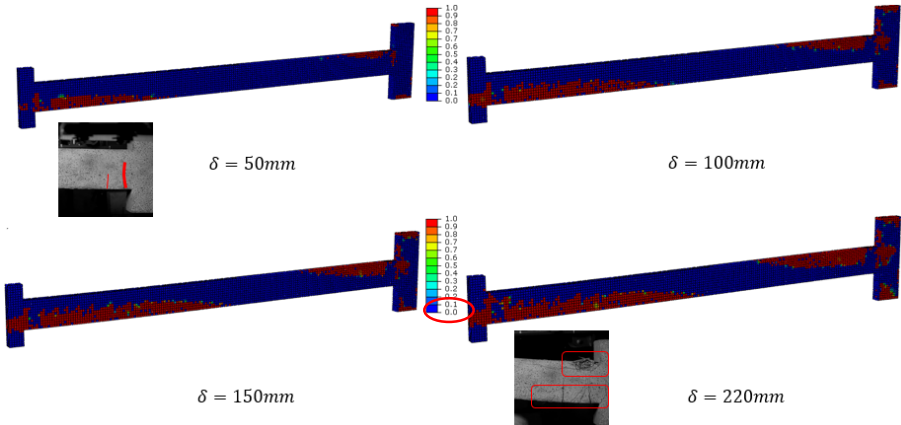
Figure 5. 18 (c) shows the damage of the Specimen 3-1. The first dominant crack was observed at the vertical displacement for approximately 50 mm. Crack began to appear at the side column when the vertical displacement increases to 100mm. The development of cracking for the specimen S3-1 was similar to that of the specimen S 2-2. It indicates that the development of cracking depends on the span of the beam. In other words, if the spans of the beam are the same, a similar development of the cracking can be observed.

In summary, the proposed method in this study that used DFH anisotropic concrete damage model and connectors can well simulate the damage process of beam-column assemblages. The calculation results show a good agreement with the experimental results. However, the

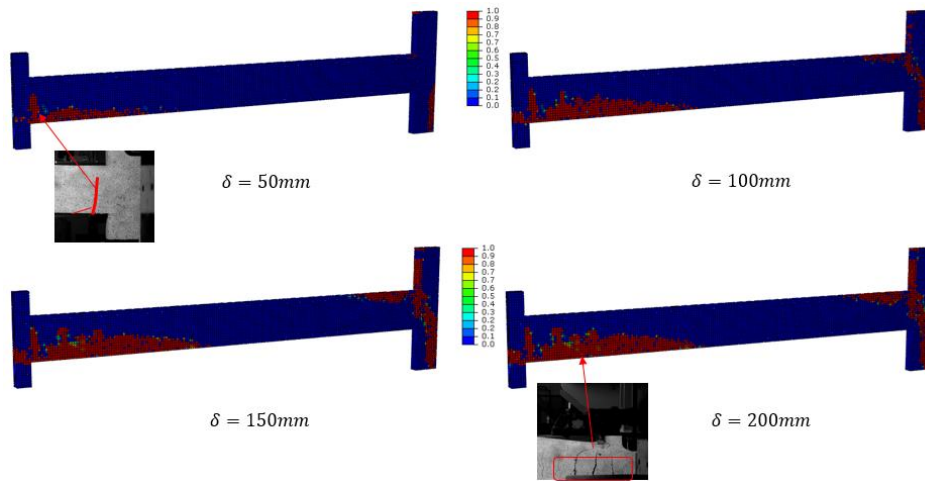
simulation results in tensile zone are relatively better than the results in the compression zone, since almost no damage of the concrete in the compression zone has been shown.



(a) Specimen S1-1 2m 180x110



(b) Specimen S2-2 3m 180x110



(c) Specimen S3-1 3m 270x110

Figure 5. 18 Damage development in the specimen

## **Chapter 6 Conclusions and Recommendations**

### **6.1 Conclusions**

The present research work aimed at contributing to the understanding and modelling of the behavior of reinforced concrete beam-column subassemblies under a middle column sudden removal scenario in the framework of an experimental program and numerical simulation. The large challenge of the present study was to design a proper support for the side column and an unloading device for the middle column in order to simulate a sudden loss of the bearing capacity of a column in a realistic circumstance. Another challenge was to describe the interaction between reinforcing bar and concrete in the numerical simulation.

This dissertation presents the dynamic experimental program conducted with three beam-column subassemblies, including the fabrication of specimens, the design of support, the design of experimental equipment and the design of the loading system. The dynamic tests for three specimens were conducted considering a middle support removal scenario. Laser and high-speed cameras were used to gather the experimental results. The pseudo-harmonic damped validation of the subassembly was first studied, and the level of damage in the beams was estimated for each level of load. Meanwhile, a finite element numerical model was used to reproduce the experimental dynamic loading of the beam-column structure. Several interaction laws between reinforcing bars and concrete were considered and, spring connectors were adopted in the numerical model. The parameters of the model were validated according to pull-out tests conducted with rebars. This interaction model was then introduced into the beam-column dynamic test simulation.

Through the dynamic experiment and simulation work above, a more comprehensive understanding of the behaviors of RC structures resisting progressive collapse can be offered. The conclusions are given in the following.

#### **Dynamic characteristic of the beam-column assemblages**

In this study, dynamic properties of the beam-column subassemblies such as the frequency, period of vibration and damping ratio were obtained from tests with a small load applied to the

top surface of the middle column. The period of vibration is 0.303s and 0.233s for the specimen S2-1 and S3-1, respectively. These experimental values are in agreement with the analytical values. The damp ratio is 2.9% and 1.9% for the S2-1 and S3-1, respectively. For a perfect beam, the influence of damping ratio on the vibration period is very small because the value of damping ratio of the reinforced concrete structure is small. With repeating loads, the damping ratio gradually decreases and the period of vibration has a significant increase due to slight damage of the RC component.

The damping ratio is generally in the range from 2% to 5% for typical reinforced concrete structures [95]. Most people assumed the damping ratio as 5% when they carry out a seismic analysis with some numerical simulation software for reinforced concrete structures [96][97]. According to these authors of the analysis object is a building, the damping ratio can be set to 5%. However, if the analysis object is a component or an assemblage like the beam-column, the value of 5% is obviously larger.

### **The mechanical behavior in resisting progressive collapse**

In experimental and analytical progressive collapse behavior of the beam-column subassemblies, three main resisting mechanisms are observed that help to resist to progressive collapse, flexural action, compressive arch action and catenary action.

Flexural action happens in the initial stage of the removal of the middle support. The ends of the beam show cracks and plastic hinges begin to form, which indicate that flexural action has devoted all capacity. This action can only provide smaller resistance but the resistance capacity increases rapidly.

Compressive arch action is the dominant mechanism in the process of the progressive collapse resistance. It plays an important role in the transformation of mechanical mechanism. In the force-displacement curve (vertical displacement of the middle column), this action can make the curve keep growing steadily after the flexural action. Compared to the flexural action, it can sustain a little more time so that the plastic hinges develops in this period. However, compared to the quasi-static test, the plastic hinges may have not enough time to develop in the dynamic test. The components enter next stage quickly. i.e. catenary action. That means that for the

quasi-static test, the capacity of catenary action can be estimated by the value of the yield of the reinforcing steel bars [20]. But for the dynamic test, it may have a deviation if the same method is used.

Both experimental and numerical simulation results show that after compressive arch action, the contribution of catenary action will become more significant as the slope of the force-displacement curve increases. When the structure enters into Catenary action, the collapse resistance is mainly driven by the plastic behavior of reinforcing bars. Different from previous two kinds of action, development of catenary action depends on the size of rebars and the anchoring strength in the side column. In conventional design, the anchorage of the reinforcements into the joint of the beam-column is never considered. It only meets the detailing requirements according to the standard. However, the development of positive bending moment in the joint, the end of bars are susceptible to be pulled out due to anchorage. The design of this joint needs to be improve for resisting progressive collapse.

The whole process of transferring mechanism is related to the vertical displacement of the middle column. With increasing the vertical displacement, these mechanisms can be gradually activated. The magnitude of the displacement is not only related to the load, but also refers to the span-depth ratio and stiffness of the structure. Among them, the span-depth ratio of the components plays the most significant role in the mechanical behavior and bearing capacity of the structure.

### **Experimental technology**

The main object of this experimental study is to reproduce the progressive collapse process of the structure by an economic and simple method. By the tests done on three specimens, it demonstrates that all the design parts of the equipment performed very well, including the loading system, the supporting system, and the unloading device. It offers a better choice for similar dynamic experiments.

The measurement methods in such experiments are very important. However, it is a pity that the reaction force of the support cannot be directly measured. In addition, the high-speed camera

can only cover a part of the component. While the fracture process of the entire component would need to be recorded at the same time. But such configuration would need to add another high-speed camera and accessory equipment.

### **Numerical simulation skill**

DFH constitutive model can describe well the character and behavior of concrete in numerical simulation on progressive collapse analysis of reinforced concrete framed structures. Either under quasi-static or dynamic loading, the stress and strain of concrete and development of cracking can be captured. It is beneficial for assessing and analyzing the bearing capacity of the component and the damage level.

The function of connector in ABAQUS can simulate bond-slip behavior between steel bars and concrete. It can be used not only to simulate simple pull-out test but also complex reinforced concrete structure tests. It has many advantages such like various models, abundant parameters and flexible setting modes. Parameters of connector model should refer to pull-out test data to improve the accuracy of simulation. Meanwhile, the function of embedded default in ABAQUS is not suitable to calculate large deformation problems since it exists a relative displacement between steel bars and concrete. To sum up, this research can offer a solution for simulating reinforced concrete structure under progressive collapse in dynamic circumstances.

## **6.2 Recommendations for future research**

Due to limited time, many thoughts and ideas still have to be explored. The following topics are recommended for further research to assist future studies and better understand the progressive collapse behavior of structures.

### **6.2.1 Experimental research**

1. In the measurement method, gathering test data mainly relies on the laser and High speed camera. However, many different kinds of information cannot be captured in these dynamic tests, such as the strain of the steel bars, and the support reaction force. In addition, a camera could only record data from a part of the beam. If the test data of the entire component need to be recorded, the only way is to add equipment for measuring data. Future tests should be

considered to record overall data and new measurement means and strategies are worth to investigate.

2. On the mode of dynamic loading, the distributed load is not considered. Because the impact load or the accidental load is greater than the distributed load. However, in fact, the distributed load may effect on local damage. Therefore, changing the loading mode and load distribution are also worth trying in the future experiments.
3. In this study, the specimens were designed with different sections and spans. Considering that the form of reinforcing steel bars also affected the behavior and the carrying capacity of the structure, and in practice seismic design also needs to set up bend-up bars nearby the beam-column joint. The effect of both types of bars on the mechanical behavior of the structure needs to be study.
4. This test only studied the progressive collapse resistance of the beam-column structure. It did not consider the effect of the reinforced concrete slab on the bearing capacity and the mechanical behavior. Thus, further studies are required to evaluate the contribution of floor slabs in mitigating progressive collapse under dynamic loading.
5. In this test, sometimes the side stub column of the specimen may have rotate due to the connection with the supporting system such as between upper case and screw or the specimen and steel case. Therefore, more rigid supporting modes for the side columns should be tried.

### **6.2.2 Numerical simulation**

1. Different from simulating the whole frame collapse, simulating components experiment concerns many problems of contact between different materials such like steel and steel or steel and concrete. Such contact should affect the boundary conditions. Setting the contact relationship between different parts and different materials needs to be studied.
2. Both experiments and numerical simulations show that the behavior of the beam-column joint plays an important role in the failure of the component and the bearing capacity. Therefore, simulating the behavior of the joint where grow out plastic hinges needs to be improved, for example adding some springs or connector components in this joint.

3. The numerical simulation work in this study only simulated the failure process of beam-column assemblages subjected to accidental loading. The collapse process of the entire building should be simulated with connectors between reinforcing bars and concrete and using concrete damage model in order to assess the damage of the building in progressive collapse.
4. In order to improve the calculation accuracy and to simulate the crack process in concrete, the grid size of the model mesh need to be very small. It is a problem that the calculation time is then pretty long. Hence, balancing accuracy and efficiency in numerical calculation needs to be studied.
5. The progressive collapse always concerns the problems of large displacements and large rotations. With the development of discrete element method and appropriate tools, discrete elements, or discrete elements associated with finite elements could be considered to simulate the collapse process.

## Reference

- [1] “United States General Services Administration (GSA). Progressive collapse analysis and design guidelines for new federal office buildings and major modernization projects, Washington D.C., 2003.”
- [2] “American Society of Civil Engineers (ASCE). (2010). ‘Minimum Design Loads for Buildings and Other Structures.’ American Society of Civil Engineers, Reston, Virginia.”
- [3] R. S. Nair, “Preventing disproportionate collapse,” *J. Perform. Constr. Facil.*, vol. 20, no. 4, pp. 309–314, 2006.
- [4] Linenthal, Edward, *The Unfinished Bombing: Oklahoma City in American Memory*. New York: Oxford University Press., 2001.
- [5] Serkan Sagiroglu, “Analytical and experimental evaluation of progressive collapse resistance of reinforced concrete structures,” Doctor thesis, Northeastern University, 2012.
- [6] Lawrence, *Looming Tower*. Knopf Doubleday Publishing Group, 2006.
- [7] Mengzhu Diao; Lanping Qian; Yi Li, Hong Guan, “Experimental Study of the Horizontal Progressive Collapse of RC Frames,” presented at the Structures Congress 2018.
- [8] Shuang Li, Sidi Shan, Changhai Zhai, Lili Xie, “Experimental and numerical study on progressive collapse process of RC frames with full-height infill walls,” *Eng. Fail. Anal.*, no. 59, pp. 57–68, 2016.
- [9] Sidi Shan, Shuang Li, Shuang Li, Shiyu Xu, Lili Xie, “Experimental study on the progressive collapse performance of RC frames with infill walls,” *Eng. Struct.*, no. 111, pp. 80–92, Mar. 2016.
- [10] S. P. Tastani, and S. J. Pantazopoulou, “Experimental Evaluation of The Direct Tension Pullout Bond Test,” *J. Struct. Eng.*, vol. 136, no. 6, 2010.
- [11] “European Committee for Standardization. EN 1991-1-7:2006, Eurocode 1: Actions on structures. Part 1-7: General Actions Accidental actions. Brussels, Belgium, 2006.”
- [12] C. A. Vidalis, “Improving the resistance to progressive collapse of steel and composite frames,” Doctor thesis, Imperial College London, 2014.
- [13] “American Concrete Institute (ACI). Building code requirements for structural concrete and commentary (ACI 318m-08). Detroit, Michigan, 2008.”
- [14] A. R. Santhakumar and M. U. Maheshwari, “Capacity Design for Tall Buildings with Mixed System,” presented at the 13th World Conference on Earthquake Engineering, 2004.
- [15] Ali Kheyroddin, H. Naderpour, “Plastic Hinge Rotation Capacity of Reinforced Concrete Beams,” *Int. J. Civ. Eng.*, vol. 5, no. 1, pp. 30–42, Jan. 2007.
- [16] David Stevens, Brian Crowder, Bruce Hall, Krik A. Marchand, “Unified Progressive Collapse Design Requirements for DOD and GSA,” presented at the Structures Congress 2008.
- [17] “Department of Defense (DoD). Unified Facilities Criteria (UFC): Design of Structures to Resist Progressive Collapse, Washington D.C., 2005.” 2005.
- [18] Sasani, M. and Serkan, S., “Progressive Collapse Resistance of Hotel San Diego,” *J. Struct. Eng.*, vol. 134, no. 3, pp. 478–488, Mar. 2008.
- [19] Tiecheng Wang, Qingwei Chen, Hailong Zhao, Lei Zhang, “Experimental Study on Progressive Collapse Performance of Frame with Specially Shaped Columns Subjected to Middle Column Removal,” *Shock Vib.*, no. 2016, 2016.
- [20] W.-J. Yi, Q.-F. He, Y. Xiao, and S. K. Kunnath, “Experimental study on progressive

- collapse-resistant behavior of reinforced concrete frame structures,” *ACI Struct. J.*, vol. 105, no. 4, 2008.
- [21] Pascal forquin, Wen Chen, “An experimental investigation of the progressive collapse resistance of beam-column RC sub-assemblages,” *Constr. Build. Mater.*, vol. 152, no. 15, pp. 1068–1084, Oct. 2017.
- [22] W. Chen and P. Forquin, “Experimental and numerical study of the damage process in RC beam - column sub - assemblages during a progressive collapse scenario,” *Int. J. Numer. Anal. Methods Geomech.*, Mar. 2019.
- [23] Sezen, H. and Song, B., “Progressive Collapse Analysis of the Ohio Union Steel Frame Building,” *EuroSteel 2008*, vol. 3, no. 5, pp. 508–526, 2008.
- [24] Qing-Feng He, Wei-Jian Yi, Y. Xiao, and Sashi Kunnath, “experimental study of progressive collapse due to sudden column removal.pdf,” in *Steel Building Symposium: Blast and Progressive Collapse Resistance: December 4-5, 2003, McGraw-Hill Auditorium, New York City*, 2009, p. 97.
- [25] M. Sasani and J. Kropelnicki, “Progressive collapse analysis of an RC structure,” *Struct. Des. Tall Spec. Build.*, vol. 17, no. 4, pp. 757–771, Nov. 2008.
- [26] Y. Su, Y. Tian, and X. Song, “Progressive collapse resistance of axially-restrained frame beams,” *ACI Struct. J.*, vol. 106, no. 5, 2009.
- [27] J. Yu and K. H. Tan, “Progressive collapse resistance of RC beam-column sub-assemblages,” *Progress. Collapse Resist. RC Beam-Column Sub-Assem. Des. Anal. Prot. Struct. 3rd2010Singapore*, 2010.
- [28] J. Kim and H. Choi, “Progressive collapse-resisting capacity of RC beam–column sub-assemblage,” *Mag. Concr. Res.*, vol. 63, no. 4, pp. 297–310, Apr. 2011.
- [29] J. Yu and K.-H. Tan, “Experimental and numerical investigation on progressive collapse resistance of reinforced concrete beam column sub-assemblages,” *Eng. Struct.*, vol. 55, pp. 90–106, Oct. 2013.
- [30] S. L. Yap and B. Li, “Experimental investigation of reinforced concrete exterior beam-column subassemblages for progressive collapse,” *ACI Struct. J.*, vol. 108, no. 5, 2011.
- [31] K. Qian and B. Li, “Experimental and analytical assessment on RC interior beam-column subassemblages for progressive collapse,” *J. Perform. Constr. Facil.*, vol. 26, no. 5, pp. 576–589, 2012.
- [32] L. Guo, S. Gao, F. Fu, and Y. Wang, “Experimental study and numerical analysis of progressive collapse resistance of composite frames,” *J. Constr. Steel Res.*, vol. 89, pp. 236–251, Oct. 2013.
- [33] Leon RT., “Semi-rigid composite construction,” *J Constr Steel Res*, vol. 15, no. 2, pp. 99–120, 1990.
- [34] Anderson D, Najafi AA., “Performance of composite connections major axis end plate joints,” *J Constr Steel Res*, vol. 31, no. 1, pp. 31–57, 1994.
- [35] Richard Liew JY, Teo TH, Shanmugam NE, Yu CH., “Testing of steel-concrete composite connections and appraisal of results,” *J Constr Steel Res*, vol. 56, no. 2, pp. 17–50, 2000.
- [36] C. Liu, K. H. Tan, and T. C. Fung, “Dynamic behaviour of web cleat connections subjected to sudden column removal scenario,” *J. Constr. Steel Res.*, vol. 86, pp. 92–106, Jul. 2013.
- [37] J. Yu, T. Rinder, A. Stolz, K.-H. Tan, and W. Riedel, “Dynamic Progressive Collapse of an RC Assemblage Induced by Contact Detonation,” *J. Struct. Eng.*, vol. 140, no. 6, p.

04014014, Jun. 2014.

- [38] S. C. Woodson and J. T. Baylot, "Structural collapse: quarter-scale model experiments," DTIC Document, 1999.
- [39] M. Esmailnia Omran, A. Hoseini Karani, "Span Length Effects on the Progressive Collapse Behaviour in Concrete Structures," *J. Stress Anal.*, vol. 3, no. 1, pp. 81–91, 2018.
- [40] "S. Elkoly, B. El-Ariss, Progressive collapse evaluation of externally mitigated reinforced concrete beams, *Eng. Fail. Anal.*," vol. 40, pp. 33–47, 2014.
- [41] F.H. Rezvani, A.M. Yousefi, H.R. Ronagh, "Effect of span length on progressive collapse behaviour of steel moment resisting frames," *Structure*, no. 3, pp. 81–89, 2015.
- [42] B. Kordbagh, M. Mohammadi, "Influence of seismicity level and height of the building on progressive collapse resistance of steel frames," *Struct Tall Spec Build*, vol. 26, p. 1350, 2017.
- [43] M. Sasani, A. Werner, and A. Kazemi, "Bar fracture modeling in progressive collapse analysis of reinforced concrete structures," *Eng. Struct.*, vol. 33, no. 2, pp. 401–409, Feb. 2011.
- [44] Waleed Mohamed Elsayed, Mohamed A.N. Abdel Moaty, Mohamed E. Issa, "Effect of reinforcing steel debonding on RC frame performance in resisting progressive collapse," *HBRC J.*, vol. 3, no. 12, pp. 242–254, 2016.
- [45] Lynn, K.M. and Isobe, D., "Structural collapse analysis of framed structures under impact loads using ASI-Gauss finite element method," *Int. J. Impact Eng.*, vol. 34, no. 9, pp. 1500–1516.
- [46] Pekau, O.A. and Cui, Y., "Progressive collapse simulation of precast panel shear walls during earthquakes," *Comput. Struct.*, vol. 84, no. 5, pp. 400–412, 2006.
- [47] Khandelwal, K. and El-Tawil, S., "Multiscale Computational Simulation of Progressive Collapse of Steel Frames," presented at the Proceedings of the ASCE Structures Congress, 2005.
- [48] Isobe, D., and Tsuda, M., "Seismic collapse analysis of reinforced concrete framed structures using the finite element method," *Earthq. Eng. Struct. Dyn.*, vol. 32, no. 13, pp. 2027–2046, 2003.
- [49] T. H. Almusallam *et al.*, "Progressive Collapse Analysis of a Typical RC Building of Riyadh," presented at the Proceedings of the IMPLAST 2010 Conference, 2010.
- [50] B. S. Iribarren, "Progressive collapse simulation of reinforced concrete structures: influence of design and material parameters and investigation of the strain rate effects," Universite Libre de Bruxelles, 2011.
- [51] Yihai Bao; Sashi K. Kunnath; Sherif El-Tawil; and H. S. Lew, "Macromodel-Based Simulation of Progressive Collapse: RC Frame Structures," *J. Struct. Eng.*, vol. 134, no. 7, 2008.
- [52] J. Li and H. Hao, "Numerical study of structural progressive collapse using substructure technique," *Eng. Struct.*, vol. 52, pp. 101–113, Jul. 2013.
- [53] K. M. Mosalam, M. Talaat, and S. Park, "Modeling progressive collapse in reinforced concrete framed structures," presented at the The 14 th World Conference on Earthquake Engineering, 2008.
- [54] Xinzheng Lu, Xuchuan Lin, Yuhu Ma, Yi Li, Lieping Ye, "Numerical Simulation for the Progressive Collapse of Concrete Building due to Earthquake," presented at the the 14

- th World Conference on Earthquake Engineering, 2008.
- [55] M. Sasani, “Response of a reinforced concrete infilled-frame structure to removal of two adjacent columns,” *Eng. Struct.*, vol. 30, no. 9, pp. 2478–2491, Sep. 2008.
- [56] M. Sasani and J. Kropelnicki, “Progressive collapse analysis of an RC structure,” *Struct. Des. Tall Spec. Build.*, vol. 17, no. 4, pp. 757–771, Nov. 2008.
- [57] “Mohamed OA. Assessment of progressive collapse potential in corner floor panels of reinforced concrete buildings. *Eng Struct* 2009;31:749–57.”
- [58] Y. Shi, Z.-X. Li, and H. Hao, “A new method for progressive collapse analysis of RC frames under blast loading,” *Eng. Struct.*, vol. 32, no. 6, pp. 1691–1703, Jun. 2010.
- [59] Y. Shi, H. Hao, and Z.-X. Li, “Numerical derivation of pressure–impulse diagrams for prediction of RC column damage to blast loads,” *Int. J. Impact Eng.*, vol. 35, no. 11, pp. 1213–1227, Nov. 2008.
- [60] L. Kwasniewski, “Nonlinear dynamic simulations of progressive collapse for a multistory building,” *Eng. Struct.*, vol. 32, no. 5, pp. 1223–1235, May 2010.
- [61] H.-S. Kim, J.-G. Ahn, and H.-S. Ahn, “Numerical Simulation of Progressive Collapse for a Reinforced Concrete Building,” presented at the World Academy of Science, Engineering and Technology, 2014, vol. 7.
- [62] E. Masoero, F. K. Wittel, H. J. Herrmann, and B. M. Chiaia, “DEM Simulations of the Progressive Collapse of Framed Structures,” presented at the 12th International Conference on Fracture, 2009.
- [63] Munjiza A, Bangash T, John NWM., “The combined finite-discrete element method for structural failure and collapse,” *Eng Fract Mech*, no. 71, pp. 469–83, 2004.
- [64] “Luccioni BM, Lopez DE, Danesi RF. Bond-slip in reinforced concrete elements. *J Struct Eng* 2005;131:1690–8.”
- [65] E. Spacone and S. Limkatanyu, “Responses of reinforced concrete members including bond-slip effects,” *ACI Struct. J.*, vol. 97, no. 6, 2000.
- [66] E Ferrier, S Avril, P Hamelin, A Vautrin, “Mechanical behavior of RC beams reinforced by externally bonded CFRP sheets,” *Mater. Struct.*, vol. 36, no. 8, pp. 522–529, 2003.
- [67] Emmanuel Ferrier, Marc Quiertant, Karim Benzarti, Patrice Hamelin, “Influence of the properties of externally bonded CFRP on the shear behavior of concrete/composite adhesive joints,” *Compos. Part B Eng.*, vol. 41, no. 5, pp. 354–362, 2010.
- [68] K. Ahmed, Z. A. Siddiqi, and A. Ghaffar, “Effect of Rebar Cover and Development Length on Bond and Slip in High Strength Concrete,” *Engg Appl*, vol. 2, Jan. 2008.
- [69] W. Yeih, R. Huang, J.J. Chang, and C.C. Yang, “A Pullout Test for Determining Interface Properties between Rebar and Concrete,” *Adv. Cem. Based Mater.*, pp. 57–65, May 1997.
- [70] J. Humbert , J. Baroth and L. Daudeville, “Probabilistic analysis of a pull-out test,” *Mater. Struct.*, no. 43, pp. 345–355, 2009.
- [71] J. Mazars, F. Hamon, and S. Grange, “A new 3D damage model for concrete under monotonic, cyclic and dynamic loadings,” *Mater. Struct.*, Oct. 2014.
- [72] U. M. Mahran, “Theoretical Study For Bond Between Reinforcement Steel And Concrete,” *Int. J. Sci. Basic Appl. Res.*, vol. 12, no. 1, pp. 93–102, 2013.
- [73] A. G. Vlassis, B. A. Izzuddin, A. Y. Elghazouli, and D. A. Nethercot, “Progressive collapse of multi-storey buildings due to sudden column loss—Part II: Application,” *Eng. Struct.*, vol. 30, no. 5, pp. 1424–1438, May 2008.

- [74] Poinard, C, Malecot, Y, and Daudeville, L, “Damage of concrete in a very high stress state: experimental investigation,” *Mater. Struct.*, vol. 43, no. 2, pp. 15–29, 2010.
- [75] Gabet, T, Malecot, Y, and Daudeville, L, “Triaxial behaviour of the concrete under high stresses: influence of the loading path on compaction and limit states,” *Cem. Concr.*, vol. 38, 2008.
- [76] Vu, X.H, Malecot, Y, and Daudeville, L, “Experimental analysis of concrete behavior under high confinement: effect of the saturation ratio,” *Int J Solides struct*, vol. 46, pp. 1105–1120, 2009.
- [77] B. Erzar and P. Forquin, “Analysis and modelling of the cohesion strength of concrete at high strain-rates,” *Int. J. Solids Struct.*, vol. 51, no. 14, pp. 2559–2574, Jul. 2014.
- [78] B. Erzar and P. Forquin, “Experiments and mesoscopic modelling of dynamic testing of concrete,” *Mech. Mater.*, vol. 43, no. 9, pp. 505–527, Sep. 2011.
- [79] Forquin P., “Influence of free water and strain-rate on the shear behaviour of concrete.,” *Applied Mech.Mat.*, no. 82, pp. 148–153.
- [80] Dupray, F, Malecot, Y, Daudeville, L, and Buzaud, E, “A mesoscopic model for the behaviour of concrete under high confinement.,” *Int.J. Num. Anal. Meth. Geomech*, no. 33, pp. 1407–1423, 2009.
- [81] Evelyne Toussaint, Sébastien Durif, Abdelhamid Bouchairid, Michel Grédiac, “Strain measurements and analyses around the bolt holes of structural steel plate connections using full-field measurements,” *Eng. Struct.*, vol. 131, no. 5, pp. 148–162, 2016.
- [82] Park, R., and Gamble, W. L., *Reinforced Concrete Slabs, second edition*, , 2000. John Wiley & Sons, 2000.
- [83] Norman W. Hanson, and Harold W. Conner, “Seismic Resistance of Reinforced Concrete Beam-Column Joints,” *J. Struct. Div.*, vol. 93, no. 5, pp. 533–560, 1967.
- [84] Anil K. Chopra, *Dynamics of structures, Third edition*. Prentice Hall, 2001.
- [85] Friedel Hartmann, Casimir Katz, *Structural Analysis with Finite Elements*. Springer, 2007.
- [86] Hajjar, J.F., and Molodan. A., “A distributed plasticity model for cyclic analysis of concrete-filled steel tube beam-columns and composite frames,” *Eng. Struct.*, no. 20(4–6), pp. 398–412, 1998.
- [87] Liew, J.Y.R. and Chen, H., “Explosion and fire element analysis of frames using fiber element approach,” *J. Struct. Eng. ASCE*, vol. 130, no. 7, pp. 991–1000, 2004.
- [88] Rassati, G. A., Leon, R. T., and Noè, S, “Component modeling of partially restrained composite joints under cyclic and dynamic loading,” *J. Struct. Eng.*, vol. 130, no. 2, pp. 343–351, 2004.
- [89] Jin, J., and El-Tawil, S, “Evaluation of FEMA-350 Seismic provisions for steel panel zones,” *J. Struct. Eng.*, vol. 131, no. 2, pp. 250–258, 2005.
- [90] P. Forquin and F. Hild, “A Probabilistic Damage Model of the Dynamic Fragmentation Process in Brittle Materials,” in *Advances in Applied Mechanics*, vol. 44, Elsevier, 2010, pp. 1–72.
- [91] C. Denoual and F. Hild, “A damage model for the dynamic fragmentation of brittle solids,” *Comput. Methods Appl. Mech. Eng.*, vol. 183, no. 3, pp. 247–258, 2000.
- [92] *ABAQUS 6.12, Abaqus Analysis User’s Manual 31.2.2.* .
- [93] P. Forquin, “Caractérisation expérimentale quasi-statique et dynamique de l’arrachement d’armature, Rapport, 2014.” 2014.

- [94] Amar Khennane, *Introduction to Finite Element Analysis Using MATLAB® and Abaqus*. Taylor & Francis Group, LLC, 2013.
- [95] K. Hesameddin, A. Irfanoglu, and T. J. Hacker, “Effective Viscous Damping Ratio in Seismic Response of Reinforced Concrete Structures,” presented at the 6th International Conference on Advances in Experimental Structural Engineering, 2015, p. 8.
- [96] Young J. PARK, Andrei M. REINHORN, Sashi K. KUNNATH, “Seismic damage analysis of reinforced concrete buildings,” presented at the Proceedings of ninth world conference on earthquake engineering, JAPAN, 1988, vol. Vol V, pp. 211–216.
- [97] M.J.N. Priestley<sup>1</sup>, G.M. Calvi<sup>1</sup>, and M.J.N. Priestley, G.M. Calvi, M.J. Kowalsky, “Direct displacement-based seismic design of structures,” presented at the 2007 NZSEE conference, 2007, pp. 329–341.